Corso di dottorato di ricerca in:

"Scienze Biomediche e Biotecnologiche"

in convenzione con I.R.C.C.S. Centro di Riferimento Oncologico di Aviano - CRO

Ciclo 32°

Titolo della tesi

"Chemoresistance in Epithelial Ovarian Cancer: *in vitro* selection and characterization of platinum resistant cells"

Dottorando

Ilaria Lorenzon

Supervisore

Dr.Gustavo Baldassarre

Co-supervisore

Dr.ssa Monica Schiappacassi
Dr.ssa Maura Sonego

Anno 2020

This PhD work was done
at Centro di Riferimento Oncologico (CRO, National Cancer Institute)
of Aviano, in the Division of Molecular Oncology
directed by Dr. Gustavo Baldassarre

Table of contents

Abstract 7

1. Introduction 8

1.1 Epithelial Ovarian Cancers (EOC) 8

1.2 Drug resistance in EOC 9

1.2.1 Clinical resistance 9

1.2.2 Molecular mechanisms of platinum resistance 10

1.2.2.1 Deregulation of cisplatin transporters 12

1.2.2.2 Detoxification of cisplatin 14

1.2.2.3 Proficient DNA repair 15

1.3 The most frequent modulated genes in EOC 17

1.3.1 CCNE1 amplification 17

1.3.2 BRCA1/ BRCA2 18

1.3.3 TP53 19

1.3.3.1 Mutant p53 in cancer 21

2. Aim of the study 24

3. Results 25

3.1 Generation of cisplatin resistant cell lines 25

3.2 Cell cycle progression of cisplatin resistant cells 27

3.3 Morphology and adhesion ability of cisplatin resistant cells 28

3.4 Response to cisplatin-induced damage of PT-res cells 34

3.5 PT-res cells are characterized by cell-specific alterations of cisplatin 35

transporters

3.6 MDAH PT-res cells grow slower than their parental counterpart, giving rise to large, multinucleated cells 38

3.7 Selection of MDAH PT-res single clones 38

3.8 $p53^{MUT}$ downstream targets are differently modulated in PT-res clones 48

3.9 DNA-PK_{CS} is not involved in the regulation of $p53^{MUT}$ activity in PT-res clones 52

3.10 MDAH PT-res clones gained a new TP53 missense mutation after therapy selection process 53

4. Discussion 59

5. Material and methods 63

5.1 Cell cultures 63

5.2 Compounds and drugs treatment 63

5.3 Cell viability assay 63

5.4 Vectors and transfections 64

5.5 Cell cycle analysis by flow cytometry 64

5.6 Preparation of Cell lysates, Immunoblotting, and Immunoprecipitation 65

5.7 Protein stability 65

5.8 RNA isolation and Real-time polymerase chain reaction 66

5.9 *In vitro* cell proliferation 66

5.10 EOC adhesion on mesothelial cells and Immunofluorescence analyses 66

5.11 Next Generation Sequencing (NGS) 67

5.12 Cisplatin-DNA (Pt-DNA) adduct detection by Dot-blot 67

5.13 Reactive Oxygen Species (ROS) analyses 67

5.14 Double thymidine block 68

5.15 Statistical analyses 68

Table 1 69

6. References 70

7. Publications 78

8. Acknowledgments 79

Abstract

Epithelial Ovarian Cancer (EOC) is the fifth leading cause of cancer death in women worldwide. Its high mortality rate is mainly due to late diagnosis, when tumors are spread out into the abdominal cavity. The standard care for patients combines radical surgery with platinum-taxol chemotherapy. Despite a good initial response, development of a platinum resistant disease is a frequent event in advanced EOC patients and predicts poor prognosis. Thus, improving response to platinum represent an unmet goal in EOC treatment. We have recently contributed to this issue reporting the molecular and biological characterization of three out of the seven new isogenic models of platinum resistant (PT-res) EOC cell lines we have generated in the lab: MDAH-2774, TOV-112D and OVSAHO. Our characterization pointed out a higher ability of the three isogenic PT-res cells to resolve PT-induced DNA damage, compared to parental cells, suggesting that drug uptake, detoxification and excretion, along with the DNA repair pathway, play a central role in the instauration of a resistant phenotype. Moreover, all PT-res cells displayed an evident change in their morphology, accompanied by higher ability to grow on mesothelium. This included a reorganization of cytoskeleton, cell-cell junctions and adhesion abilities. We went deeper in the biological and molecular characterization of MDAH-2774 PT-res cells reporting the appearance of a novel mutation (S185G), that accompanied the already present R273H, in TP53 gene. This additional mutation, likely induced by platinum, was associated with higher p53 phosphorylation on Ser37 that might confer increased activity to an already mutated TP53. Its expression had functional consequences, since it significantly increased PT-resistance in SKOV3 ($p53^{NULL}$) cells and was associated with the higher PT-resistant phenotype in MDAH cells. Mechanistically, our results suggest that the more active $p53^{S185G/R273H}$ protein, in MDAH cells, was at least partially responsible for an altered progression through the M phase of the cell cycle, that eventually results in deregulated mitosis with the appearance of a subpopulation of enlarged multinucleated cells (MNGCs). Indeed, $TP53^{MUT}$ specifically regulates the transcription of mitotic-regulator genes, supporting the possibility that it confers a surviving advantage to aberrant mitotic cells. Future studies are necessary to properly clarify the molecular mechanisms underlying the formation of MNGCs and how $p53^{S185G/R273H}$ contributes to this resistant phenotype.

Introduction

1.1 Epithelial Ovarian Cancer (EOC)

Ovarian cancer is the fifth leading cause of cancer death in women and the most lethal gynecologic malignancy. This is mostly due to late diagnosis, when tumors are spread out into the abdominal cavity, and to the occurrence of chemoresistance (Jayson et al., 2014). Histologically ovarian cancer is roughly composed of epithelial, germ cell and stromal tumors, with epithelial ovarian cancer (EOC) being the most common and the most deadly, with five-year survival rates below 40%.

Several distinctive morphology and molecular features can be used to classify epithelial ovarian carcinomas into different types. The serous type is the most common, and can include high grade and low grade tumors. The other main types include mucinous, endometrioid, and clear cell. Type I tumors tend to grow slowly and cause fewer symptoms. These tumors usually do not respond well to chemotherapy. Low grade serous carcinoma, clear cell, mucinous and endometrioid carcinoma are examples of type I tumors. They are frequently mutated in genes like KRAS, BRAF, PTEN and β-catenin. Type II tumors grow fast and tend to spread sooner. These tumors tend to respond better to chemotherapy. High grade serous carcinoma is an example of a type II tumor. They are characterized by a high genomic instability and mutations in TP53 gene. Moreover homologous recombination repair pathways are altered in roughly 50% of high grade serous ovarian cancers in fact, hereditary tumors associated with BRCA1 and BRCA2 mutations belong to Type II (Jayson et al., 2014; Kurman and Shih, 2010).

The International Federation of Gynecology and Obstetrics (FIGO) proposes a four-steps staging for EOC: Stage I) The cancer is only in the ovary or fallopian tubes; Stage II) The cancer is in one or both ovaries or fallopian tubes and has spread to other organs (such as the uterus, bladder, the sigmoid colon, or the rectum) within the pelvis or there is primary peritoneal cancer; Stage III) Tumor involves one or both ovaries or fallopian tubes, or primary peritoneal cancer, with cytologically or histologically confirmed spread to the peritoneum outside the pelvis and/or metastasis to the retroperitoneal lymph nodes and Stage IV) Distant metastasis excluding peritoneal metastases (Prat, 2015).

Standard care for patients combines radical surgery with platinum-based chemotherapy. The standard first-line treatment combines two different types of drugs, a platinum compound (usually cisplatin or carboplatin) and a taxane (usually paclitaxel or docetaxel). Paclitaxel is an antitumoral drug that enhances the polymerization of tubulin to stable

microtubules and also interacts directly with microtubules, stabilizing them against depolymerization. The fact that the drug has a specific binding site on the microtubule polymer makes it unique among chemotherapeutic agents (Horwitz, 1994). The chemotherapeutic mechanism of platinum compounds is typical of DNA-binding alkylating agents. Platinum compounds exert their anti-tumor activity through the formation of intrastrand and interstrand cross-links, interfering with DNA repair mechanisms, causing single-strand and double-strand breaks (DNA damage), and subsequently inducing cell cycle arrest in S and G2 phases, if the damage is limited, or inducing apoptosis in cancer cells, when the DNA damage is extended (Cook and Brenton, 2011). Although this treatment regime is effective as the first-line treatment, recurrence occurs in up to 75% of ovarian cancer patients. Patients with recurrent ovarian cancer ultimately develop resistance to chemotherapy that led to the progression of the disease (Jayson et al., 2014).

1.2 Drug resistance in EOC

1.2.1 Clinical resistance

Improving response to platinum represents an unmet goal in EOC treatment, since platinum resistance is the main contributing factor in cancer-associated mortality. Time to relapse after first-line platinum-based therapy affects the subsequent treatment options (Figure 1). Platinum-refractory patients, who have progressive disease during initial treatment, represent about 14% of cases and have an intrinsic drug resistance. Despite of good initial response, the majority of patients relapse and are classified according to likelihood of response to secondary platinum treatment. Those who have a platinum free interval (PFI) within 6 months of ending first treatment are classified as platinum resistant. Patients who relapse more than 12 months later are termed platinum sensitive. Patients who relapse between 6 and 12 months are classified as partially sensitive (Cooke and Brenton, 2011).

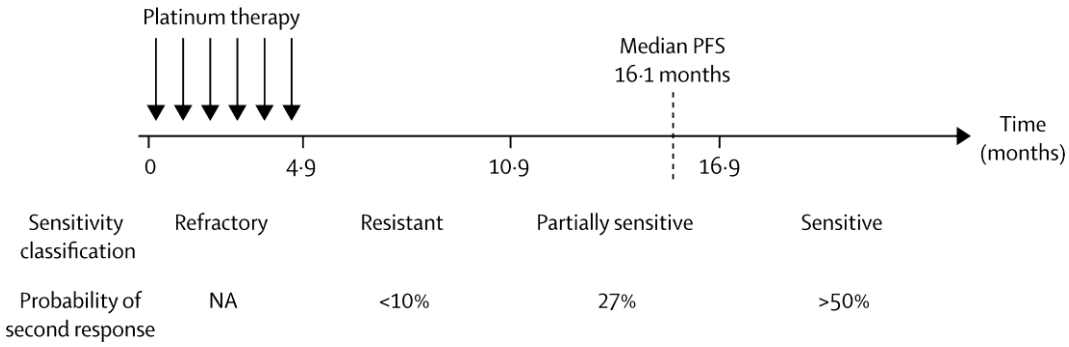

Figure 1. Likelihood of patients response to secondary platinum treatment. Patients are classified as refractory, platinum resistant, platinum sensitive and partially sensitive according to time to relapse after initial platinum treatment (from Cooke and Brenton, 2011).

EOC is described as having an extensive intra-tumoral heterogeneity with multiple, genetically distinct clones forming the entire tumor bulk. Intrinsic platinum-resistant cancer cells exist in ovarian tumors before treatment and are selected once treatment has killed their platinum-sensitive counterparts (Figure 2). This results in repopulation of the tumor, and a low probability that it will respond to further treatments with platinum-based drugs (Holmes, 2015; Cooke and Brenton, 2011). In the absence of any pre-existing resistant cells within the cancer mass, relapse in patients with platinum-sensitive EOC is caused by regeneration of tumor bulk by residual platinum-sensitive cells. Cell divisions during the regrowth can lead to the occurrence of resistance mutations. Whether further relapses are sensitive or not to platinum, therefore, reflects the stochastic nature of mutation (Cooke and Brenton, 2011). The process that lead to refractory disease might be basically different from those that lead to initially sensitive EOC.

1.2.2 Molecular mechanisms of platinum resistance

The platinum-resistant cells use a complex repertoire of mechanisms to mitigate the effects of platinum therapy, including DNA damaging repair, decreased drug uptake, increased platinum removal, sequestration of the metal into lysosomes and occurrence of resistance mutations (Figure 3) (Galluzzi et al., 2014).

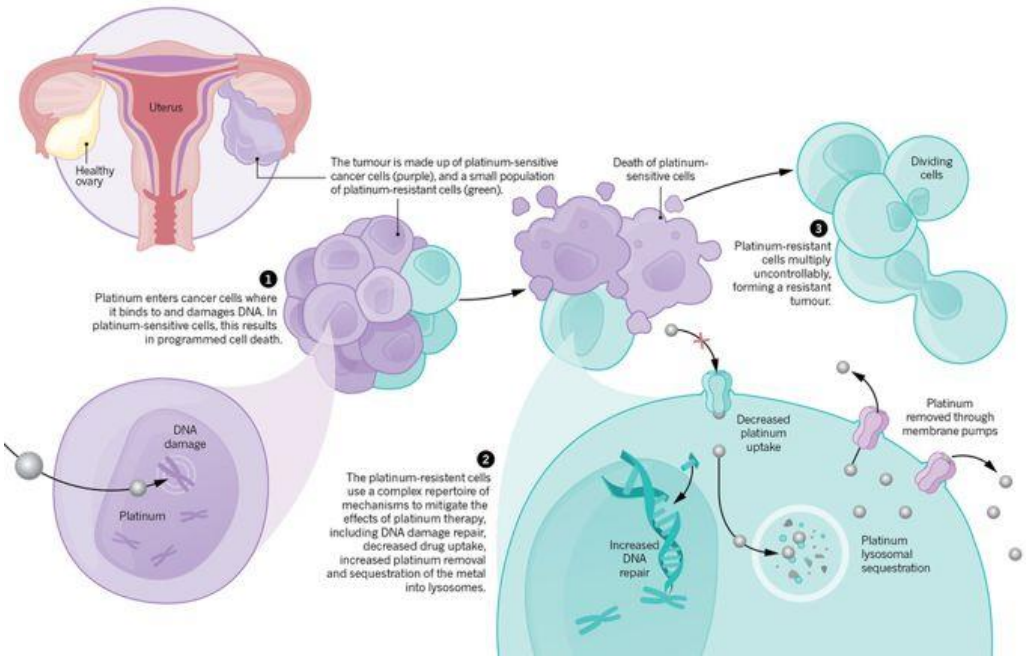

Figure 2. Platinum resistance development in EOC. As indicated, platinum-resistant cells (green) are present in the tumor before treatment and they are selected once the chemotherapy has killed their platinum-sensitive counterparts (purple) (from Holmes, 2015).

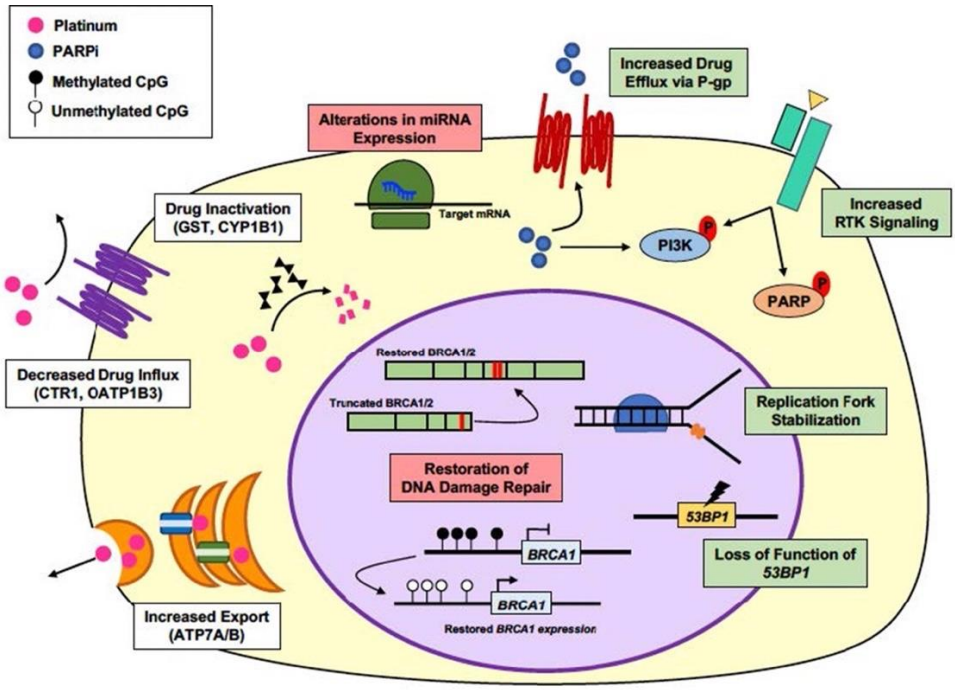

Figure 3. Major mechanisms of primary and acquired resistance in EOC. Resistant cells develop resistance mechanisms, including DNA damaging repair, decreased drug uptake, increased platinum removal, sequestration of the metal into lysosomes and occurrence of resistance mutations (from Freimund et al., 2018).

The therapeutic activity of platinum compounds is mediated by an active species, formed by aqueous hydrolysis as the drug enters the cell. This active species interacts with DNA, RNA and protein, but the cytotoxic effect seems to be primarily mediated via the formation of DNA interstrand and intrastrand crosslinks (Argawal and Kaye, 2003). Two categories of resistance to platinum have been identified: those that limit platinum-DNA adduct formation and those that prevent cell death after the formation of platinum-DNA adduct (Freimund et al., 2018).

1.2.2.1 Deregulation of cisplatin transporters

One of the most prominent characteristics of cellular resistance to cisplatin is the reduced accumulation of the compound into the cell. As a consequence of reduced uptake or retention, the formation of platinum-DNA adducts is decreased. Several transporters, which are expressed on the cell membranes, have been associated with cisplatin transport across the plasma membrane and with resistance: the copper transporter 1 (Ctr1), the copper transporter 2 (Ctr2), the P-type copper-transporting ATPases ATP7A and ATP7B, and the ATP-binding cassette transporter known for years as P-glycoprotein or MDR1 (Ciarimboli, 2014). The two copper transporters, ATP7A and ATP7B, are expressed at higher levels in platinum-resistant cell lines and have been functionally implicated in resistance to several platinum agents, including cisplatin (Samimi et al., 2004; Katano et al., 2004; Katano et al., 2003). ATP7A and ATP7B are members of the P-type ATPase family of transporters. Their primary function is to transport copper into the lumen of the *trans*-Golgi network (TGN) for the biosynthesis of copper-dependent enzymes and to facilitate export of excess copper from the cell by sequestering copper into exocytic vesicles. Cu-ATPases bind copper at their large NH_2-terminal domain and then transfer copper across the membrane using the energy of ATP hydrolysis. Therefore, the major mechanism through which overexpression of ATP7B increases resistance to cisplatin seems to involve blockade of drug access to the nucleus. This may be due either to ATP7B pumping cisplatin into the lumen of the TGN and, similarly to copper exposure, cisplatin also alters the subcellular localization of ATP7B, resulting in its translocation from the Golgi apparatus to peripheral vesicles, presumably lysosomes (Zhitomirsky et Assaraf, 2016). Studies have demonstrated that small interfering RNA silencing of ATP7B increases DNA adduct formation in platinum-resistant EOC lines, and when used with cisplatin *in vivo*, a decrease in tumor growth was observed, highlighting a potential method to circumvent platinum resistance (Mangala et al., 2009).

The copper transporter Ctr1 is a major determinant of cisplatin uptake and sensitivity, which could be modulated by copper levels. It has been observed that in different cisplatin-resistant cell lines and ovarian cancer cell lines derived from patients, where the platinum-based chemotherapy failed, the resistance against cisplatin is associated with reduced expression of the Ctr1 (Liang et al., 2012). Other lines of evidence of the importance of Ctr1 expression for efficacy of treatment with platinating agents derive from the study of the Ctr1-mRNA expression in 40 women with ovarian carcinoma: high Ctr1 expression was significantly associated with sensitivity to platinum-based chemotherapy and progression-free survival. Conversely, low Ctr1 expression was significantly associated with resistance to platinum-based chemotherapy and the shortest survival (Lee et al., 2011). Copper transporter 2 (Ctr2) is in the same family as Ctr1, and primarily localized in intracellular vesicles, in particular in lysosomes and late endosomes as well as on the plasma membrane of several tumor cell lines (Huang et al., 2014; van den Berghe et al., 2007). Based on its structural similarity to the plasma membrane Ctr1, it has been postulated that Ctr2 may mediate copper and cisplatin efflux from lysosomes and late endosomes into the cytoplasm (Huang et al., 2014). Thus, it seemed reasonable that Ctr2 overexpression would increase cell sensitivity to cisplatin, due to increased release of cisplatin from lysosomes. Accordingly, one would suggest that reduced expression of Ctr2 could render cells resistant to cisplatin due to reduced drug efflux from the lysosomes into the cytoplasm. Surprisingly, an analysis of Ctr2 expression levels and cisplatin cytotoxicity in six ovarian carcinoma cell lines identified a direct correlation between Crt2 expression levels and cisplatin resistance (Blair et al., 2009). A possible explanation for this Ctr2-mediated cisplatin resistance is based on its ability to mediate cisplatin endocytosis (Zhitomirsky et Assaraf, 2016).

ABC transporters catalyze the ATP-dependent transport of various anticancer drugs out of tumor cells (van Veen and Konings, 1998; Borst and Elferink, 2002). Overexpression of ABC drug transporters is related to gene amplification, transcriptional and epigenetic changes (Choi and Yu, 2014) and has been shown to be responsible for the major portion of multidrug resistance (Choi, 2005). The most widely studied ABC transporter is the P-glycoprotein or human MDR1. It has been proposed to act as ‘hydrophobic vacuum cleaner’ because of its ability to remove both lipids and drugs as they intercalate and diffuse through the cell membrane. The protein sequences of lipid and drug ABC transporters are similar and probably reflect a common transport mechanism. Human MDR3, for example, is a well-characterized phosphatidyl-choline flippase and has 73%

protein sequence identity to human MDR1. In fact, human MDR1 is itself a lipid flippase transporting short chain phospholipids (Chang, 2003; Choi and Yu, 2014). In addition to facilitate drug export from the cell, other mechanisms of ABC transporters-mediated drug resistance have been reported; these include active lysosomal drug sequestration mediated by these transporters (Figure 4) (Zhitomirsky and Assaraf, 2016). Therefore, to improve therapeutic response of patients, should be used anticancer agents which do not interact with any of this kind of transporters (despite an extremely wide recognition pattern). Thus, MDR modifying agents which inhibit the function of the MDR proteins, either competitively or non-competitively, are good candidates for such a pharmacological modulation (Glavinas et al., 2004).

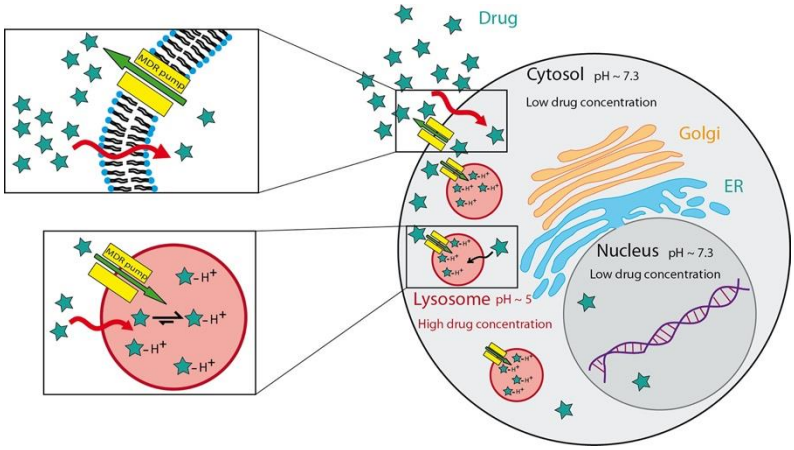

Figure 4. MDR transporters mediate platinum resistance. Transporters from the ABC superfamily localize on the plasma membrane, and facilitate drug efflux from the cell. In addition, some ABC transporters were found to localize on lysosomes and mediate active transport of drugs into the lysosome, facilitating lysosomal drug sequestration (from Zhitomirsky and Assaraf, 2016).

1.2.2.2 Detoxification of cisplatin

There is also an extensive body of evidence implicating the enzyme that catalyzes GSH synthesis (γ-glutamylcysteine synthetase), or the enzyme that mediates the conjugation between cisplatin and GSH (glutathione S-transferase, GST) in platinum resistance through their role in the conversion of cisplatin to inactivated conjugates and detoxification of cisplatin, respectively. GSTs make the compound more anionic and more readily exported from cells by the ATP-dependent glutathione *S*-conjugate export (GS-X) pumps (MRP1 or MRP2). Increased levels of other low-molecular-weight thiol-containing proteins that are involved in heavy-metal binding and detoxification, the metallothioneins, have also been shown to lead to resistance to cisplatin (Kelland, 2007).

1.2.2.3 Proficient DNA repair

After platinum-DNA adducts have been formed, cellular survival can occur either by DNA repair or removal of these adducts, or by tolerance mechanisms. Platinum compounds bind to DNA and create intra-strand/ inter-strand DNA cross-links that induce a DNA damage response (Figure 5). Repair of DNA lesions occurs through different DNA repair pathways, including nucleotide excision repair (NER), mismatch repair (MMR), and homologous recombination (HR) (Kelland, 2007).

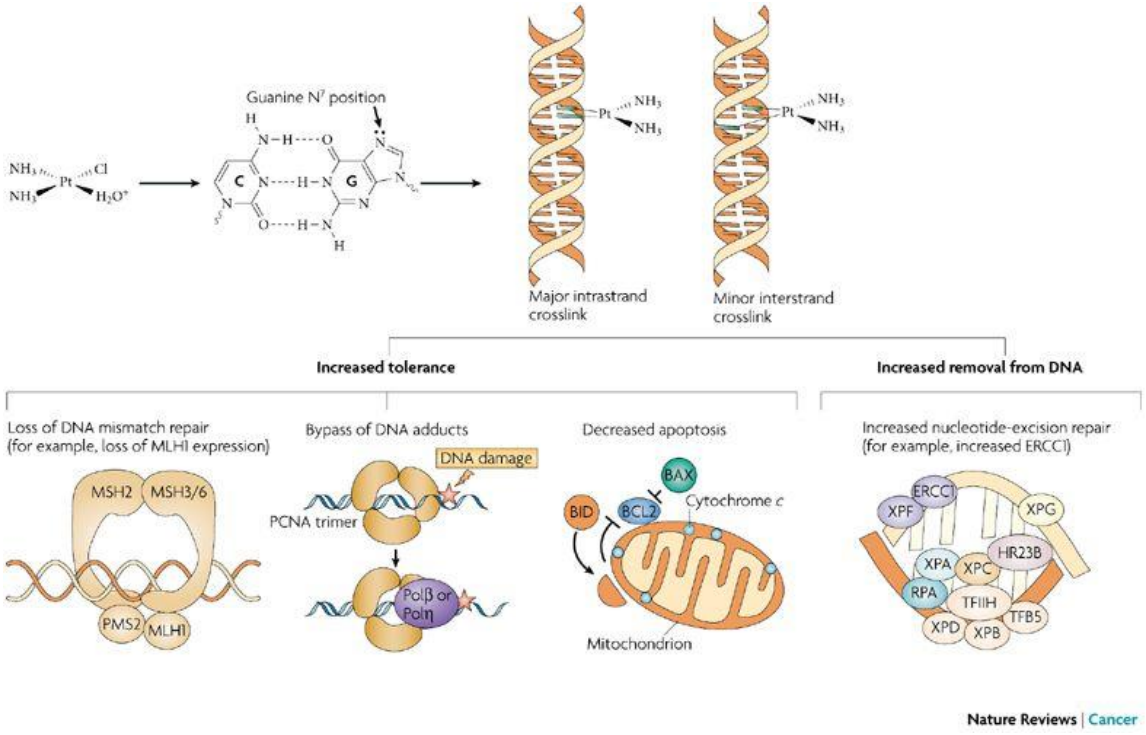

Figure 5. Tumor resistance to platinum drugs mediated after DNA binding. The main removal pathway for DNA adducts is the nucleotide-excision repair (NER); increased NER, especially through increased activity of the endonuclease protein ERCC1 (excision repair cross-complementing-1) can occur in tumors, and can lead to platinum drug resistance (as adducts are removed before apoptotic signaling pathways are triggered). In addition, resistance can occur through increased tolerance to platinum-DNA adducts - even though the DNA adducts are formed - either through loss of DNA mismatch repair, bypassing of adducts by polymerase β and η, or through downregulation of apoptotic pathways (from Kelland, 2007).

NER is the major pathway known to remove cisplatin lesions from DNA (Kelland, 2007). Increased NER in cisplatin-resistant ovarian cancer cells was associated with increased expression of ERCC1 (excision repair cross-complementing-1) and XPF (xeroderma pigmentosum (XP), complementation group F) (Kelland, 2007). ERCC1 forms a heterodimer with XPF and acts to make a 5´ incision into the DNA strand, relative to the

site of platinated DNA. Increased tolerance to platinum-induced DNA damage can also occur through loss of function of the MMR pathway. Loss of this repair pathway leads to low-level resistance to cisplatin and carboplatin (Fink et al., 1996). During MMR, cisplatin-induced DNA adducts are recognized by the MMR proteins MSH2, MSH3 and MSH6. It is postulated that cells then undergo several unsuccessful repair cycles, finally triggering an apoptotic response; loss of MMR with respect to cisplatin-DNA adducts therefore results in reduced apoptosis and, consequently, drug resistance (Kelland, 2007). The clinical relevance of the loss of MMR to platinum-drug-containing chemotherapy resistance, for example, in patients with ovarian cancer, is under active study; some data indicate a possible role in acquired drug resistance, whereas other data show no correlation with intrinsic resistance (Gifford et al., 2004; Kelland, 2007).

HR is another major DNA repair pathway that plays an important role in repairing the DNA lesions induced by platinum-based agents. After NER-mediated identification and resolution of a DNA lesion, the process of HR “fills in” the resulting DNA gaps. HR-dependent interstrand-crosslinking repair occurs during late S or G2 phase. It is well-documented that critical components of the HR mechanism which mediate the repair of double-strand breaks (DSBs) are BRCA1 and BRCA2 (Couch et al., 2014). Although BRCA1 and BRCA2 have many pivotal roles in DNA repair, one of the most crucial roles seems to be direct binding of BRCA2 to the RAD51 protein to form a complex on the DNA. This complex leads to the recruitment of proteins, including MAPK, ATR, and p53, to the DNA lesions that initiates the HR repair process. HR repair of DNA lesions requires a second, homologous DNA that can act as a template for the repair reaction (Johnson and Jasin, 2001; Sung and Klein, 2006). Information from the homologous sequence is copied into the damaged site, allowing for the precise restoration of the original DNA sequence. EOC patients with germline mutations in BRCA1 and/or BRCA2 exhibit impaired ability to repair DNA lesions via HR. This event could potentially explain the increased sensitivity that these tumors have to platinum-based drugs (Cass et al., 2003).

NHEJ is also involved in the repair of interstrand-crosslinking DNA lesions, but in contrast to HR, which repairs DSBs maintaining the genetic information contained in the homologous DNA strand, NHEJ often introduces errors while repairing the DNA lesion. First, the end-binding KU70/80 heterodimer complex binds to the DNA ends and activates DNA-dependent protein kinase catalytic subunits (DNA-PKs). Then the DNA lesion is removed, and finally, a DNA ligase IV-XRCC4 rejoins the two DNA ends. In contrast to

HR, NHEJ can generate translocations and/or deletions and is generally considered to be error-prone (Deans and West, 2011; Peng and Lin, 2011).

Finally, tolerance might occur to platinum, and other cancer drugs, through decreased expression or loss of apoptotic signaling pathways (either the mitochondrial or death-receptor pathways) as mediated through various proteins such as p53, anti-apoptotic and pro-apoptotic members of the BCL2 family, and JNK.

1.3 The most frequent modulated genes in EOC

To understand clonal origin and mutational adaptations associated with recurrent disease, whole-genome sequencing of tumors has been done by several groups (Cancer Genome Atlas Research Network, 2011; Castellarin et al., 2013; Patch et al., 2015). They reported that ubiquitous TP53 mutations were prevalent, extensive copy number changes, like CCNE1, inactivation of tumor suppressors RB1, NF1, RAD51B and PTEN genes and functional inactivation of homologous recombination repair genes. They observed multiple independent reversions of germline BRCA1 or BRCA2 mutations, loss of BRCA1 promoter methylation and recurrent promoter fusion associated with overexpression of the drug efflux pump MDR1 (Patch et al., 2015).

1.3.1 CCNE1 amplification

Cyclin E, a regulatory subunit for CDK2 that plays a key role in centrosome duplication, frequently is overexpressed in human cancers. Cyclin E1 overexpression and CCNE1 copy-number gain occurred in 23.3% and 14.8% of ovarian clear cell carcinomas, respectively, but they were not detected in any of the other endometriosis-related tumors. The amplification and subsequent overexpression of CCNE1 have been reported as one of the major molecular mechanisms that promote the progression of ovarian high-grade serous carcinoma, the most common and aggressive type of ovarian cancer. Cyclin E1 has been established as a critical factor in the regulation of cell cycle progression, and overexpression of cyclin E1 has been reported to result in genomic instability. Cyclin E1 can inappropriately initiate DNA replication and centrosome duplication, which leads to chromosomal instability, aneuploidy, and eventually tumorigenesis (Kuhn et al., 2016; Kawamura et al., 2004). Further studies are required to determine whether cyclin E1 also contributes to the maintenance of telomeres in ovarian clear cell carcinomas and to determine the mechanisms involved. These results suggest the importance of CCNE1 in the progression of ovarian clear cell carcinoma and support

cyclin E1 as a possible therapeutic target in ovarian clear cell carcinoma; indeed, the presence of partially functional DNA repair pathway gives CCNE1-amplified cancers an advantage in surviving both platinum-based therapy and poly-ADP-ribose polymerase (PARP) inhibitor treatments (Kanska et al., 2016).

1.3.2 BRCA1 / BRCA2

BRCA1 and *BRCA2* are genes mapping on two different chromosomes (17q21 and 13q12.3, respectively). These genes are considered tumor suppressor genes, since they are deputed to the maintenance of genomic stability and hence to the control of cell growth (Yoshida and Miki, 2004). Germline BRCA1/2 mutations confer an increased risk of breast and High Grade Serous EOC (HGSOC), and, to a lesser extent, of other type of cancers (Madariaga et al., 2019). Approximately 15–20% of HGSOCs may be inherited with germ line mutations of BRCA1 and BRCA2 genes; however, the majority of HGSOC are sporadic, and a proportion of these present alterations in BRCA function through somatic mutations in BRCA1/2 genes or as a result of methylation (The Cancer Genome Atlas Research Network, 2011).

Retrospective studies suggest that heterozygosity for a BRCA hereditary pathogenic variant ("BRCAness concept) in EOC patients is associated with a significantly more favorable prognosis and is predictive of sensitivity to combination therapies containing platinum derivates. BRCA1/2 gene mutations are a biomarker of sensitivity to treatment with PARP inhibitors in patients with advanced ovarian cancer. PARPs compose a family of more than 18 enzymes that play fundamental roles in DNA replication, DNA transcription and DNA damage repair. Many of these enzymes play a catalytic role in repairing damaged DNA. PARP-1, the most studied member of the PARP family, is an important factor for repairing single-strand breaks. Activation of PARP leads to increased activities of the BER and NER pathways in cells with a fully functional DDR/DNA repair capacity, but not in cells in which PARP is inhibited. PARP binds to SSBs through its N-terminal zinc finger motifs, which activate its C-terminal domain to hydrolyze NAD+ (Figure 6). This event produces long chains of ADP-ribose units (PARylation) and recruits factors of the BER complex (Krishnakumar and Kraus, 2010; Rouleau et al., 2010). The therapeutic effect of PARP inhibitors is due to "synthetic lethality", which occurs in cells with non-functional double-strand DNA repair mechanism (homologous recombination, HR), like BRCA mutated cells. Once PARP-1 gene is deleted, it has been shown that SSBs collapse at the points of replication forks and result in DSBs. DSBs trigger HR repair

pathways to restore the DNA sequences that were disrupted. Farmer et al. showed that when BRCA1 or BRCA2 are defective, cells become sensitized to PARP inhibition, and this event results in chromosomal instability, cell cycle arrest, and apoptosis (Farmer et al., 2005; Sonnenblick et al., 2015).

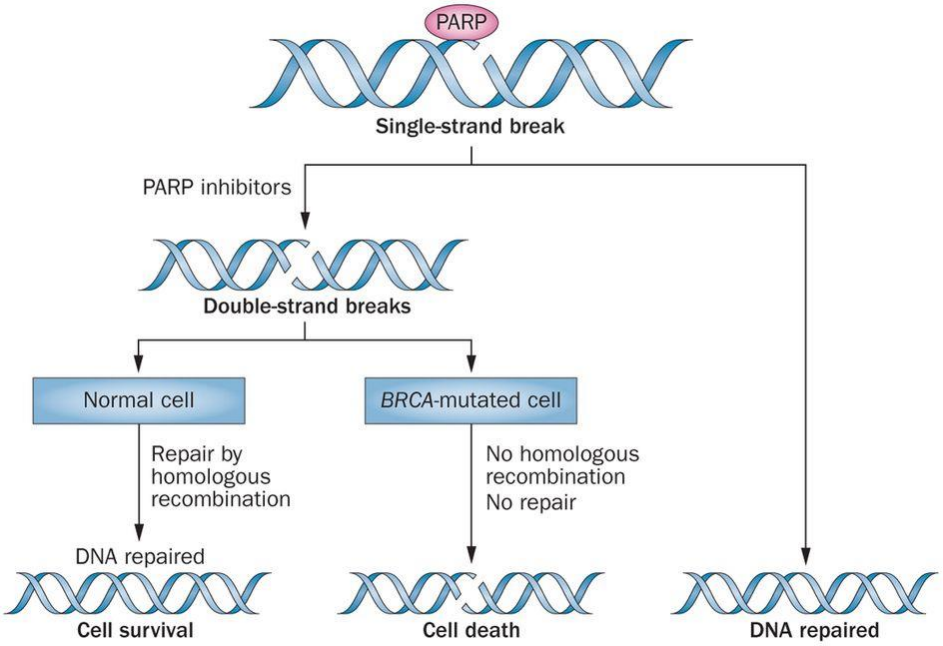

Figure 6. The therapeutic effect of PARP inhibitors is due to "synthetic lethality" in a "BRCAness" background. *BRCA1* or *BRCA2* mutation, resulting in a lack of homologous recombination, sensitizes cells to inhibition of PARP activity, which in turn leads to chromosomal instability, cell-cycle arrest, and subsequent apoptosis (from Sonnenblick et al., 2015).

PARP inhibitors (e.g. Olaparib, Niraparib, Rucaparib) perform their anticancer effects only via their catalytic inhibition of PARPs in a landscape of BRCA deficiency and are used as maintenance therapy in patients with relapsed HGSOCs (Basourakos et al., 2017). BRCA testing is a prerequisite to agree upon PARP inhibitor therapy.

1.3.3 TP53

TP53 gene is the most frequently mutated tumor suppressor gene in human malignancy. Beyond the indisputable importance of p53 as a tumor suppressor, a wide number of new roles have recently been reported. It is known that p53 is a transcription factor and regulates the expression of a myriad of different target genes that then mediate the p53 response. p53 binds specifically to DNA and regulates genes involved in cell cycle arrest, DNA repair, senescence, apoptosis, autophagy, angiogenesis and metabolic changes,

leading to inhibition of tumorigenesis (Figure 7) (Vousden and Prives, 2009; Yamamoto and Iwakuma, 2018; Kruiswijk et al., 2015; Vogelstein et al., 2000; Bieging and Attardi, 2012).

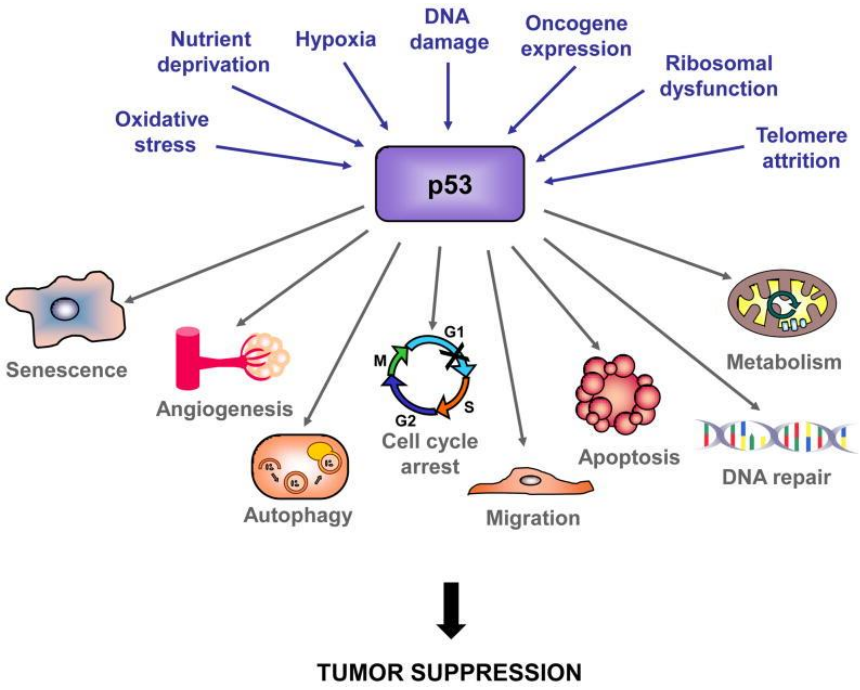

Figure 7. p53 responses in mediating tumor suppression. p53 is a key tumor suppressor implicated in the regulation of cell survival, proliferation and apoptosis by the transcriptional activation of p53 target genes (from Bieging and Attardi, 2012).

The discovery of vast and varied transcriptional targets controlled by p53 raises new questions about how these networks coordinate to promote tumor suppression. The activation of p53 efficiently inhibit cell proliferation and cancer development. This activation is driven by a diversification of stress signals that a cell might run into during cancer progression, like genotoxic damage, oncogene activation, loss of cell-cell contacts, hypoxia. But the mechanisms of action are more intricated. The p53 protein has a short half-life under normal conditions. Because of the negative effects of p53 on cell proliferation and growth, eukaryotic organisms have evolved a feedback autoregulation to maintain low levels of the protein, in the absence of cellular stress. The protagonists are two oncoproteins: MDM2 and MDMX (Khoo et al., 2014; Lu, 2017; Eischen, 2017; Zhou et al., 2017; Wiman, 2010). MDM2 is a RING finger-containing protein, encoded by a p53 target gene, that utilizes several mechanisms to inhibit p53 activity. First, it possesses an intrinsic E3 ligase to mediate p53 polyubiquitination and proteasomal degradation (Wiman, 2010). Also, it targets p53 for monoubiquitination and nuclear export, thus preventing it

from binding to its target promoters into nucleus (Li et al., 2003). Additionally, it inhibits p53 by directly associating with and hiding the trans-activation domain (TA) (Oliner et al., 1993). Lastly, it can suppress TP53 mRNA translation by promoting RPL26 degradation and dissociating the RPL26-p53 mRNA interaction (Ofir-Rosenfeld et al., 2008). MDMX, an MDM2 homologue without any apparent intrinsic E3 ligase activity, repress p53 activity partnering with MDM2 (Wade et al., 2013). It associates with MDM2 through their C-terminal RING domains and drives the E3 ligase activity of the second towards p53. MDMX can also suppress p53 activity by directly interacting with the N-terminal TA domain (Badciong and Haas, 2002). This MDM2-MDMX-p53 loop is critically important for normal growing of cells but is often hijacked by cancer cells for their growth benefits. Several type of cancers express high levels of MDM2 and/or MDMX that inactivate p53 and its downstream pathways (Zhou et al., 2017; Wiman, 2010). Like most transcription factors, p53 contains distinct domains responsible for sequence-specific DNA binding and transcriptional activation. The DNA binding domain comprises residues 100–300 and directs p53 to p53-response elements (p53 RE). The DNA binding domain is the most common site for mutations in cancer (Brosh and Rotter, 2009), underscoring the importance of p53 DNA binding function for tumor suppression. Two distinct transcriptional activation domains (TADs), spanning residues 1–40 and 40–83, cooperate for full p53 transactivation capacity. These domains were defined initially by their ability to confer activation potential on a Gal4 DNA binding domain in reporter assays, and residues within these domains critical for transactivation were pinpointed through additional reporter assays (Venot et al., 1999). Recently, the specific contributions of each domain to various p53 functions *in vivo* have been clarified through the generation of TAD mutant knock-in mice, and we now appreciate that the TADs are differentially required for the activation of distinct sets of p53 target genes and for different biological functions (Johnson et al., 2005; Brady et al., 2011). This knowledge can now be harnessed to map the transcriptional networks critical for p53 function in tumor suppression.

1.3.3.1 Mutant p53 in cancer

Perturbations in p53 signaling pathways are believed to be required for the development of many cancers. The significance of p53 in tumor suppression in humans is highlighted by its inactivation in over half of all human cancers. Unlike wild-type p53, which under normal conditions has a short half-life curtailed when it is targeted by MDM2 for degradation, mutant p53 proteins are outside this negative feedback loop and accumulate to high levels

in cancer cells. Alterations in this gene have been found in every region, but only few of the most frequently occurring mutations have been studied. In some cases, frameshift or non-sense mutations result in loss of p53 protein expression and function (LOF), however, more frequently, alterations in p53 result in missense mutations, with the substitution of a single amino-acid that can be stably expressed in the tumor cell. These substitutions occur through the entire gene, but mostly accumulate in the DNA-biding domain of p53, affecting six hot-spot residues (R175, G245, R248, R249, R273, R282) of the protein translating into various impact on its structure- function activity (Figure 8). Moreover, categorized into structural (R175, G245, R249, R282) and contact (R248 and R273) mutations with effects of gross conformational alterations and loss of anchorage to DNA, respectively.

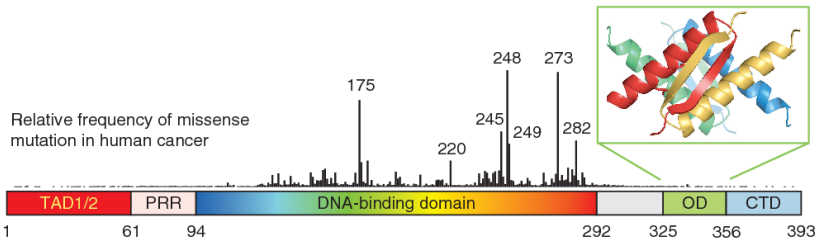

Figure 8. The TP53 hot-spot mutations. p53 contains a natively unfolded amino-terminal transactivation domain (TAD), followed by a proline-rich region (PRR). The structured DNA-binding and tetramerization domains (OD) are connected through a flexible linker region. Similarly to the TAD region, the regulatory domain at the extreme carboxyl terminus (CTD) is also intrinsically disordered. The vertical bars indicate the relative missense-mutation frequency in human cancer for each residue based on the TP53 Mutation Database of the International Agency for Research on Cancer (www-p53.iarc.fr), showing that most cancer mutations are located in the DNA-binding domain (from Joerger and Fersht, 2010).

These conformational alterations disrupt its function as a transcription factor in recognizing its DNA targets thereby inactivating its tumor suppressor activity (Muller and Vousden, 2014; Olotu and Soliman, 2017). This classification is an over-simplification, because different mutations can lead to different alterations in the structure and conformational stability of the p53 protein. Notably, not only the position of the mutation, but also the nature of the substitution may influence the activity of the resulting mutant protein (Brachova et al., 2013).

p53 contact with the DNA's major and minor groove is at the loop-sheet-helix-motif conserved residues and R248 of the L3 (large loop), respectively (Joerger and Fersht, 2007). Moreover, p53 contact and structural mutations affect its DNA interaction both

directly and indirectly by perturbing the conformation of the binding surface thereby prompting its transition from the folded active wild-type state to an unfolded non-active state. Restoration of DNA binding has, therefore, been the subject of interest in most mutant p53 translational research with the design of reactivators, which are able to interact with p53 mutants and restore its wild-type transcriptional activities. Mutants displays structural distortion, reduction in flexibility and increase in rigidity hence its kinetic stability (Olotu and Soliman, 2017). However, some of these variants not only lose their tumor-suppressive capacity, but also enrich cells with oncogenic gain-of-function (GOF) properties, like enhanced proliferation, invasion and migration, genomic instability and resistance to chemotherapy, that contribute to tumor aggressiveness (Oren and Rotter, 2010). Therefore, distinct p53 mutations could display variable transactivation capacity towards different target sequences, affecting distinct cellular pathways (Variant-specific effects) (Kato et al., 2003). Furthermore, different p53 mutants may also possess a set of target genes that are shared among all the mutants (Pan-mutant effects) (Figure 9).

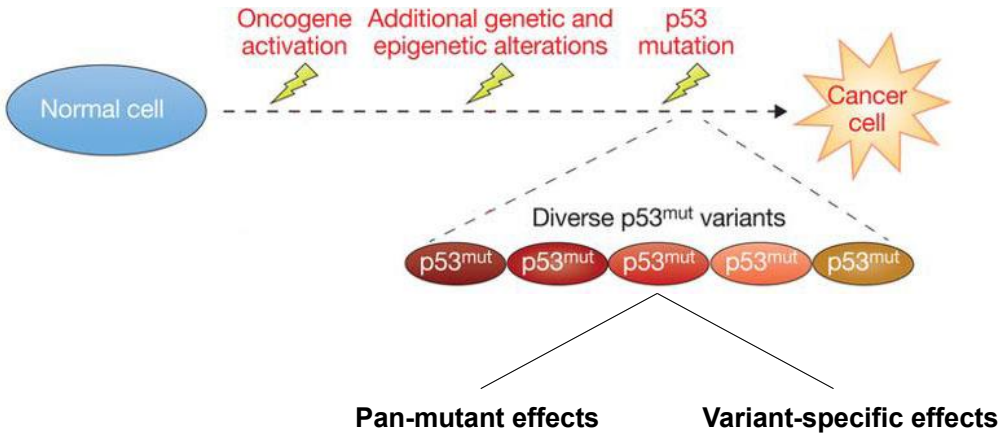

Figure 9. Mutant p53 gain-of-function effects. Different mutant p53 gain-of-function could have Pan-mutant effects, shared among all the mutants, or Variant-specific effects, for which every mutant has single specific targets (adapted from Oren and Kotler, 2016).

So the identification of common pan-mutant mechanisms of action, shared by most of cancer-associated p53 mutants, is very attractive, especially if those mechanisms can be targetable by specific drugs (Oren and Kotler, 2016; Girardini et al., 2011; Muller et al., 2011). This approace is considered more workable than targeting mutant p53, which lacks a well-defined common site for binding reactivating small molecules, and presents structural heterogeneities induced by specific mutations (Wiman, 2010).

Aim of the study

Improving response to platinum-based agents represents an unmet goal in EOC treatment. Few models of isogenic ovarian cancer platinum resistant cell lines exist. Therefore, we contributed to this issue selecting and characterizing three isogenic platinum resistant cell lines (MDAH-2774, TOV-112D and OVSAHO) to study and understand the molecular mechanisms at the basis of the onset of acquired resistance to platinum. This approach suggests new possible strategies to overcome resistance and represents a very relevant topic in ovarian cancer research. Moreover, the characterization of MDAH-2774 PT-res cells underlined the link between p53 mutational status and regulation of mitosis, suggesting their role in the acquisition of novel cellular phenotypes at the base of acquired resistance to platinum.

Results

3.1 Generation of cisplatin resistant cell lines

We have contributed to understand the mechanisms underlying acquired platinum resistance, through the selection of seven new models of platinum resistant isogenic EOC cell lines encompassing the principal EOC histotypes as defined by published results (Domcke et al., 2013; Beaufort et al., 2014; Dai et al., 2009; Sonego et al., 2017). In particular we selected: MDAH-2774 (hereafter referred as MDAH) and TOV-112D as models of high grade endometrioid cancer; OVSAHO and OVCAR-8 as models of high grade serous-carcinomas; SKOV-3 cell line is frequently cited as "serous", but it is better to report it as "adenocarcinoma cell line derived from the ascitic fluid"; TOV-21G and ES-2 as models of clear-cell ovarian carcinomas.

First, we treated cells with increasing concentrations of cisplatin (CDDP) for 72 hours and established the cisplatin concentration to obtain 50% of cell death (IC50) of the different cell lines. All these cell lines can be considered cisplatin sensitive with a platinum IC50 ranging from 3.6 to 9.1 μM (Figure 10).

cell line	IC50(μM)
TOV-112D	4.7 ± 1.0
MDAH	3.6 ± 1.1
OVSAHO	3.6 ± 0.9
OVCAR-8	9.1 ± 0.4
ES-2	4.3 ± 0.5
SKOV-3	5.1 ± 0.3
TOV-21G	5.9 ± 0.3

Figure 10. IC50 of parental EOC cells treated with cisplatin (CDDP). EOC cells were treated with increasing doses of CDDP for 72 hours to evaluate their cisplatin IC50. EOC cell lines can be considered cisplatin sensitive. Data are expressed as the mean (±SD) of percentage of viable cells respect to untreated cells (n=3 biological replicates each performed in triplicate).

Cisplatin resistant EOC cell lines were generated using the "pulse" method (Figure 11), that has been considered the most appropriate strategy to generate drug resistant ovarian cancer cells *in vitro*, since it is similar to that used in the clinic with pulse dosage according to plasma peak concentration in patients (Yan et al., 2007). However, using this approach we were not able to select SKOV-3, OVCAR-8 and ES-2 cell lines. Thus, we used another method, the low-dosage intermittent one, that we called "incremental" method, increasing

the dose every 5 treatments (Figure 11) (Yan et al., 2007). As shown in Figure 11, cells were plated at high confluence (step 1) and treated for 2 hours with a CDDP dose 10-fold higher than their calculated IC50 ("pulse method") (step 2) or for 48 hours with a low dose of CDDP ("incremental method"). After a recover period (step 3), "resistant" cells were subjected again to step 1-3 for additional 20 cycles (Figure 11). By performing this schedule of cisplatin treatments, we selected two different CDDP resistant populations (hereafter named PT-res) from each cell line.

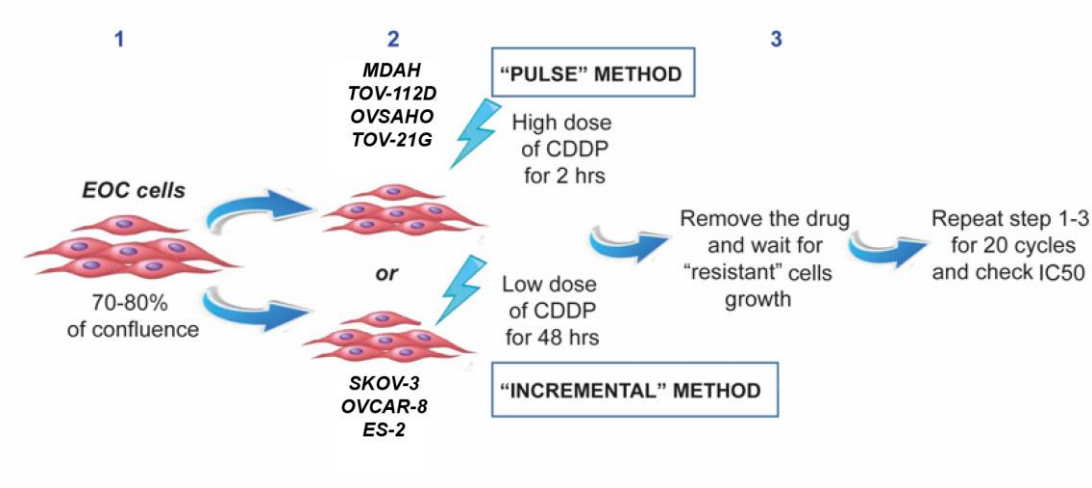

Figure 11. Generation of cisplatin resistant cell lines. Experimental design used to select cisplatin resistant (PT-res) cells. Cells were plated at high confluence (step 1) and treated for 2 hours with a cisplatin dose 10-fold higher than their calculated IC50 ("pulse method" or for 48 hours with a low dose of CDDP ("incremental method") (step 2). After a recover period (step 3), "survived" cells were subjected again to step 1-3 for additional 20 cycles, and then their cisplatin sensitivity tested again. Adapted from Sonego et al., 2017.

After 20 cycles of treatment, we tested again the CDDP sensitivity of the resulting cells. PT-res cells displayed a CDDP IC50 3- to 5-fold higher than parental cells (Figure 12). We experimentally verified that the resistant phenotype was stable and maintained independently from the presence of CDDP in the culture medium.

In this work is presented only the characterization of the first three cisplatin resistant cell lines generated: MDAH, TOV-112D and OVSAHO.

Even in this simplified model system, it was clear that CDDP resistance is a multifactorial phenotype associated with the development of numerous resistance mechanisms. It is well accepted that ovarian cancers, that become resistant to aggressive cisplatin-based

chemotherapy, are unlikely to respond to the other drugs commonly used in the therapy of EOC.

A

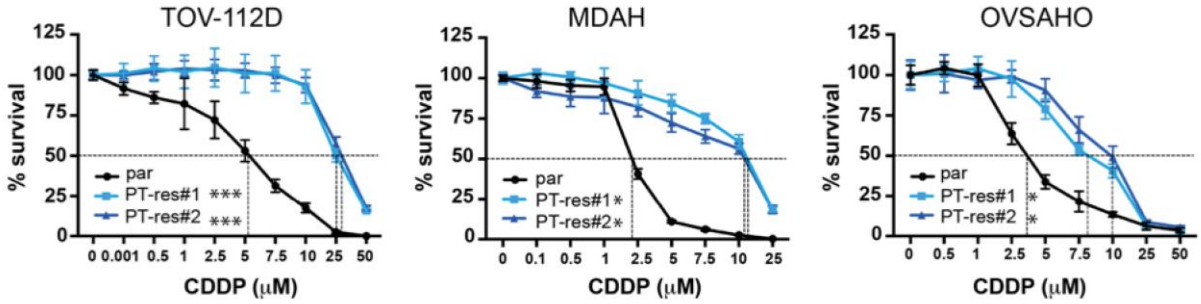

B

cell line	IC50(μM)
TOV-112D	4.7 ± 1.0
MDAH	3.6 ± 1.1
OVSAHO	3.6 ± 0.9
OVCAR-8	9.1 ± 0.4
ES-2	4.3 ± 0.5
SKOV-3	5.1 ± 0.3
TOV-21G	5.9 ± 0.3

Figure 12. Dose-response curves of parental and PT-res cells. (A) Cisplatin dose response curves of parental and PT-res cells. Results are expressed as percentage of viable cells respect to untreated cells. IC50 (half maximal inhibitory concentrations) are reported (n = 3 biological replicates each performed in triplicate). Statistical significance was determined by repeated-measures analysis of ANOVA test (*p < 0.05; **p < 0.01; ***p < 0.001; ns = not significant). Graphs of the first 3 cell lines used, taken as an example; (B) in the table all the cell lines. Adapted from Sonego et al., 2017.

For these reasons we tested if PT-res cells acquired cross-resistance to Taxol and Doxorubicin, two other chemotherapeutic drugs commonly used to treat EOC patients. MDAH and OVSAHO, but not TOV-112D, PT-res cells displayed an IC50 for Taxol of 2- to 5-fold higher than parental cells (Figure 13A). In the case of Doxorubicin, MDAH and TOV-112D, but not OVSAHO, PT-res cells were more resistant than parental cells (Figure 13B).

3.2 Cell cycle progression of cisplatin resistant cells

We next checked if this PT-resistant phenotype was linked to an altered cell cycle progression. We performed FACS analyses of DNA content under basal conditions and we observed that PT-res cells did not highlight any significant variation in cell cycle distribution compared to parental ones (Figure 14A). This result was confirmed by immunofluorescence analyses of phosphorylated Histone H3, a marker of mitotic cells,

showing no differences in the percentage of pH3 positive cells (mitotic index) of parental and PT-res cells (Figure 14B).

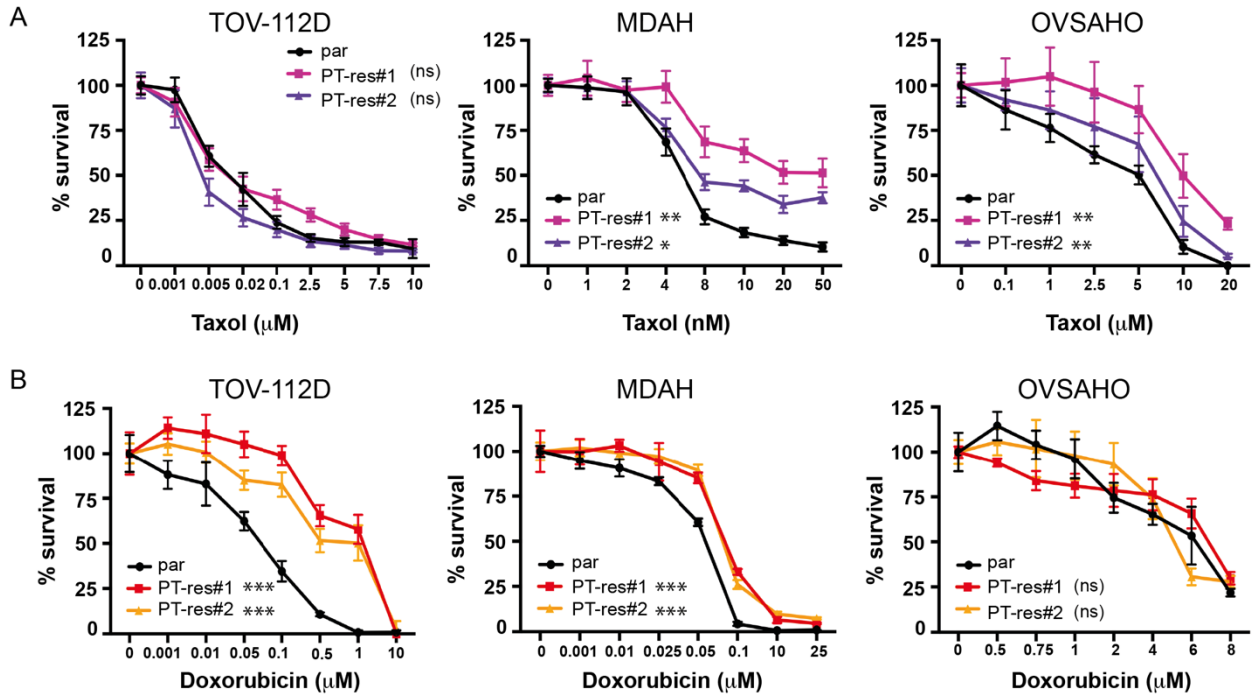

Figure 13. Dose-response curves of parental and PT-res cells. Taxol (A) and Doxorubicin (B) dose response curves of parental and PT-res cells. Results are expressed as percentage of viable cells respect to untreated cells. IC50 (half maximal inhibitory concentrations) are reported (n = 3 biological replicates each performed in triplicate). In the lower table, the IC50 calculated for each drug and cell line is shown. In figure the difference between parental cells and each PT-res pool is reported. Statistical significance was determined by repeated-measures analysis of ANOVA test (*p < 0.05; **p < 0.01; ***p < 0.001; ns = not significant). Adapted from Sonego et al., 2017.

3.3 Morphology and adhesion ability of cisplatin resistant cells

A key change associated with the cisplatin resistant phenotype was a clear alteration of PT-res cells morphology, respect to parental cells (Figure 15). Parental TOV-112D cells are small and comprise both rounded and spindled-shaped cells, while the correspondent PT-res cells were frankly polygonal. Conversely, MDAH cells are large epithelial-like cells and the correspondent resistant ones displayed a significantly tapered shape. Finally, OVSAHO parental cells are small round-shaped cells growing in small epithelial-like islets, while OVSAHO PT-res cells were larger and more elongated.

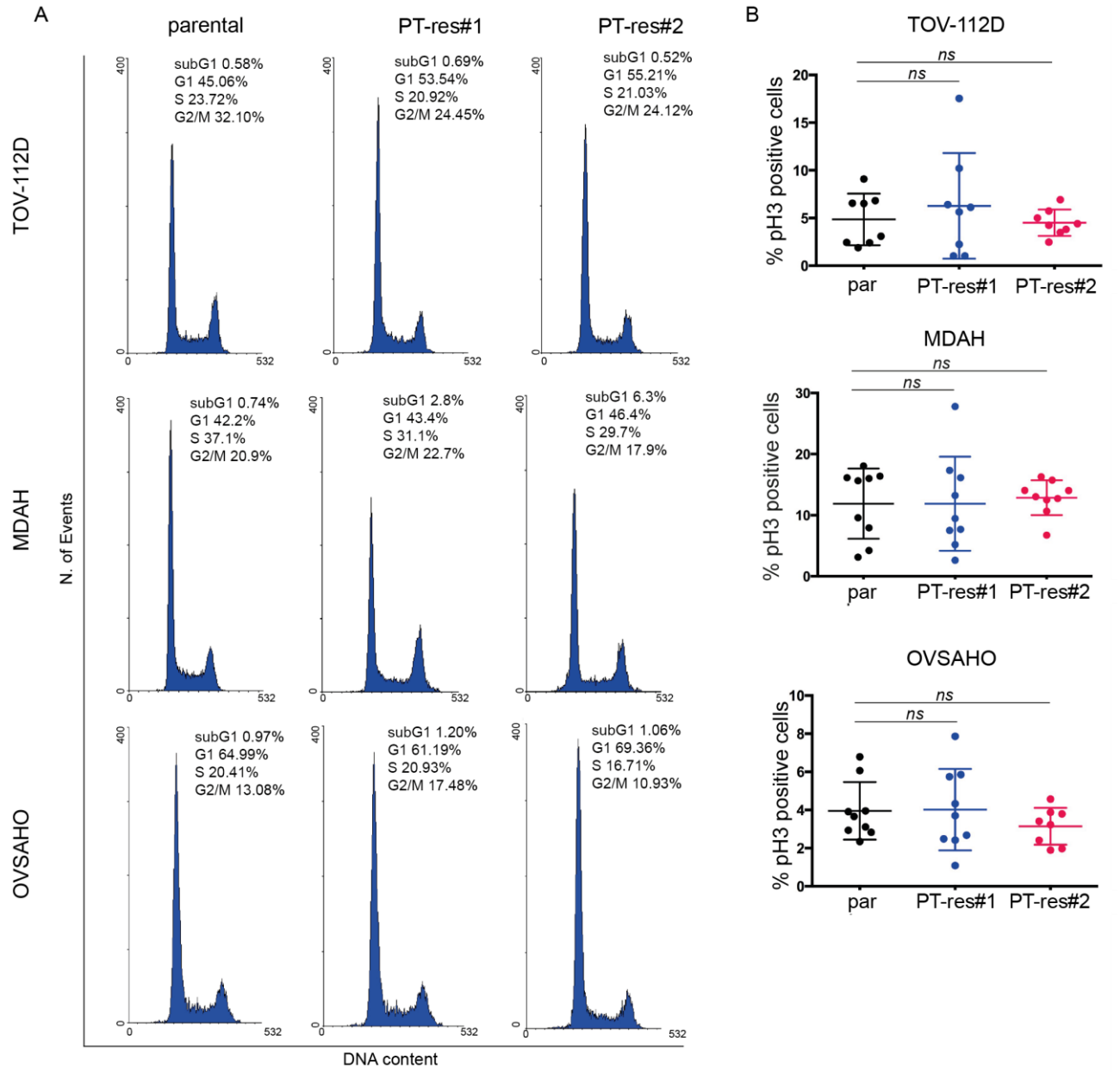

Figure 14. Cell cycle distribution of cisplatin resistant cells. (A) FACS analyses of DNA content of parental and PT-res cells in exponentially growing conditions. Parental and PT-res cells show a similar cell cycle progression. (B) Evaluation of mitotic index of parental and PT-res cells in exponentially growing conditions. Mitotic index was calculated by immunofluorescence analyses, using the expression of pS10-H3 as a marker of mitotic cells. Data are expressed as percentage of pH3-positive cells. Statistical significance was determined by a two-tailed, unpaired Student's t-test (ns = not significant). Adapted from Sonego et al., 2017.

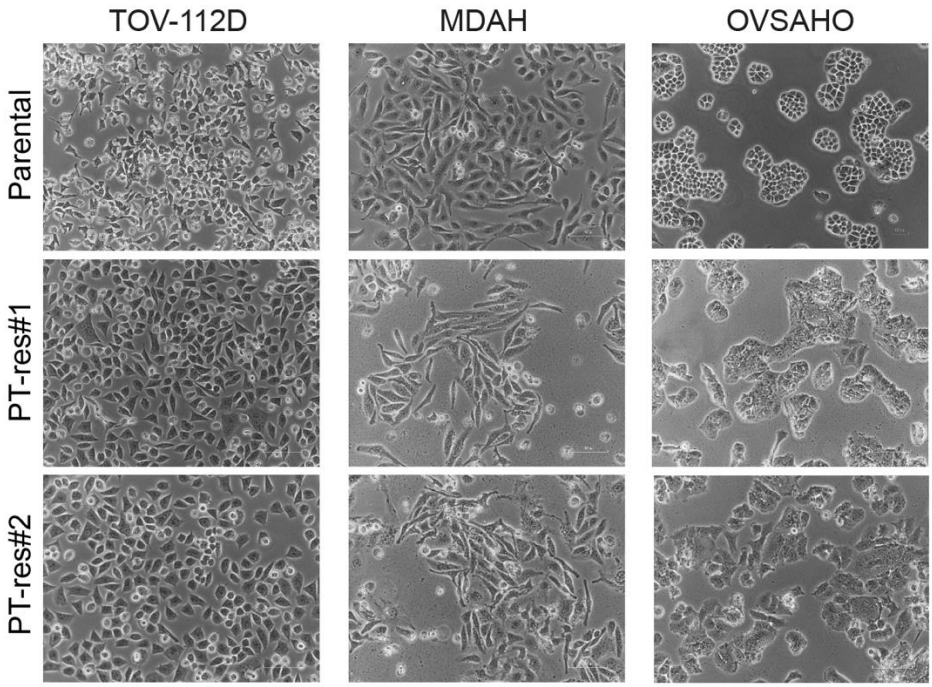

Figure 15. PT-res cells show an altered cell morphology. Representative phase-contrast photomicrographs of EOC parental (top) and PT-res (middle and bottom) cells in exponential phase (20X, original magnification). Adapted from Sonego et al., 2017.

We observed that all PT-res cells avoided the formation of an uniform monolayer, also when plated at high density (Figure 15). These morphological modifications suggested that the balance between epithelial and mesenchymal status could be altered in PT-res cells, possibly through alteration of the Epithelial-Mesenchymal Transition (EMT) and/or Mesenchymal-Epithelial Transition (MET) processes. It has been proposed in EOC that an EMT-like process, characterized by alternation of EMT and MET, could confer the ability to spread, attach and grow in the peritoneal lining and, eventually, favour the appearance of chemoresistant clones (Ahmed et al., 2010). To verify this hypothesis in our models, we tested the expression of known modulators of EMT and MET, like ZEB-1, SNAIL, SLUG and TWIST-1, by Western Blot analysis. The results of our analysis showed changes, that were essentially cell line specific, in the expression of the tested transcription factors in PT-res cells. Specifically, OVSAHO cells showed an increase of ZEB-1 protein while TOV-112D PT-res cells had increased levels of SNAIL and TWIST-1 compared to parental cells (Figure 16). Minor changes were observed in MDAH cells with only a slight increase in SNAIL expression in PT-res cells (Figure 16). These data suggest that an altered balance

between epithelial and mesenchymal status could be common among platinum resistant cells.

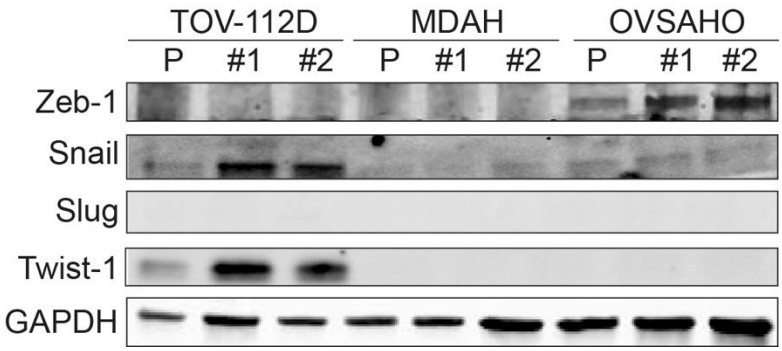

Figure 16. Western Blot analysis of EMT/MET markers expression in parental and PT-res cells. The expression levels of ZEB-1, Snail, Slug and Twist-1 in parental and PT-res cells. GAPDH was used as loading control. PT-res cells showed an altered expression of these EMT/MET markers respect to parental cells. P= parental cells; #1 and #2= the two PT-res populations. Adapted from Sonego et al., 2017.

Using immunofluorescence analyses we evaluated the expression and distribution of defined markers of cytoskeleton organization and cell-cell junctions, including F-actin, α-tubulin, ZO-1 (marker of tight junctions) and γ-catenin (marker of adherens junctions). The obtained result confirmed that PT-res cells displayed a different organization of actin and microtubular cytoskeleton, with respect to their parental counterparts, showing a more radial distribution that resulted in a more spreaded cells morphology (Figure 17).

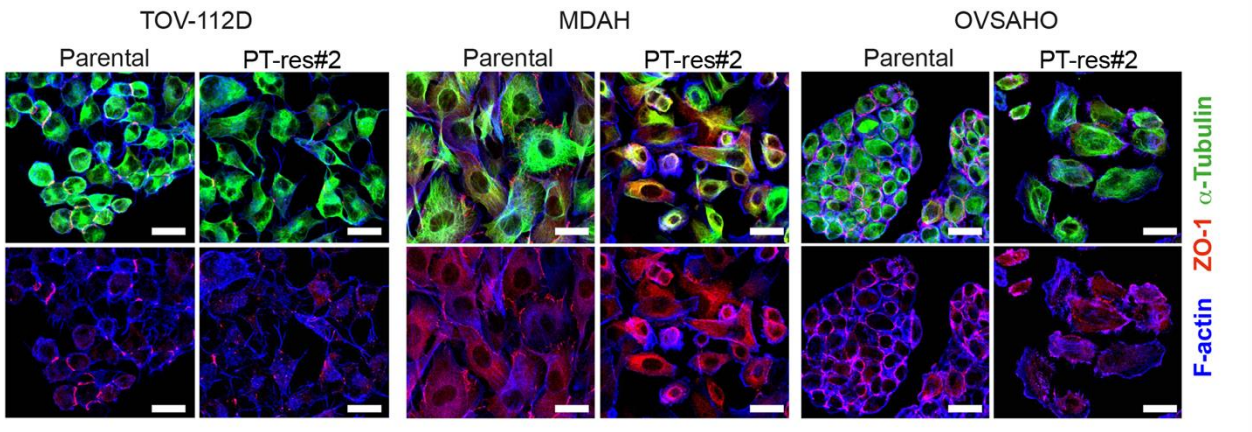

Figure 17. PT-res cells fail cytoskeleton organization. (**A**) Representative images of parental and PT-res cells, immunostained for the expression and localization of α-tubulin (green), ZO-1 (red) and F-Actin (blue), are reported. Scale bar = 25 μm. Adapted from Sonego et al., 2017.

Importantly, PT-res cells failed to form well-organized cell-cell junctions, as demonstrated by ZO-1 and γ-catenin redistribution in the cytosol rather than at the cell membrane, and by the fact that ZO-1 and γ-catenin failed to properly locate at the cell-cell contacts, as observed in parental cells (Figure 18).

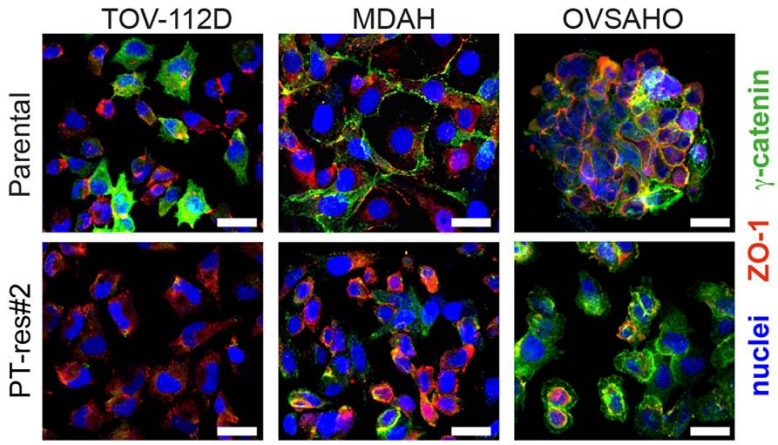

Figure 18. PT-res cells show non-organized cell-cell junctions. Representative images of γ-catenin (green) and ZO-1 (red) in parental and PT-res cells cultured in exponentially growing conditions. Nuclei are in blue. Scale bar = 25 μm. Adapted from Sonego et al., 2017.

Mesothelial cells represent the cellular component on which platinum resistant EOC cells attach and grow *in vivo*, when spreading from the primary lesions. Since PT-res cells seemed to display an altered balance between epithelial and mesenchymal status and a disorganization in the space-growth, we tested the growth of parental and PT-res cells on a mesothelial cell layer. To this aim, parental and PT-res EOC cells were labeled with the lipophilic green fluorescent dye, DiO, and then seeded on a mesothelial cell layer allowing to attach and grow for 24 hours. The DiO lipophilic tracer is in fact used in several biological assays to characterize the behaviour of a difend cell population including detection of cell-cell fusion and cell adhesion, tracing of migrating cells, labeling of lipoproteins, etc (Spötl et al., 1995; Bastiat et al., 2013; Huerta et al., 2006). Using this assay coupled with immunofluorescence and confocal microscopy we observed that all PT-res cells adhered and grew on the mesothelium at higher rate than the parental ones (Figure 19A). Three-dimensional reconstruction of the fields (Figure 19B) and representative XY planes of confocal images (Figure 19C) confirmed and reinforced the obtained result that is consistent with an increased ability to disseminate in the peritoneal cavity and to adhere at distant sites, proposed as key and common properties of platinum resistant cells.

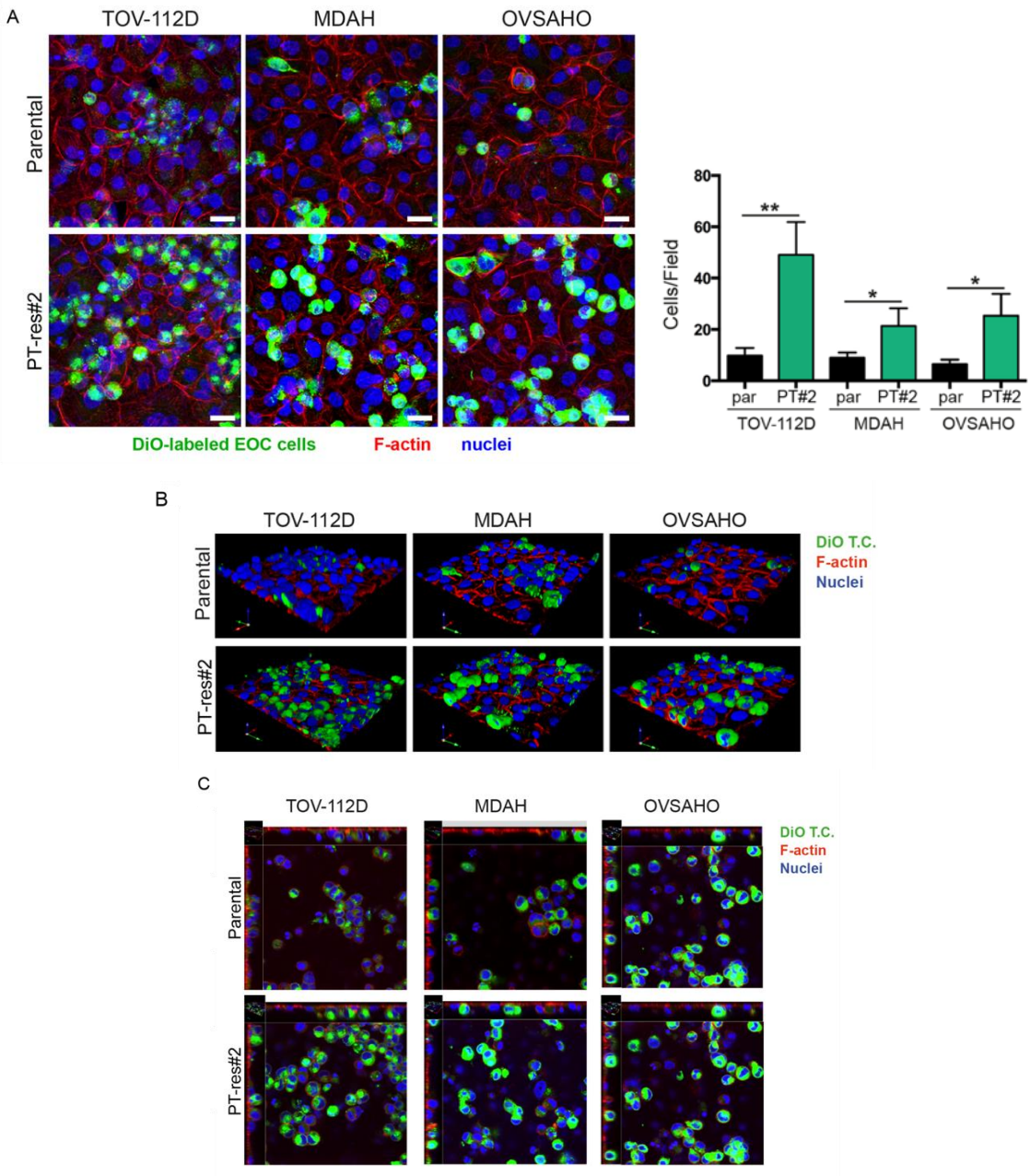

Figure 19. PT-res cells growth on a mesothelial cell layer. (A) Maximal projections of images of parental and PT-res cells labeled with the green fluorescent marker DiO (green) and cultured on a monolayer of mesothelial cells for 24 hours. Cells were then fixed and stained with Phalloidin (F-Actin, red) and TO-PRO-3 (nuclei, blue). In the right graph, the number (mean ± SD) of cancer cells/field is reported. Statistical significance was determined by a two-tailed, unpaired Student's t-test (*$p < 0.05$ and **$p < 0.01$) (PT#2 = PT-res#2). (B) 3D reconstruction of confocal stack images of DiO-labeled parental and PT-res cells (green) cultured on a monolayer of mesothelial cells for 24 hours in the absence of serum. Cells were then fixed and stained with Phalloidin (F-Actin, red) and TO-PRO-3 (nuclei, blue). (C) Representative XY planes of confocal images of parental and PT-res cells labeled as in B. YZ and XZ projections show the contacts between mesothelial (well flat and delineated by red F-actin) and EOC cells ("spheric" and green labeled). B and C are projections of the images reported in (A). Adapted from Sonego et al., 2017.

3.4 Response to cisplatin-induced damage of PT-res cells

We next investigated the response of parental and PT-res EOC cells to cisplatin treatment looking at the appearance of DNA damages and at the resolution of DNA platination. To this aim, cells were treated with cisplatin (50 μM) for 16 or 24 hours, the phosphorylation levels of Histone H2AX (Ser 139) (γH2AX), a well-known marker of damaged DNA, were evaluated by Western Blot analyses. In all tested models, PT-res cells showed a reduced expression of γH2AX indicating that they accumulated less DNA damage (Figure 20A). Accordingly, using a specific anti cisplatin-DNA adducts antibody in dot blot analyses, we observed a reduced DNA platination after CDDP exposure, more evident after 24 hours of treatment, followed by a faster removal of platinum from the DNA, already resolved after 24 hours of treatment release (Figure 20B).

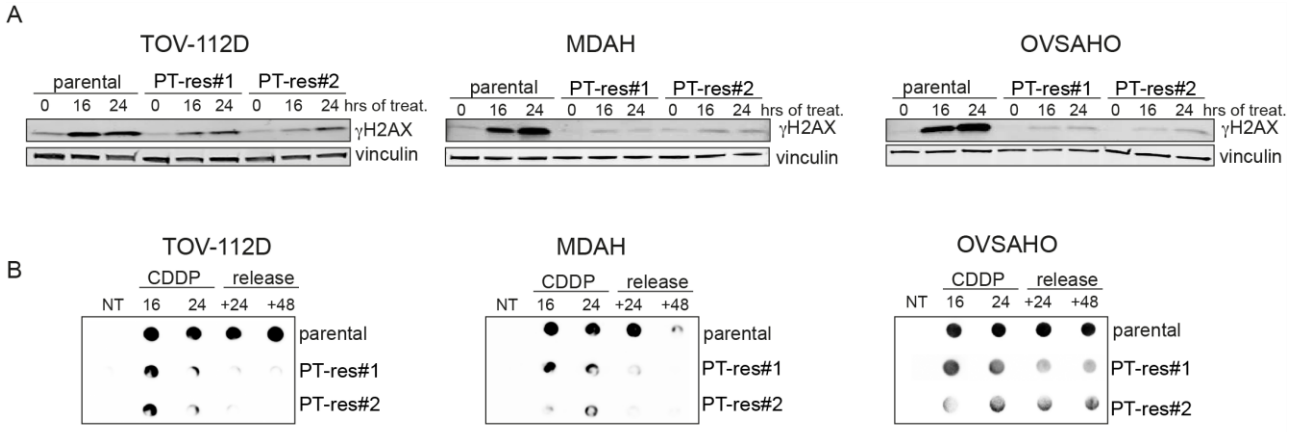

Figure 20. PT-res cells accumulate less DNA damage after cisplatin treatment. (A) Western blot analyses of Ser 139 phosphorylated Histone H2AX (γH2AX) expression, used as marker of DNA damage, in parental and PT-res cells untreated (0) or treated with cisplatin for 16 and 24 hours, as indicated. Vinculin was used as loading control. (B) Dot blot analyses evaluating the amount of platinated-DNA in parental and PT-res cells untreated (NT) or treated with cisplatin for 16 and 24 hours and then released in cisplatin-free medium for additional 24 (+24) or 48 (+48) hours to allow for DNA repair. Adapted from Sonego et al., 2017.

Based on these results, we next compared the cell cycle distribution of PT-res cells and parental ones under cisplatin treatment for 16 and 24 hours and after treatment removal for additional 24 hours. The data collected in the TOV-112D model, showed that parental cells exposed to cisplatin remained blocked in their cell cycle distribution and started undergo apoptosis (sub-G1 population) 24 hours after the somministration of treatment and failed to reenter the cell cycle up to 24 hours after the removal of the drug. Conversely, PT-res cells were resistant to platinum-induced apoptosis and were able to

resolve the cisplatin-induced cell cycle block, massively restarting to recycle within 8 hours from the drug release (Figure 21). Similar results were observed using both MDAH and OVSAHO models, overall suggesting that PT-res cells are more prone to bypass the cell cycle arrest induced by platinum treatment.

3.5 PT-res cells are characterized by cell-specific alterations of cisplatin transporters

The above results showing reduced DNA platination and DNA damage response and faster resolution of cisplatin-induced cell cycle block, suggested that PT-res cells could have acquired defects in the uptake and/or efflux of cisplatin into/from the cell. The cisplatin influx into cells is mainly regulated by the copper transporter CTR1, while the cisplatin efflux from the cells is mediated mainly by MDR1, ATP7A and ATP7B transporters. CTR2 is a copper uptake protein substantially homologous to CTR1, but it plays an opposite role in platinum drugs transport (Galluzzi et al., 2014; Blair et al., 2010).
Through qRT-PCR analyses we confirmed that all PT-res cells displayed a deregulation in the expression of the known cisplatin transporters CTR1, CTR2, MDR1, and/or ATP7A, although not in a common way. A significant decreased expression of CTR1 (Figure 22A), that could be responsible of a reduction in cisplatin influx, was observed in MDAH and TOV-112D PT-res respect to parental cells together with an upregulated expression of MDR1 gene (Figure 22B), that controls the efflux of cisplatin from the cell. On the contrary, these cells displayed a more or less downregulation of the efflux transporters ATP7A/B, and a non univocal variation in CTR2 (Figure 22B), suggesting that they more likely rely on the overexpression of MDR1 to excrete the drug. OVSAHO PT-res cells, instead, expressed similar amount of MDR1, but strongly increased the expression of ATP7A, ATP7B and CTR2 (Figure 22B) respect to parental cells. Unexpectedly, they showed an upregulated expression of the influx transporter CTR1. Taken together, these data suggest that all PT-res cell lines commonly displayed a deregulation in platinum transport that, however, could be due to different molecular alterations specific for each cell line.

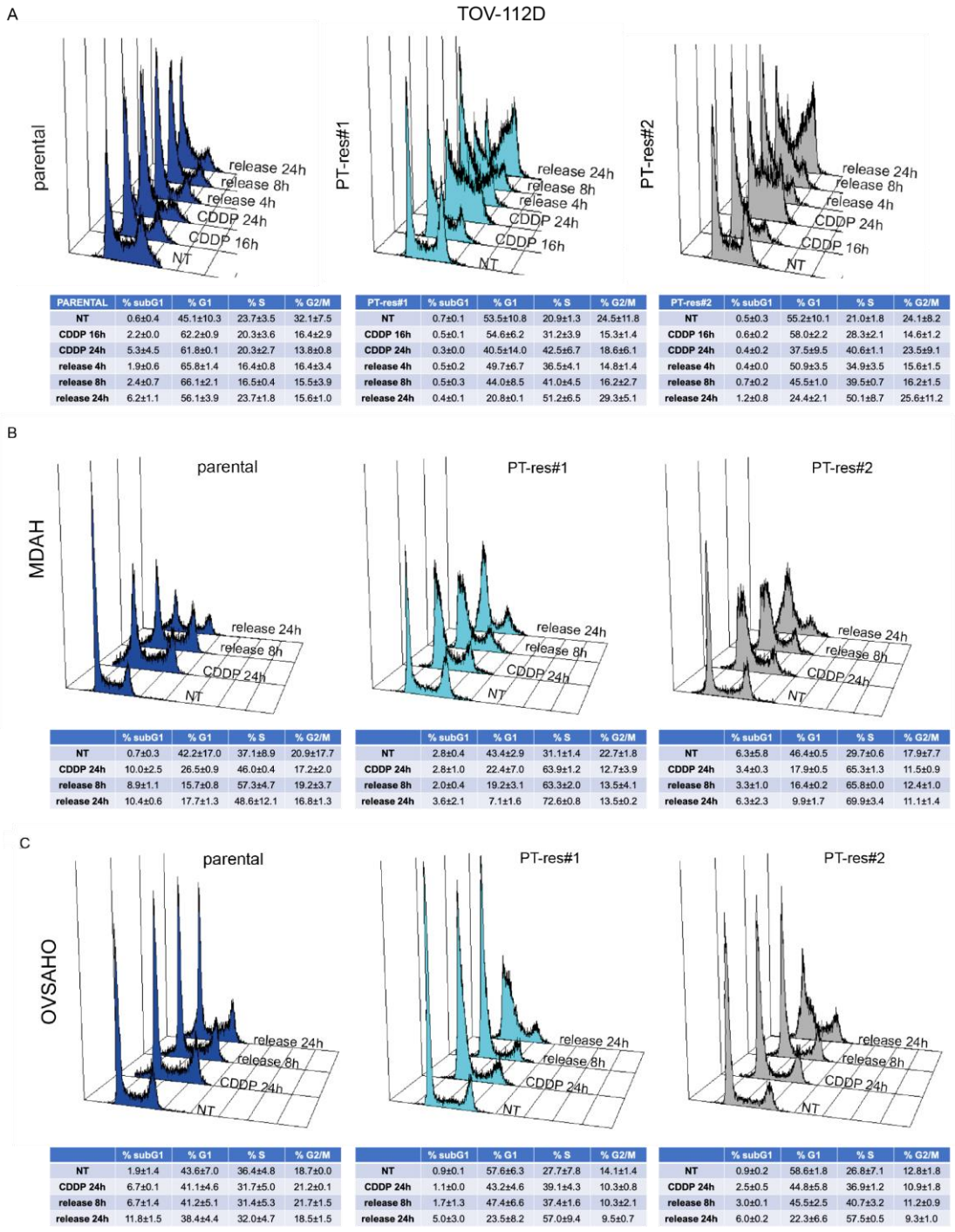

PARENTAL	% subG1	% G1	% S	% G2/M
NT	0.6±0.4	45.1±10.3	23.7±3.5	32.1±7.5
CDDP 16h	2.2±0.0	62.2±0.9	20.3±3.6	16.4±2.9
CDDP 24h	5.3±4.5	61.8±0.1	20.3±2.7	13.8±0.8
release 4h	1.9±0.6	65.8±1.4	16.4±0.8	16.4±3.4
release 8h	2.4±0.7	66.1±2.1	16.5±0.4	15.5±3.9
release 24h	6.2±1.1	56.1±3.9	23.7±1.8	15.6±1.0

PT-res#1	% subG1	% G1	% S	% G2/M
NT	0.7±0.1	53.5±10.8	20.9±1.3	24.5±11.8
CDDP 16h	0.5±0.1	54.6±6.2	31.2±3.9	15.3±1.4
CDDP 24h	0.3±0.0	40.5±14.0	42.5±6.7	18.6±6.1
release 4h	0.5±0.2	49.7±6.7	36.5±4.1	14.8±1.4
release 8h	0.5±0.3	44.0±8.5	41.0±4.5	16.2±2.7
release 24h	0.4±0.1	20.8±0.1	51.2±6.5	29.3±5.1

PT-res#2	% subG1	% G1	% S	% G2/M
NT	0.5±0.3	55.2±10.1	21.0±1.8	24.1±8.2
CDDP 16h	0.6±0.2	58.0±2.2	28.3±2.1	14.6±1.2
CDDP 24h	0.4±0.2	37.5±9.5	40.6±1.1	23.5±9.1
release 4h	0.4±0.0	50.9±3.5	34.9±3.5	15.6±1.5
release 8h	0.7±0.2	45.5±1.0	39.5±0.7	16.2±1.5
release 24h	1.2±0.8	24.4±2.1	50.1±8.7	25.6±11.2

	% subG1	% G1	% S	% G2/M
NT	0.7±0.3	42.2±17.0	37.1±8.9	20.9±17.7
CDDP 24h	10.0±2.5	26.5±0.9	46.0±0.4	17.2±2.0
release 8h	8.9±1.1	15.7±0.8	57.3±4.7	19.2±3.7
release 24h	10.4±0.6	17.7±1.3	48.6±12.1	16.8±1.3

	% subG1	% G1	% S	% G2/M
NT	2.8±0.4	43.4±2.9	31.1±1.4	22.7±1.8
CDDP 24h	2.8±1.0	22.4±7.0	63.9±1.2	12.7±3.9
release 8h	2.0±0.4	19.2±3.1	63.3±2.0	13.5±4.1
release 24h	3.6±2.1	7.1±1.6	72.6±0.8	13.5±0.2

	% subG1	% G1	% S	% G2/M
NT	6.3±5.8	46.4±0.5	29.7±0.6	17.9±7.7
CDDP 24h	3.4±0.3	17.9±0.5	65.3±1.3	11.5±0.9
release 8h	3.3±1.0	16.4±0.2	65.8±0.0	12.4±1.0
release 24h	6.3±2.3	9.9±1.7	69.9±3.4	11.1±1.4

	% subG1	% G1	% S	% G2/M
NT	1.9±1.4	43.6±7.0	36.4±4.8	18.7±0.0
CDDP 24h	6.7±0.1	41.1±4.6	31.7±5.0	21.2±0.1
release 8h	6.7±1.4	41.2±5.1	31.4±5.3	21.7±1.5
release 24h	11.8±1.5	38.4±4.4	32.0±4.7	18.5±1.5

	% subG1	% G1	% S	% G2/M
NT	0.9±0.1	57.6±6.3	27.7±7.8	14.1±1.4
CDDP 24h	1.1±0.0	43.2±4.6	39.1±4.3	10.3±0.8
release 8h	1.7±1.3	47.4±6.6	37.4±1.6	10.3±2.1
release 24h	5.0±3.0	23.5±8.2	57.0±9.4	9.5±0.7

	% subG1	% G1	% S	% G2/M
NT	0.9±0.2	58.6±1.8	26.8±7.1	12.8±1.8
CDDP 24h	2.5±0.5	44.8±5.8	36.9±1.2	10.9±1.8
release 8h	3.0±0.1	45.5±2.5	40.7±3.2	11.2±0.9
release 24h	6.0±0.2	22.3±6.6	57.5±0.5	9.3±1.0

Figure 21. Cell cycle distribution of PT-res cells under cisplatin treatment and during drug release. (A) FACS analyses of DNA content in TOV-112D parental and PT-res cells untreated (NT) or treated with cisplatin for 16 and 24 hours and then released in cisplatin-free medium for additional 4, 8 or 24 hours, as indicated. A typical histogram for each cell line is shown and the correspondent cell cycle distribution (mean ± SD n = 3 biological replicates) is reported in the right tables. (B-C) FACS analyses of DNA content in MDAH and OVSAHO parental and PT-res cells untreated (NT) or treated with cisplatin for 24 hours and then released in cisplatin-free medium for additional 8 or 24 hours, as indicated. A typical histogram for each cell line is shown and the correspondent cell cycle distribution (mean ± SD n = 3 biological replicates) is reported in the bottom tables. Adapted from Sonego et al., 2017.

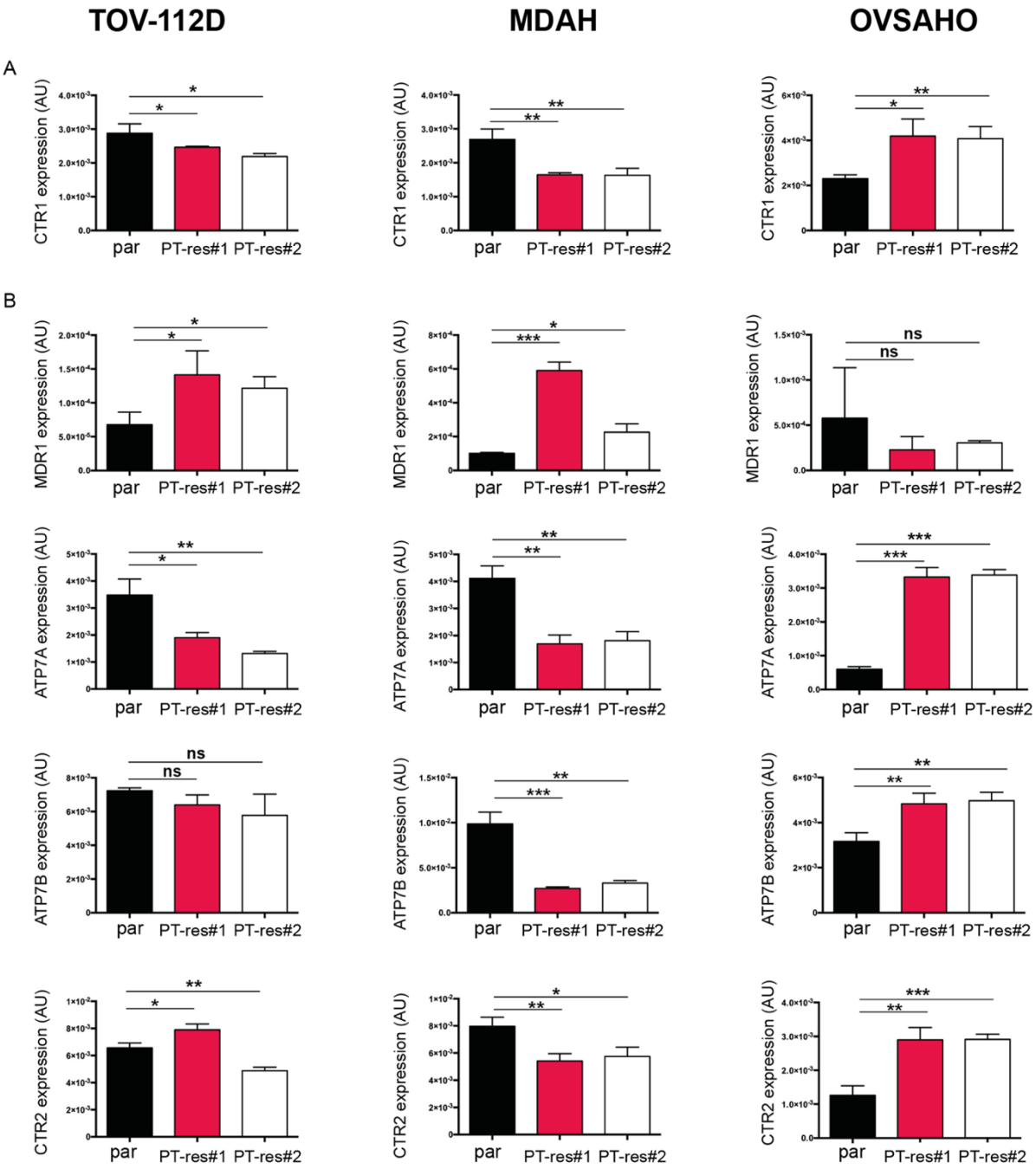

Figure 22. mRNA expression levels of cisplatin transporters in parental and PT-res cells. (A) Graphs showing the expression of CTR1 influx cisplatin-transporter in the indicated cell lines, evaluated by qRT-PCR analyses. mRNA levels was analyzed in triplicate and normalized using SDHA housekeeping gene. Data represent the mean ± SD of 3 biological replicates, performed in duplicate. Statistical significance was determined by a two-tailed, unpaired Student's t-test (ns = Not Significant, *p < 0.05, **p < 0.01, ***p < 0.001). (B) Graphs showing the expression of MDR1, ATP7A, ATP7B and CTR2 efflux cisplatin-transporters in the indicated cell lines, evaluated by qRT-PCR analyses. mRNA levels was analyzed in triplicate and normalized using SDHA housekeeping gene. Data represent the mean ± SD of 3 biological replicates, performed in duplicate. Statistical significance was determined by a two-tailed, unpaired Student's t-test (ns = Not Significant, *p < 0.05, **p < 0.01, ***p < 0.001). Adapted from Sonego et al., 2017.

3.6 MDAH PT-res cells grow slower than their parental counterpart, giving rise to large, multinucleated cells

When we analyzed the cell cycle progression pattern between parental and PT-res cells in exponentially growing conditions (DNA content in FACS analysis Figure 21), we did not observe alterations in cell cycle phases distribution, nevertheless MDAH PT-res cells presented an impaired growth rate (Figure 23). This phenotype was not observed in the two other isogenic cell lines (Figure 23).

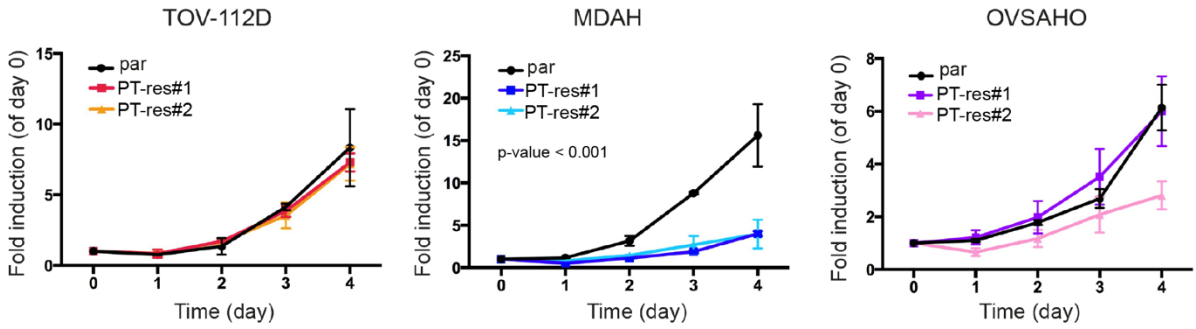

Figure 23. MDAH PT-res cells show an impaired growth rate. Growth curve analysis of parental and PT-res cells. Viable cells were counted daily in triplicate for 5 days, by trypan-blue dye exclusion method. Data are expressed as fold increase respect to day 0. Statistical significance was determined by two-way ANOVA test (*p < 0.05 and **p < 0.01 and ***p < 0.001).

We thus tested if the reduction in cell growth could be due to a different mechanism. Interestingly, a closer examination of MDAH cells by transmission microscopy (Figure 24A) and immunofluorescence analyses (Figure 24B) showed only in PT-res pools, but not in parental cells, the presence of large, frequently multinucleated cells that were often positive for the apoptotic marker cleaved caspase 3 (CC3).

3.7 Selection of MDAH PT-res single clones

To better characterize this phenotype, we performed a single cell cloning (Figure 25A) of PT-res cell pools. We isolated twenty-three PT-res single-cell clones from the two resistant PT-res pools (eleven from PT-res#1 and twelve from PT-res#2) and confirmed that all of them were platinum resistant. Among these, we randomly selected 4 PT-res clones for a more complete characterization. Kill-curve analyses performed treating parental e PT-res cells with increasing doses of CDDP for 72 hours, demonstrated that PT-res clones have a CDDP IC50 from 2.5 to 6.7 folds higher than the one of parental cells (Figure 25B), and

also higher than the IC50 observed for the PT-res pools #1 and #2 (i.e. 11 and 12 μM, respectively).

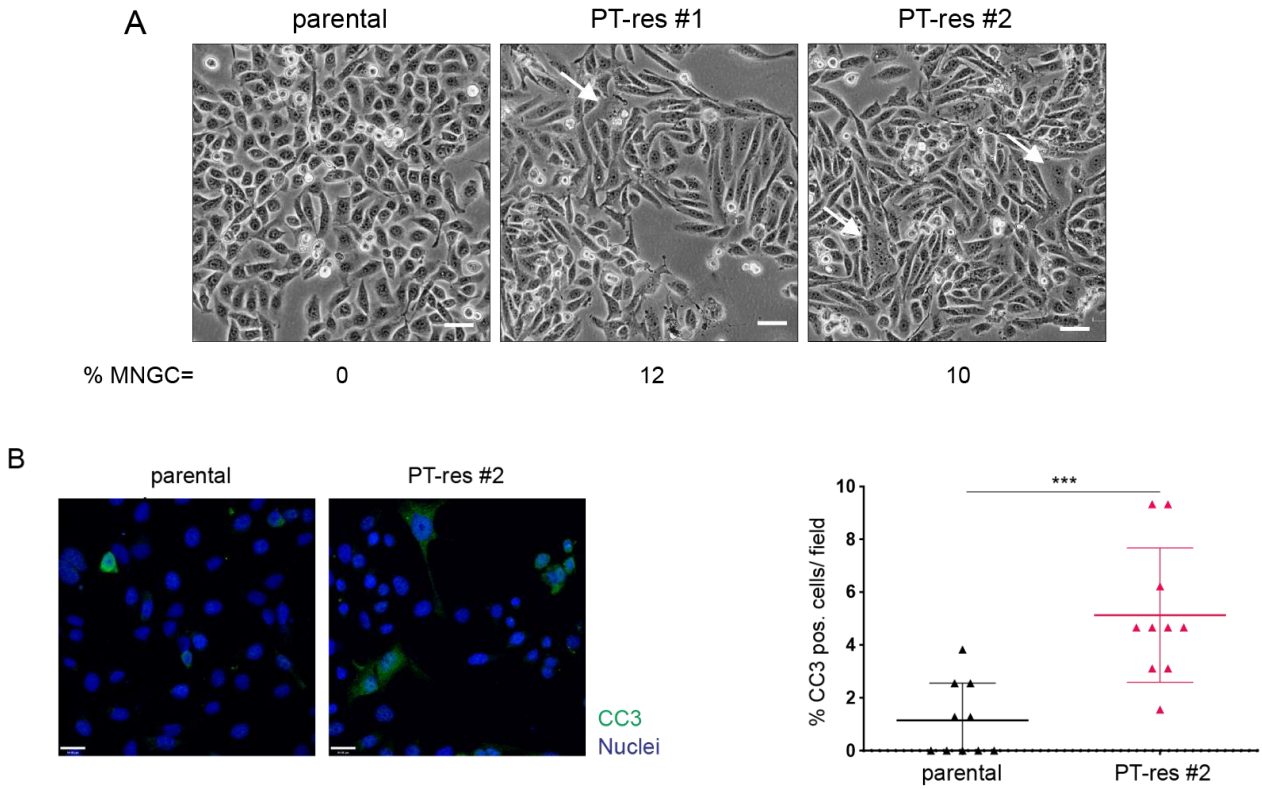

Figure 24. MDAH PT-res cells present a subpopulation of enlarged cells. (A) Representative phase-contrast photomicrographs of MDAH parental and PT-res pools in exponential growth phase (20X, original magnification). Scale bar = 25 μm. White arrows point to possible MultiNucleated Giant Cells (MNGC) here defined as cells with a cell area 1.5 fold bigger than the mean cell area of parental MDAH cells, as calculated using the ImageJ software. The percentage of MNGC in each cell line is reported under the respective images (at least 50 cells were analyzed for each cell line). (B) Representative images of Cleaved Caspase 3 (CC3) (green) in MDAH parental and PT-res cells cultured in exponentially growing conditions. Nuclei are in blue. Scale bar = 33 μm. On the right the graph reports the number (mean ± SD) of CC3 positive cells/field is reported. Statistical significance was determined by unpaired Student's t-test (*p < 0.05 and **p < 0.01 and ***p < 0.001). Adapted from Lorenzon et al., 2020.

A

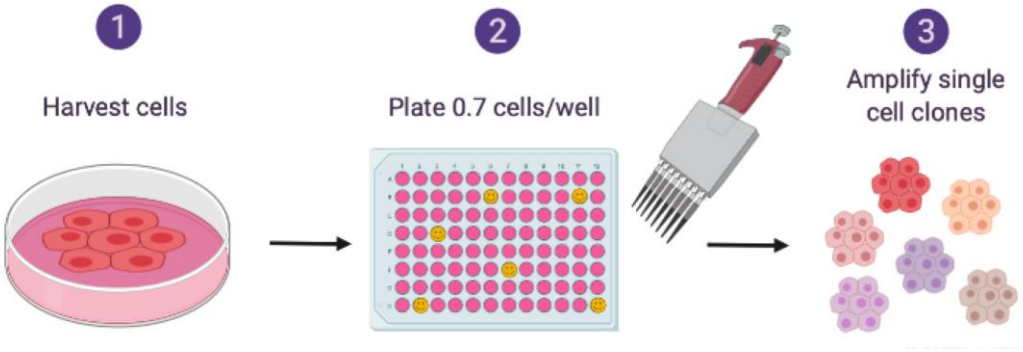

B

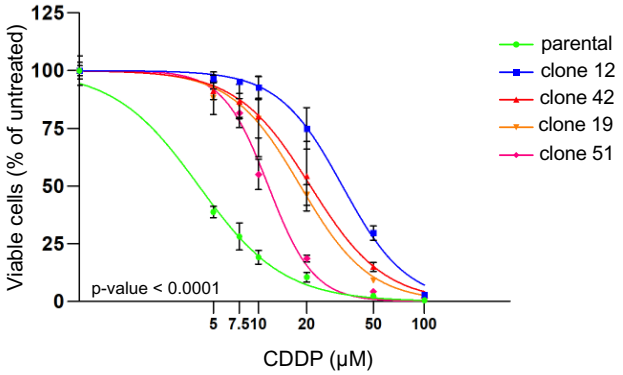

cell line	IC50(μM)	95% C.I. (μM)
parental	4.9	4.5 - 5.3
clone 12	33.8	31.7 - 36
clone 42	22	19.3 - 25.2
clone 19	19.3	18 - 20.7
clone 51	12.5	11.9 - 13.3

Figure 25. MDAH PT-res single cell cloning. (A) Experimental design used to select PT-res single clones. MDAH PT-res cells were harvested, counted (step 1) and plated 0.7 cells/well in 96wells plates (step 2). After a recover period, single cells started to grow and were amplified (step 3) to test cisplatin resistance. (B) Nonlinear regression analyses of cell viability assay of MDAH parental and PT-res single cell clones treated with increasing doses of CDDP for 72 hours. Data are expressed as percentage of viable cells respect to the untreated cells and represent the mean (±SD) of 3 biological replicates. The table on the right reports the IC50 and the confidence interval (C.I.) of each cell population. Fisher's exact test was used to calculate the global p-value reported in the graph. Adapted from Lorenzon et al., 2020.

We next evaluated their growth rate by growth curve analyses and we observed that, as PT-res pools #1 and #2, also the four PT-res clones tested had an impaired growth rate when compared to parental cells (Figure 26A). Intriguingly, MDAH PT-res cell clones also contained a subpopulation of larger multinucleated cells not present in parental cells, here defined as cells with a cell area 1.5 fold bigger than the mean cell area of parental cells (Figure 26B).

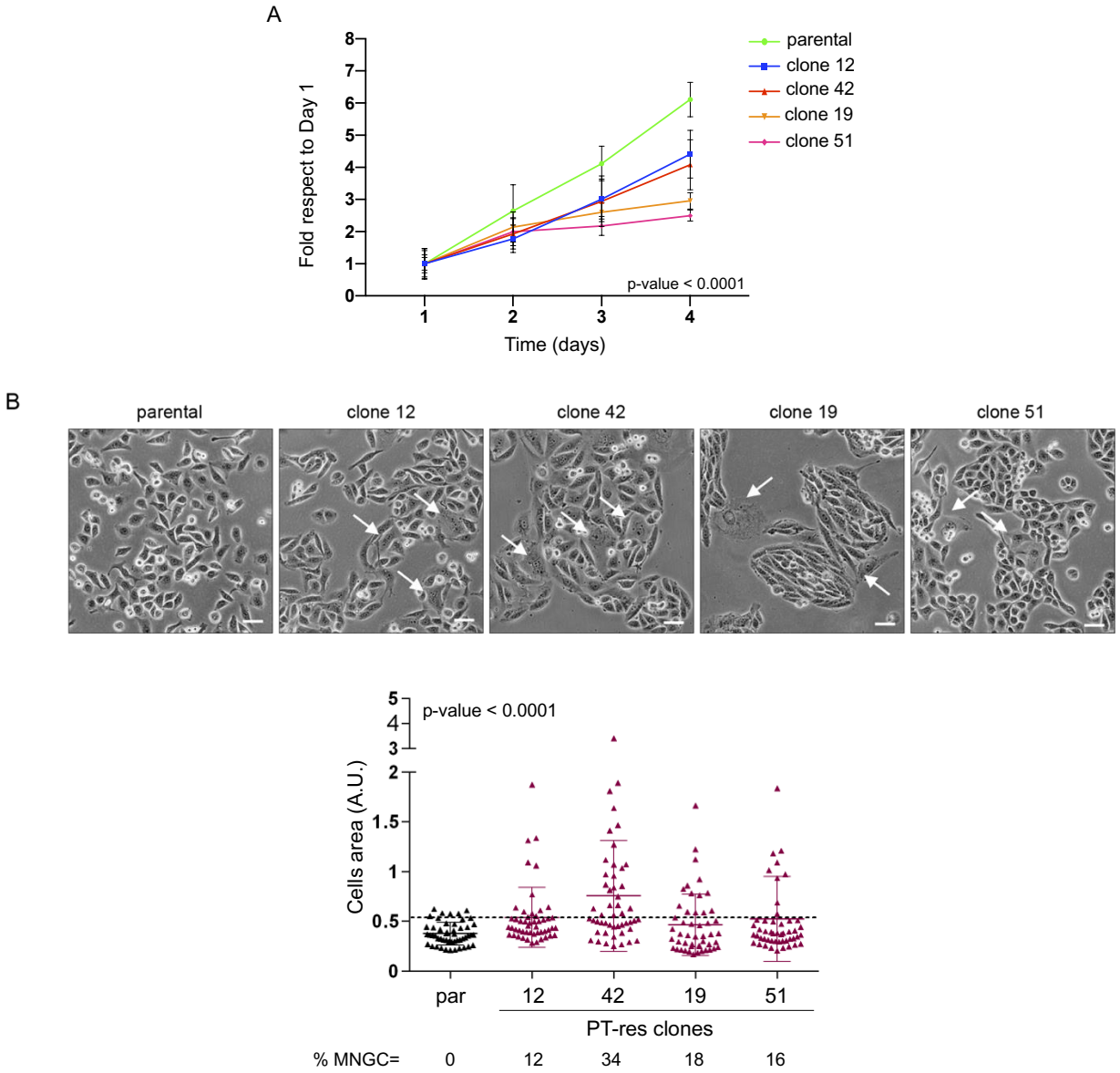

Figure 26. PT-res clones also show an impaired growth rate and the presence of enlarged cells. (A) Growth curve analysis of parental and PT-res clones. PT-res clones (#12, #19, #42 and #51) were seeded in sextuplicate in 96-well plates and cell proliferation was determined daily (for 5 days) by MTS assay using the CellTiter 96 AQueous cell proliferation assay kit (Promega). Statistical significance was determined by two-way ANOVA test, p-value reported in the graph (*p < 0.05 and **p < 0.01 and ***p < 0.001). (B) Representative phase-contrast photomicrographs of MDAH parental and PT-res clones in exponential growth phase (20X, original magnification). Scale bar = 25 μm. The graph reports the cell area (mean ± SD) expressed as arbitrary units (A.U.). A threshold has been established (dash line) to determine the percentage of MNGCs cells here defined as cells with a cell area 1.5 fold bigger than the mean cell area of parental MDAH cells. The quantification of MNGCs is reported under the graph as % of analyzed cells. Statistical significance was determined by one-way ANOVA test, global p-value < 0.0001; a multiple comparison analysis was done to determine significant differences among groups (*p < 0.05 and **p < 0.01 and ***p < 0.001 and ****p < 0.0001). Adapted from Lorenzon et al., 2020.

Since our previous results with MDAH PT-res pools demonstrated no differences in cell cycle distribution between parental and PT-res pools under exponentially growing conditions, we decided to investigate if an alteration in cell cycle progression could be highlighted in PT-res clones (Figure 27).

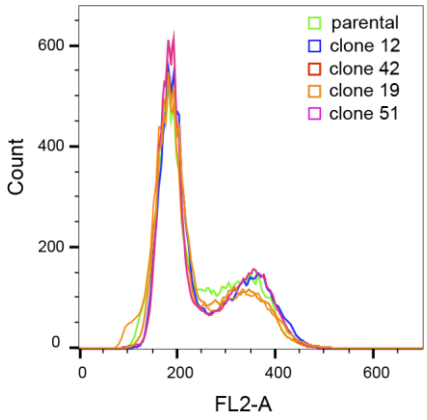

	% cells		
cell line	G1	S	G2/M
parental	42	43	15
clone 12	55	24	22
clone 42	59	23	18
clone 19	56	27	17
clone 51	54	24	22

Figure 27. PT-res clones shows a similar cell cycle progression pattern. FACS analyses of DNA content of MDAH parental and PT-res clones in exponentially growing conditions. The plots overlapping show the cell cycle distribution of each cell line. The propidium iodide (PI) stained cells were recorded by BD FACScan™ or BD FACSCalibur™ flow cytometer. The right table reports the cells percentage in G1, S or G2/M phases. Adapted from Lorenzon et al., 2020.

Cell cycle progression in exponentially growing cells showed small differences between parental and PT-res clones that displayed a slight increase in G2/M population and a low decrease in S phase cells, once compared to parental ones (Figure 27). To better study cell cycle progression and trying to force the system allowing cells to complete one mitotic division, we decided to use cell synchronization. To this aim parental and PT-res clones #12 and #42 were synchronized at the G1/S phase boundry by double thymidine block. After release into normal medium, cells were collected at different time points (i.e. 12, 16 and 24 hours), lysated and evaluated by Western Blot analyses for the expression of defined and accepted molecular makers of the different phases of the cell cycle. The results of this analysis were quite striking and informative showing that, while the phosphorylation of pRB (Ser780) (G1/S phase marker) and the expression of Cyclin A (S phase marker) and Cyclin B1 (G2/M marker) were equally regulated in parental and PT-res clones (Figure 28A, first, second and third blot lanes), PT-res cell clones displayed an earlier and prolonged phosphorylation of Histone H3 (pH3 Ser10), a recognized marker of M phase, accompanied by a higher expression of the inhibitory phosphorylation of CDK1

(Tyr15) a serine/threonine kinase that is a key player in M phase entry and progression (Figure 28A, forth and sixth blot lanes). These data suggested that MDAH PT-res cells likely had an alteration in M phase progression that indeed could explain the higher number of multinucleated cells. Based on these results, we next quantified the number of pH3 Ser10 positive cells by immunofluorescence analyses (Figure 28B), in cell synchronized by serum starvation for 72 hours and then released in complete medium for additional 24 hours. This approach allowed to exclude that differences observed in Western Blot analyses were due or enhanced by the use of the double thymidine block. Results showed that all four PT-res clones had a significanlty increased number of pH3 Ser10 positive mitotic cells/field (Figure 28C).

FACS analyses of DNA content of synchronized cells (Figure 29A) confirmed, in the PT-res clones, the persistence of an increased G2/M population 24h after release from double thymidine block, compatible with the observed increased expression of mitotic markers (Figure 28A). This analysis combined with an immunofluorescence one also revealed and confirmed that PT-res clones had an increased number of multinucleated cells with high DNA content (Figure 29B and 30). The quantification of multinucleated cells/field evidenced significant differences for all clones respect to parental cells and no significant differences among the different PT-res clones.

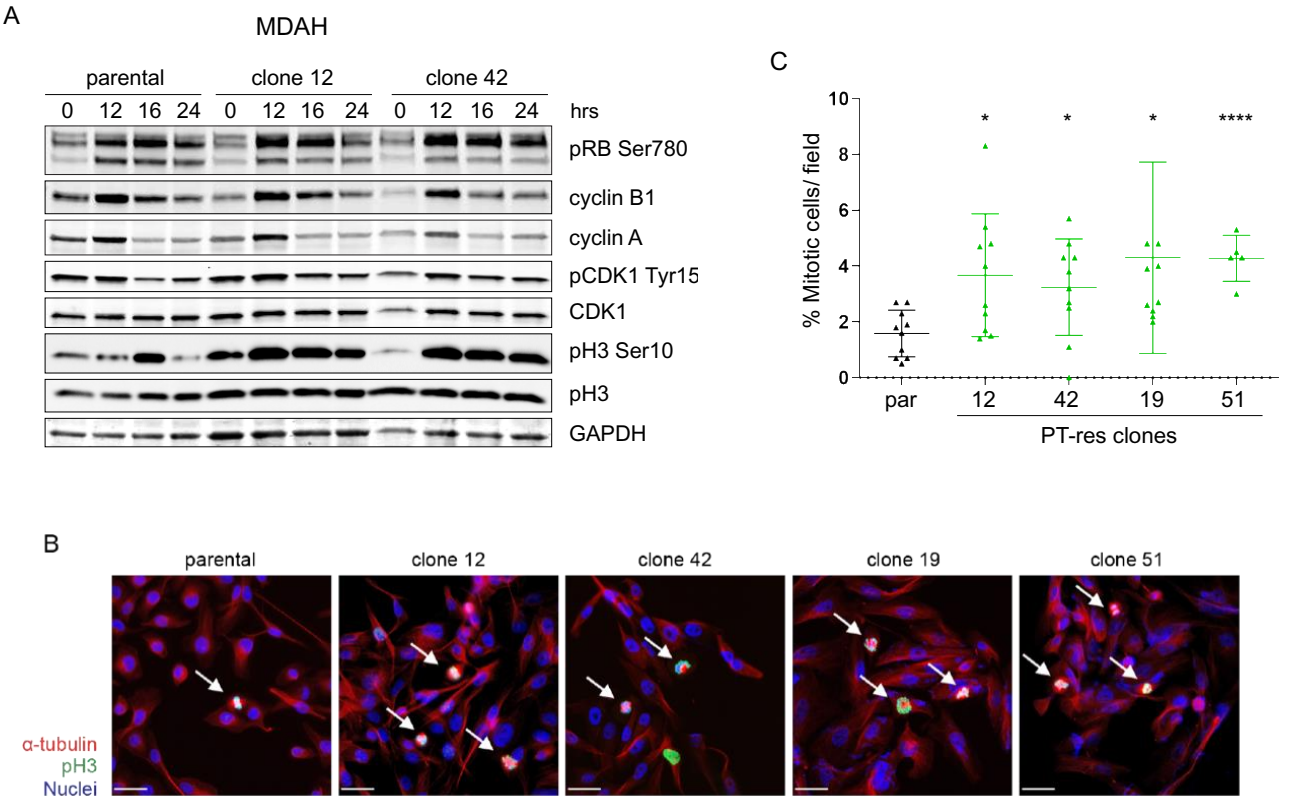

Figure 28. MDAH PT-res clones display a mitotic defect that could explain the presence of the enlarged subpopulation. (A) Western Blot analysis of MDAH parental and PT-res clones (#12 and #42) synchronized by double thymidine block and released for the indicated hours (hrs). The indicated cell cycle markers were analyzed. GAPDH was used as loading control. (B) Representative images of parental and PT-res single clones, immunostained for pH3 (green), α-tubulin (red) and TO-PRO-3 (nuclei, blue) are reported. White arrows indicate pH3-positive mitotic cells. Scale bar = 44 μm. (C) The graph reported the number (mean ± SD) of mitotic cells/field. Each dot corresponds to one field, at least 10 fields were scored for each cell line. Statistical significance was determined by a two-tailed unpaired Student's t-test (*p < 0.05 and **p < 0.01 and ***p < 0.001). Adapted from Lorenzon et al., 2020.

Based on the notion that multinucleated cells could derived from an altered mitotic division, we studied more in detail the morphology of mitotic cells in parental and PT-res clones using immunofluorescence analyses coupled with confocal analyses, and staining cells for γ-tubulin, an accepted centrosome marker, α-tubulin to evidence the mitotic spindle, and TO-PRO-3 for DNA staining (Figure 31A). These analyses demonstrated that PT-res clones, when compared to parental cells, presented an increased number of aberrant mitotic cells (Figure 31B), that represent more than 50% of all scored mitosis (Figure 31C). The most frequently observed anormality was the presence of multi-centrosome.

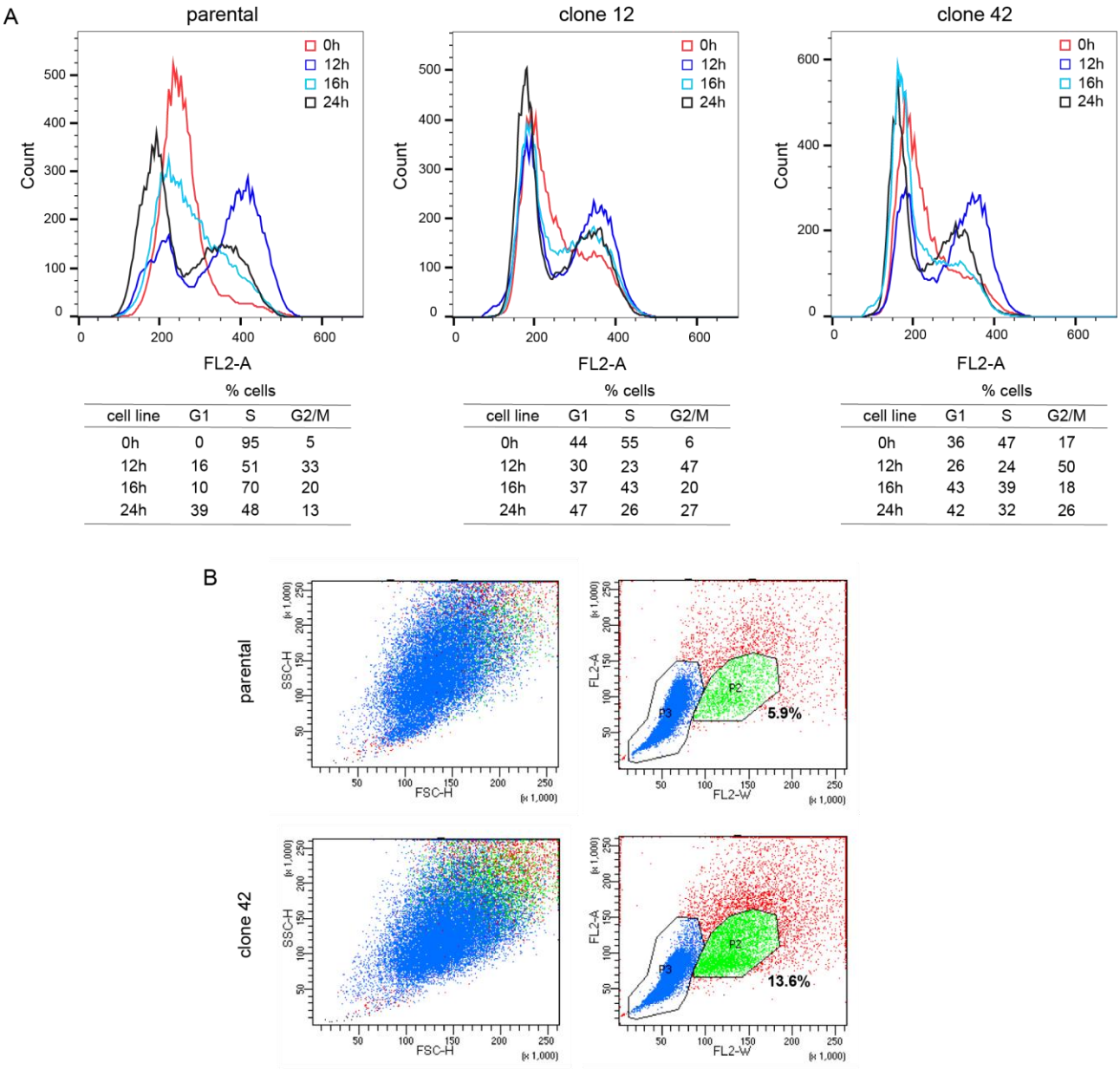

% cells

cell line	G1	S	G2/M
0h	0	95	5
12h	16	51	33
16h	10	70	20
24h	39	48	13

% cells

cell line	G1	S	G2/M
0h	44	55	6
12h	30	23	47
16h	37	43	20
24h	47	26	27

% cells

cell line	G1	S	G2/M
0h	36	47	17
12h	26	24	50
16h	43	39	18
24h	42	32	26

Figure 29. (A) FACS analyses of DNA content of MDAH parental and PT-res clones (#12 and #42) synchronized by double thymidine block and then released in thymidine free medium for the indicated hours. The histogram overlay shows the cell cycle distribution of each cell line at the different time points, as indicated by the color code. The bottom tables report the cells percentage in G1, S or G2/M phases. (B) FACS analyses of MDAH parental and PT-res clone 42 cells evaluating the size and the cell cycle distribution of analyzed living cells. The left panels show cell size as determined by forward and side scatter fluorescence. The right panels show the DNA content distribution evaluated by the analyses of PI fluorescence read as FL2-Width and FL2-Area. In blue (P3) is highlighted the cycling population analyzed in the histograms reported in (A). In green (P2) is highlighted the giant cells population which also shows a DNA content >2n. The percentage of P2 cells is reported in plots. In red are marked dead cells or cells that cannot be properly classified. Adapted from Lorenzon et al., 2020.

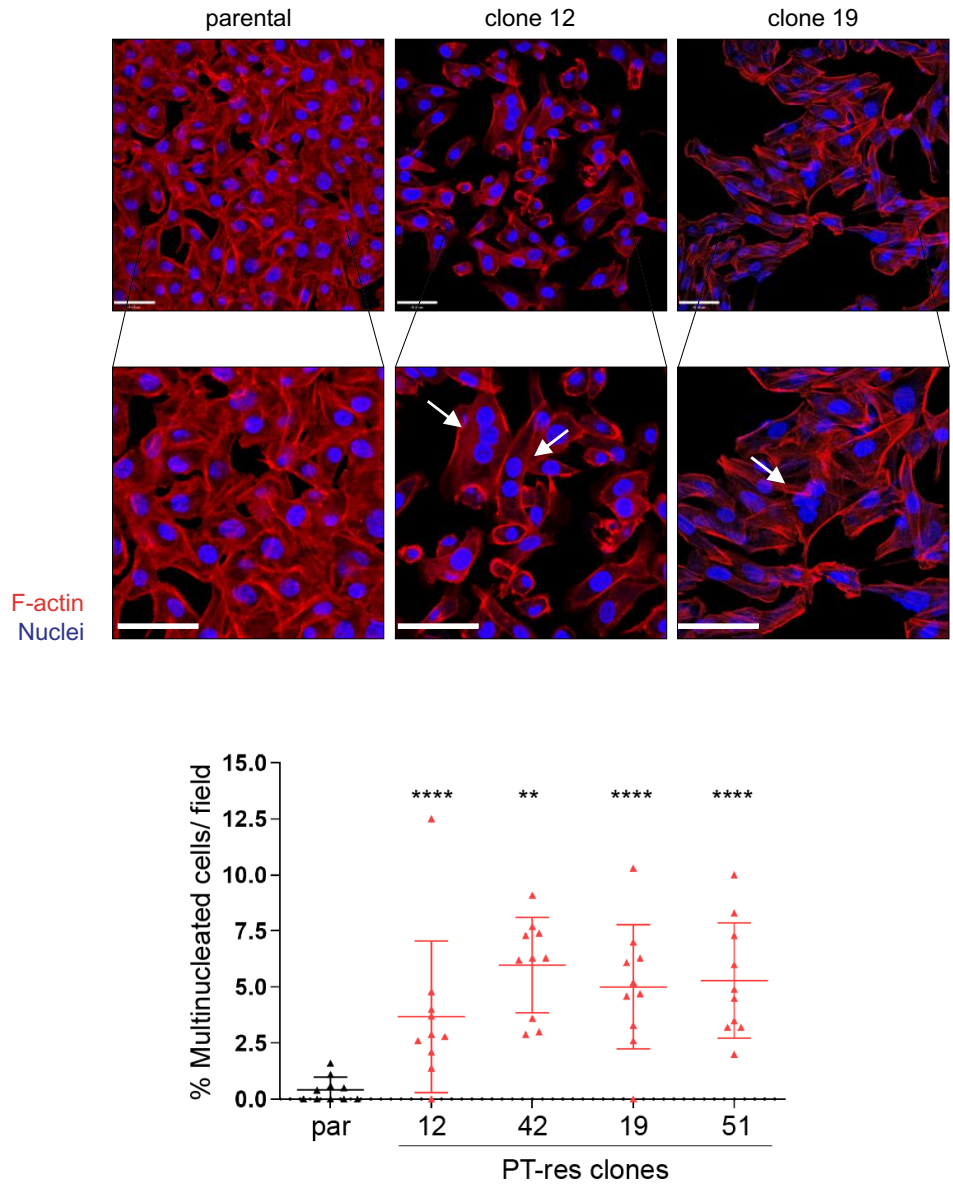

Figure 30. PT-res clones are characterized by a high number of multinucleated cells. Representative images of MDAH parental and PT-res clones stained for F-actin with Phalloidin (F-actin, red). Nuclei are pseudo colored in blue (TO-PRO-3). In the lower magnifications white arrows indicate multinucleated cells. Scale bar = 44 μm. On the bottom, the number of multinucleated cells/field is reported (mean ± SD). Statistical significance was determined by a two-tailed unpaired Student's t-test (*p < 0.05 and **p < 0.01 and ***p < 0.001). Adapted from Lorenzon et al., 2020.

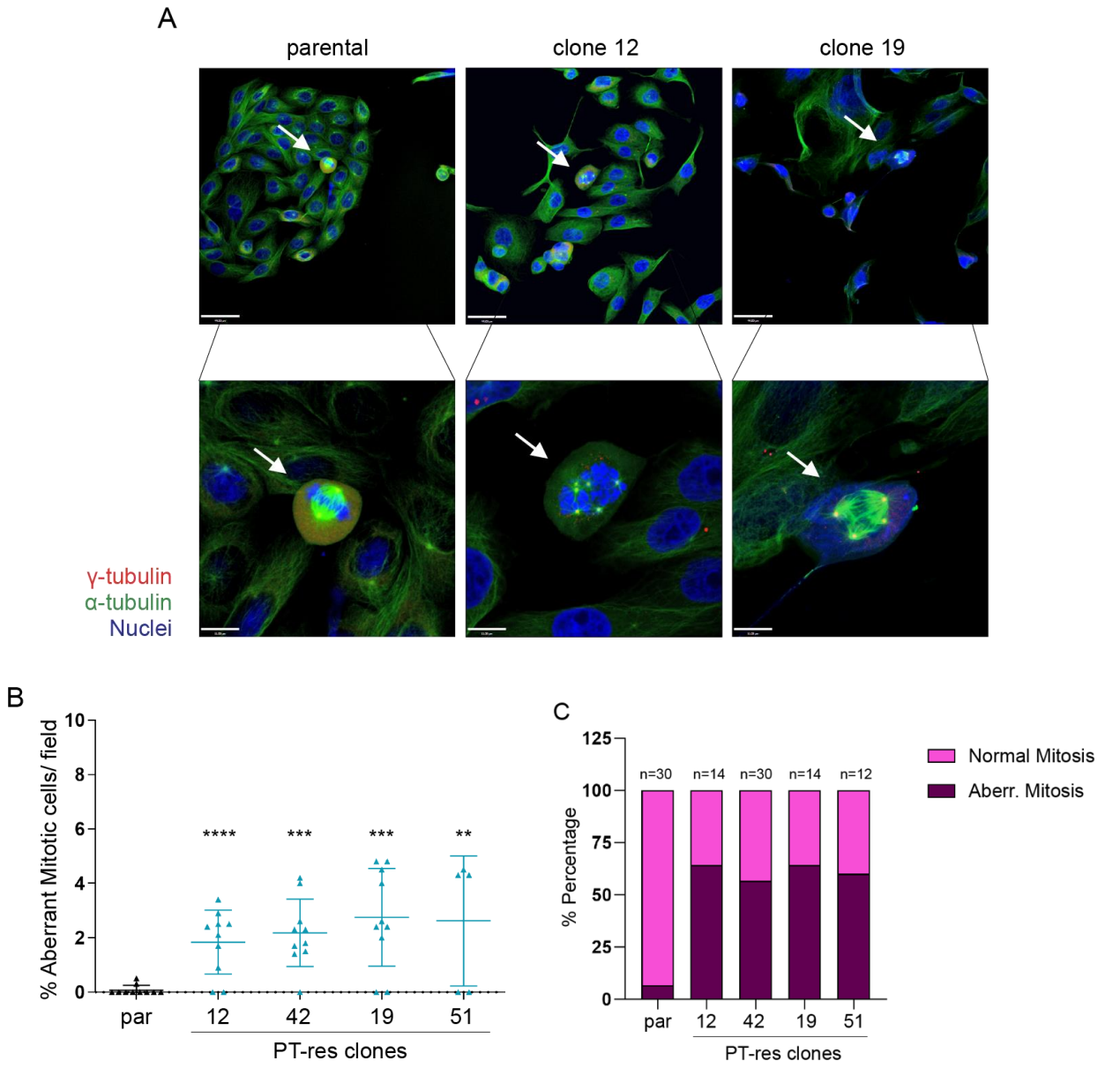

Figure 31. PT-res clones presented an increased number of aberrant mitotic cells. (A) Representative images of MDAH parental and PT-res clones, stained for α-tubulin (green), γ-tubulin (red) and TO-PRO-3 (nuclei, blue). Scale bar = 44 μm. In the lower magnifications white arrows indicate mitotic cells. Scale bar = 11 μm. (B) On the bottom-left, the graph reports the number of aberrant mitosis/field (mean ± SD). Statistical significance was determined by a two-tailed unpaired Student's t-test (*$p < 0.05$ and **$p < 0.01$ and ***$p < 0.001$). (C) The lower graph (right) reports the fraction of aberrant and normal mitosis expressed as percentage of total mitosis. Numbers above each column indicate the total number of mitosis analyzed for each cell type. Adapted from Lorenzon et al., 2020.

Interestingly, as observed in PT-res pools, PT-res clones were more positive than parental cells for the expression of cleaved caspase 3 (Figure 32), and the increase in cleaved caspase 3 positive cells paralleled the increase in the percentage of aberrant mitosis.

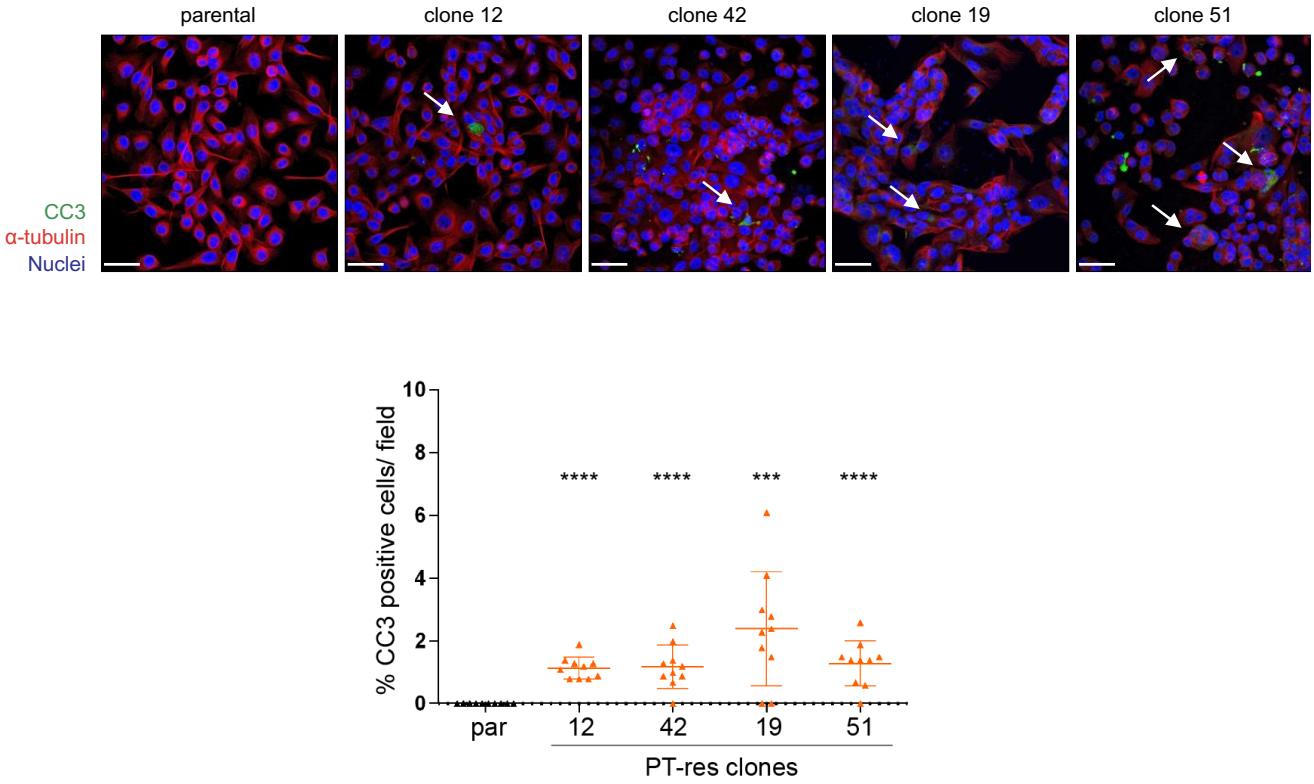

Figure 32. MDAH PT-res clones present an increased number of CC3 positive cells. Representative images of Cleaved Caspase 3 (CC3) (green) and α-tubulin (red) immunofluorescence staining in MDAH parental and PT-res clones in exponentially growing conditions. Nuclei are pseudo colored in blue (TO-PRO-3). White arrows indicate CC3 positive cells. Scale bar = 44 μm. The bottom graph reports the number (mean ± SD) of CC3 positive cells/field. Statistical significance was determined by a two-tailed unpaired Student's t-test (*p < 0.05 and **p < 0.01 and ***p < 0.001). Adapted from Lorenzon et al., 2020.

Overall the data collected so far suggested that defects in M phase progression accompanied the acquisition of the platinum resistant phenotype of MDAH cells, and likely resulted in an increased number of multinucleated giant cells (MNGCs) and an increase in cleaved caspase 3 positive cells. Both these phenotypes in turn could explain the lower growth rate of PT-res MDAH clones respect to the parental counterpart, without a clear evidence of cell distribution in the different phases of the cell cycle in FACS analyses, as reported previously (Figure 21).

3.8 $p53^{MUT}$ downstream targets are differently modulated in PT-res clones

A very recent report suggests that MNGCs could contribute to the chemoresistant phenotype of MDA-MB231 breast cancer cells, by increasing the production of Reactive Species of Oxygen (ROS) (Parekh et al., 2018). Accordingly, we showed that MDAH PT-

res clones presented a higher production of ROS than parental cells, both under basal conditions and after 24 hours of CDDP treatment (Figure 33), supporting the possibility that in MDAH cells MNGCs contribute to the onset of PT-resistance.

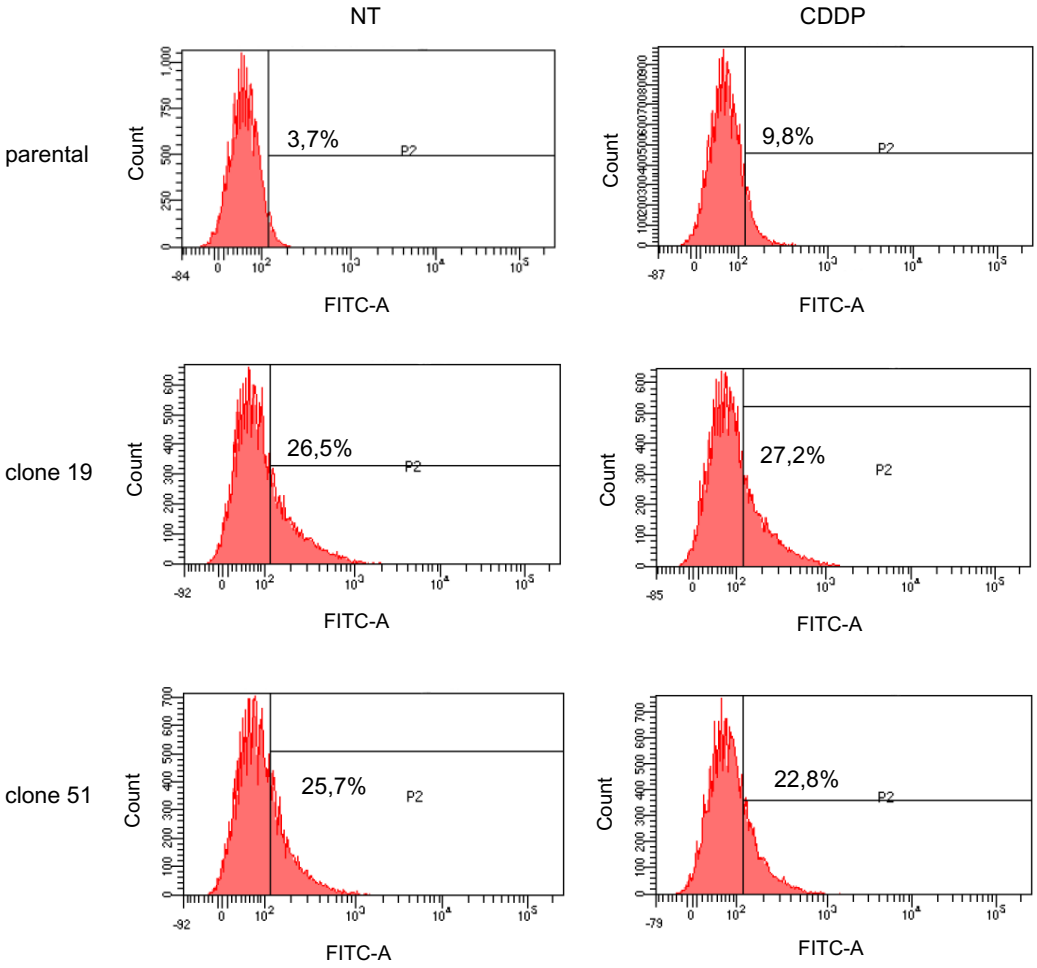

Figure 33. ROS production in MDAH PT-res clones. Flow cytometry profiles of 2',7'-dichlorodihydrofluorescein diacetate (H2-DCF-DA) fluorescence (FITC-A) used as an indicator for reactive oxygen species (ROS) generated in MDAH parental and PT-res clones, treated or not with cisplatin for 24 hours. The emission wavelength (529 nm) was detected and recorded by BD FACSCanto™ II flow cytometer. The percentages of positive cells for oxidized H2-DCF-DA are indicated in the plots. Adapted from Lorenzon et al., 2020.

Based on the above results, we tried to understand why MDAH PT-res cells acquired a MNGCs population and focused on the possible role of the tumor suppressor TP53, which plays a pivotal role in the control of M phase progression after therapy-induced DNA damage. Indeed, several reports suggest that cells lacking a functional TP53 enter mitosis even in the presence of a mutated DNA, especially when a mutated TP53 ($p53^{MUT}$) is expressed (Lukin et al., 2015; Sonego et al., 2013; Jackson et al., 2012). Accordingly,

cells lacking wild-type p53 functions escape cell cycle checkpoints and may undergo mitosis even after DNA damage and chromosomal aberrations, leading to the generation of MNGCs (Parekh et al., 2018; Lukin et al., 2015; Mirzayans et al., 2017). These evidences support the possibility that the presence of $p53^{R273H}$ in MDAH cells could be relevant for the onset, in MDAH PT-res cells, of the multinucleated phenotype. Interestingly, others and we demonstrated that $p53^{MUT}$ specifically regulates the expression of genes involved in the correct M phase progression and subsequent cell division (Girardini et al., 2011; Sonego et al., 2013; Mantovani et al., 2019). Our lab recently reported, in MDAH cells, that the proper expression, stability and activity of $p53^{R273H}$, regulated by stathmin/ DNA-PK_{CS} interaction, was necessary for the completion of a timely cell division and for the increased resistance to platinum-induced cell death via the regulation of several mitotic regulators like BUB1, CENPA, C21orf45 and NCAPH (Sonego et al., 2013); all belonging to the so-called $p53^{MUT}$ signature (Girardini et al., 2011). For these reasons, we first analyzed the expression of the 10 genes belonging to this signature, in parental and PT-res clones. Among the tested genes, we observed a consistent increase in mRNA expression levels of CCNE2 and DEPDC1, and a decreased mRNA expression for NCAPH and C21orf45 in PT-res clones respect to parental cells (Figure 34A). On the other hand, no significant variations were detected in the mRNA expression of BUB1, CENPA, WDR67, CPSF6, FAM64A and EPB41, once compared PT-res clones to parental counterpart, although a tendency for the overexpression of CENPA and CPSF6 was noted (Figure 34B).

These alterations were also confirmed at protein level, by Western Blot analysis (Figure 35). All these genes play a key role in mitotic cell division regulation: CCNE2 is linked to endoreplication and genomic instability (Caldon et al., 2013; Motwani and Schwartz, 2000), C21orf45, also known as MIS18A, is a kinetocore protein belonging to the Mis18 complex assembly that is crucial for CENPA deposition at the centromere (Pan et al., 2017; Spiller et al., 2017), DEPDC1 is highly expressed in M phase and its silencing caused mitotic defects (Chen et al., 2017; Zhou et al., 2019) and NCAPH is a regulatory subunit of the condensin complex, required for the conversion of interphase chromatin into condensed chromosomes (Batty and Gerlich, 2019; Yin et al., 2017). Overall, their altered expression could participate to the development of an aberrant mitotic phenotype, like the one observed in our model.

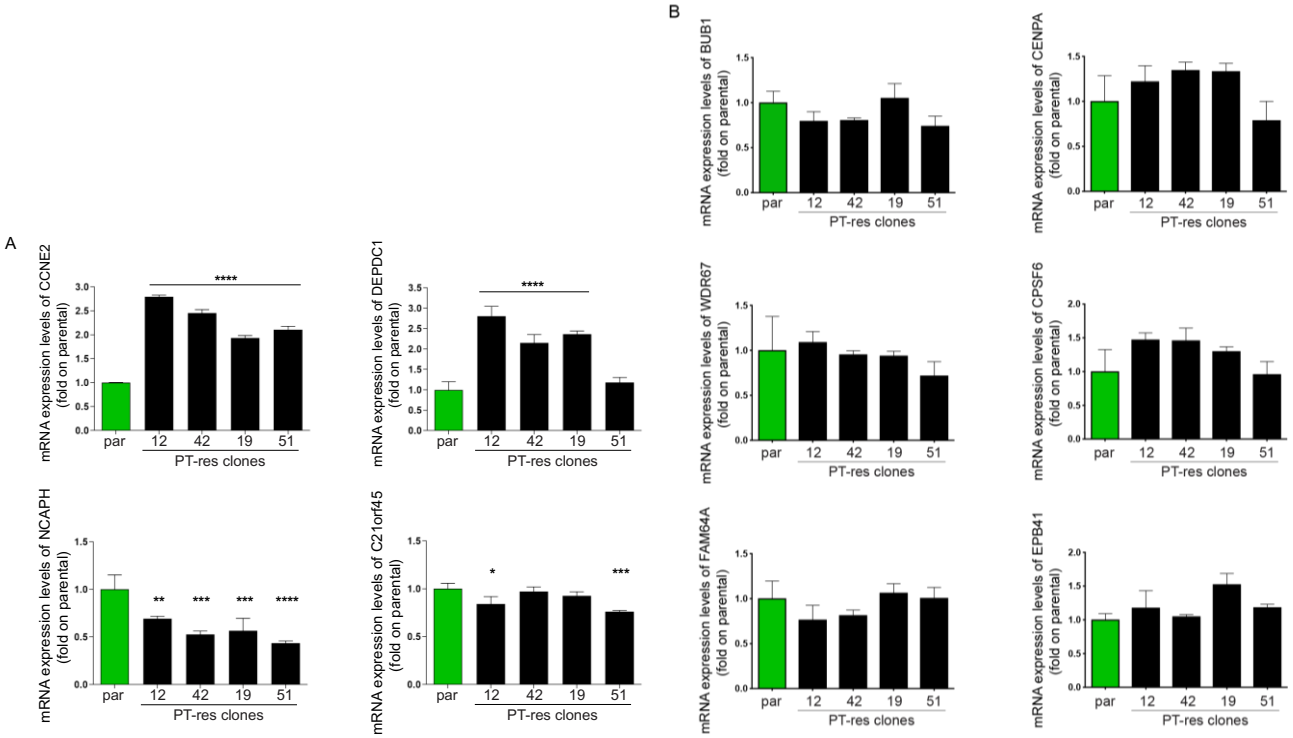

Figure 34. mRNA expression levels of several genes belonging to the so-called p53^{MUT} signature. (A) qRT-PCR analyses of the indicated genes in MDAH parental and PT-res clones. mRNA levels were analyzed in triplicate and normalized using GAPDH housekeeping gene. Data are expressed as fold of mRNA expression in PT-res cells respect to parental cells and represent the mean (± SD) of at least of three independent experiments. (B) qRT-PCR analyses evaluating the mRNA expression of the indicated p53^{MUT} transcriptional target genes in parental and PT-res single clones. mRNA levels were analyzed in triplicate and normalized using GAPDH as housekeeping gene. Data are expressed as fold of mRNA expression in PT-res cells respect to parental one and represent the mean (± SD) of at least of three independent experiments. Statistical significance in (A) and (B) was determined by one-way ANOVA test; a multiple comparison analysis was done to determine significant differences among groups (*p < 0.05 and **p < 0.01 and ***p < 0.001 and ****p < 0.0001). Adapted from Lorenzon et al., 2020.

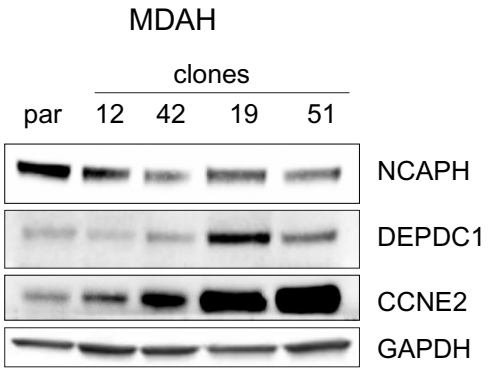

Figure 35. Protein expression levels of genes found altered by qRT-PCR in MDAH PT-res clones. Western Blot analysis of NCAPH, DEPDC1, CCNE2 expression in parental and PT-res clones. GAPDH was used as loading control. Adapted from Lorenzon et al., 2020.

3.9 DNA-PKcs is not involved in the regulation of p53MUT activity in PT-res clones

The collected data supported the possibility that MDAH PT-res clones displayed a different activity of p53MUT and, based on our previous results, suggested a role for DNA-PKcs/ stathmin in the regulation of p53MUT in EOC cells. First, we tested the expression of p53, stathmin and DNA-PKcs in PT-res clones and parental cells finding no significant changes in their expression levels, except for a slightly reduction of stathmin when assayed in exponentially growing conditions (Figure 36A). Considering that DNA-PKcs plays a major role in p53MUT regulation via phosphorylation of Ser 37, affecting its stability and/or its transcriptional activity (Sonego et al., 2013), we next checked p53 expression and phosphorylation levels in MDAH parental and PT-res cells, treated with high dose of CDDP for 16 hours and released in complete medium for 24 hours. All tested PT-res clones presented a higher phosphorylation of Ser37 and Ser15 of p53 respect to parental cells, both under platinum treatment and after the release, without significant changes in total protein levels. In the same settings, no differences in the expression of stathmin and DNA-PKcs were observed (Figure 36B).

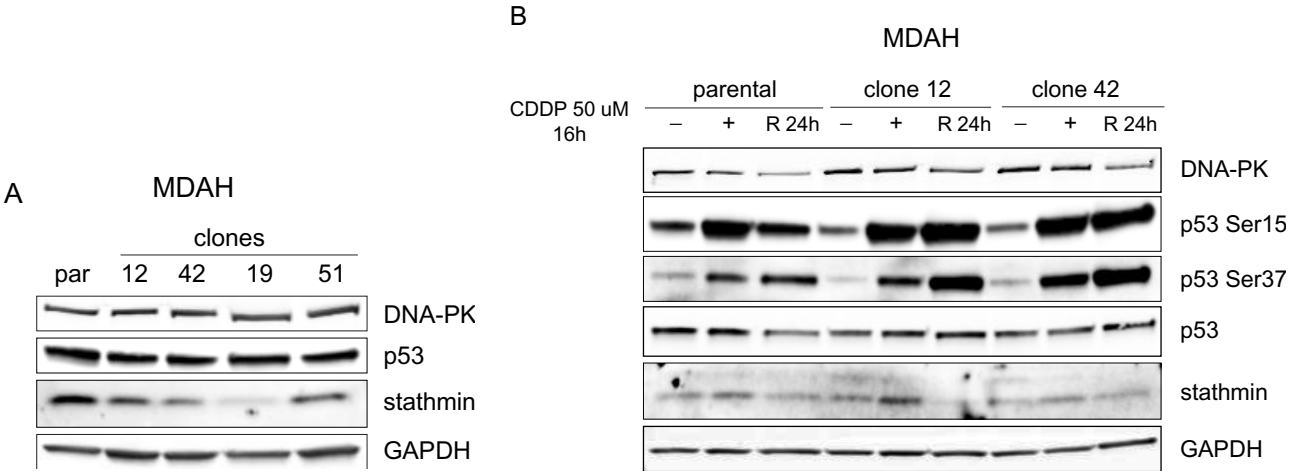

Figure 36. The expression of p53, stathmin and DNA-PKcs in PT-res clones. (A) Western Blot analysis of DNA-PK, p53, stathmin expression in parental and PT-res clones. GAPDH was used as loading control. (B) Western Blot analysis of DNA-PK, phosphorylated p53 forms (Ser15 and Ser37), p53 and stathmin expression in parental and PT-res clones (#12 and #42), treated with CDDP for 16 hours and allowed to repair DNA for 24 hours (R24h). GAPDH was used as loading control. Adapted from Lorenzon et al., 2020.

This increased phosphorylation was, however, not associated to an increased binding to DNA-PKcs (Figure 37A), neither to an increased p53MUT protein stability, at least in basal conditions. In fact, to determine the p53 protein half-life of MDAH parental and PT-res clones we performed a time course treatment with the inhibitor of protein synthesis

cycloheximide (CHX). Cells treated with CHX for the indicated times were then lysated and cell lysated evaluated by Western Blot for the expression of p53. Densitometric analyses of the blots show that in parental and PT-res clones p53 had similar half life of about 12 hours (Figure 37B).

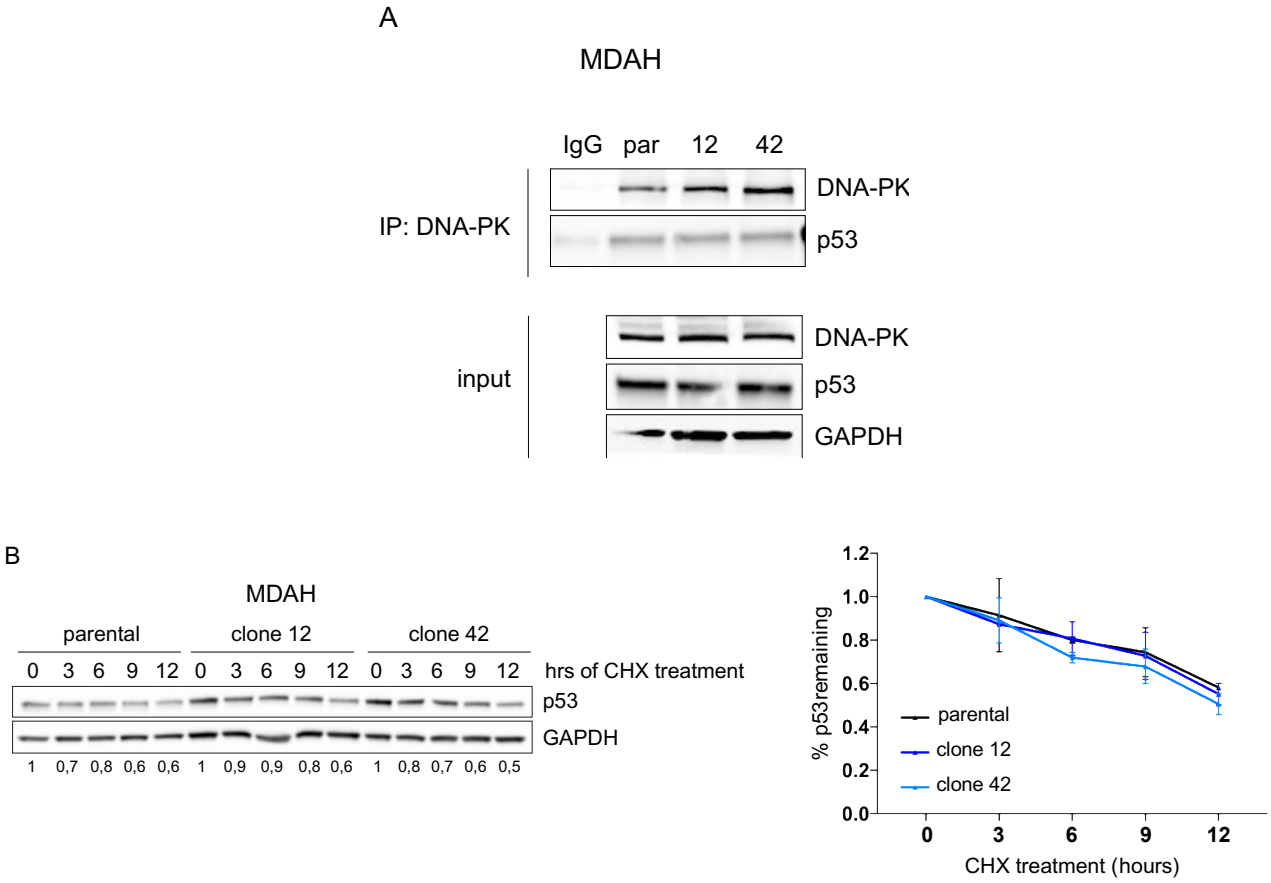

Figure 37. DNA-PK$_{CS}$ is not involved in the regulation of p53^{MUT} activity in PT-res clones. (A) Co-IP analysis of endogenous DNA-PK and p53 proteins in parental and PT-res single clones (#12 and #42). Input shows the expression of the indicated proteins in the lysates used for IP experiments; IgG represents the control IP using an unrelated antibody. GAPDH was used as loading control. (B) Western blot analyses of p53 expression in parental and PT-res single clones (#12 and #42) treated with cycloheximide (CHX) for the indicated times. The graph reports the p53 expression as remaining fraction respect to T0 (mean ± SD of 3 different experiments), normalized respect to GAPDH expression. Adapted from Lorenzon et al., 2020.

3.10 MDAH PT-res clones gained a new TP53 missense mutation after therapy selection process

To confirm the reported presence of p53^{R273H}, we analyzed the complete coding sequence of TP53 from genomic DNA extracted from parental cells, PT-res pools and PT-res single clones, by targeted Next Generation Sequencing (NGS). Surprisingly, we found that all

PT-res clones (and pools, data not shown) presented an additional mutation c.553A>G in exon 5, that determines a substitution of Serine residue in pos.185 to Glycine (p.S185G), that was not present in parental cells and that accompanied the p.R273H, c. 818G>A in exon 8 (Figure 38).

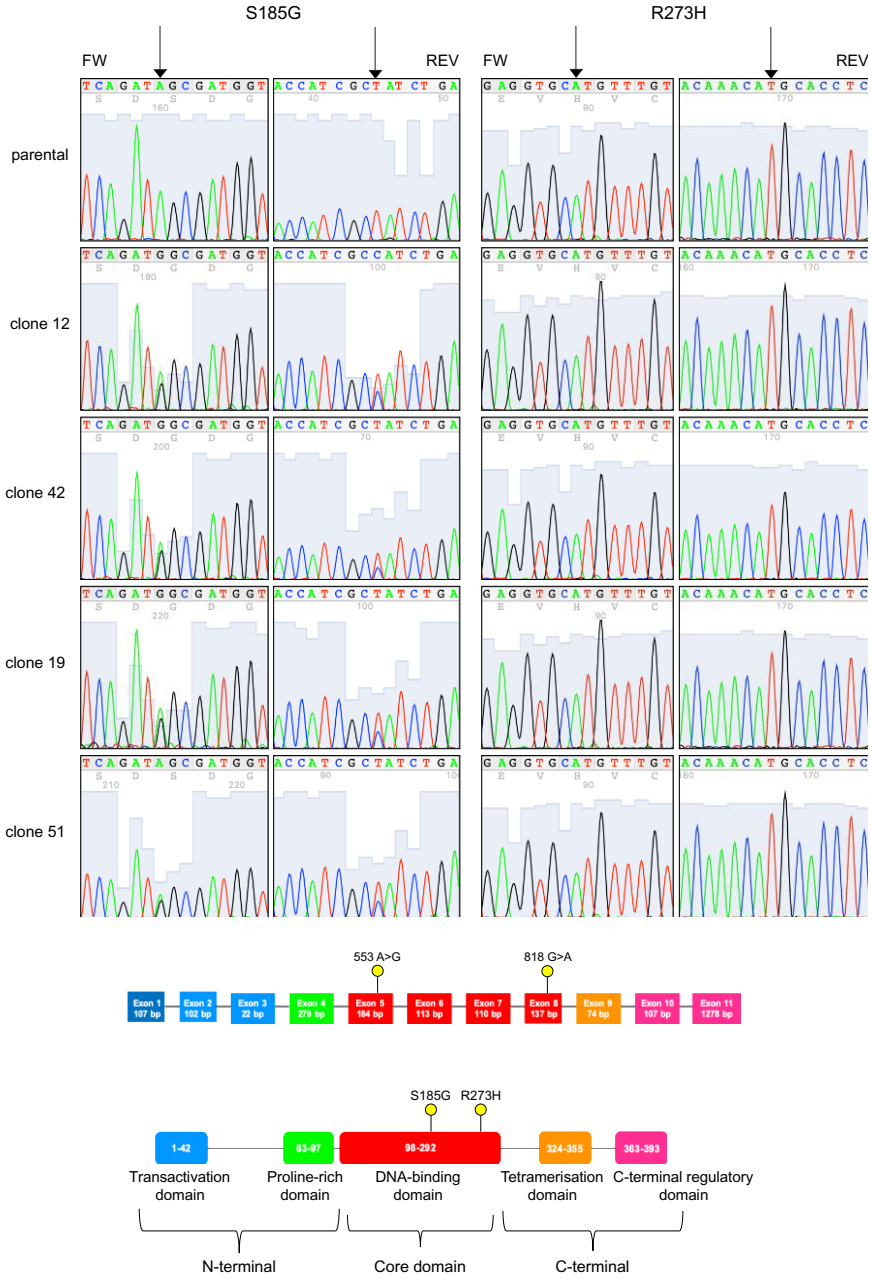

Figure 38. MDAH PT-res clones gain a new TP53 missense mutation. Representative four-color fluorescence electropherograms of p53 Sanger sequencing (top) performed on parental and PT-res clones, black arrows indicate residues 273 and 185. Schematic diagram (bottom) of p53 gene (first) and protein (second). Exons are colour-coded according to the corresponding protein functional domains. Yellow dots depict the mutations found. Adapted from Lorenzon et al., 2020.

Therefore, we asked if this double mutant p53$^{S185G/R273H}$ could play a role in some of the biological characteristics observed in MDAH PT-res pools and clones described above. In order to verify this hypothesis, we silenced TP53 in both parental and PT-resistant clones and then treated cells with CDDP for 16h (Figure 39).

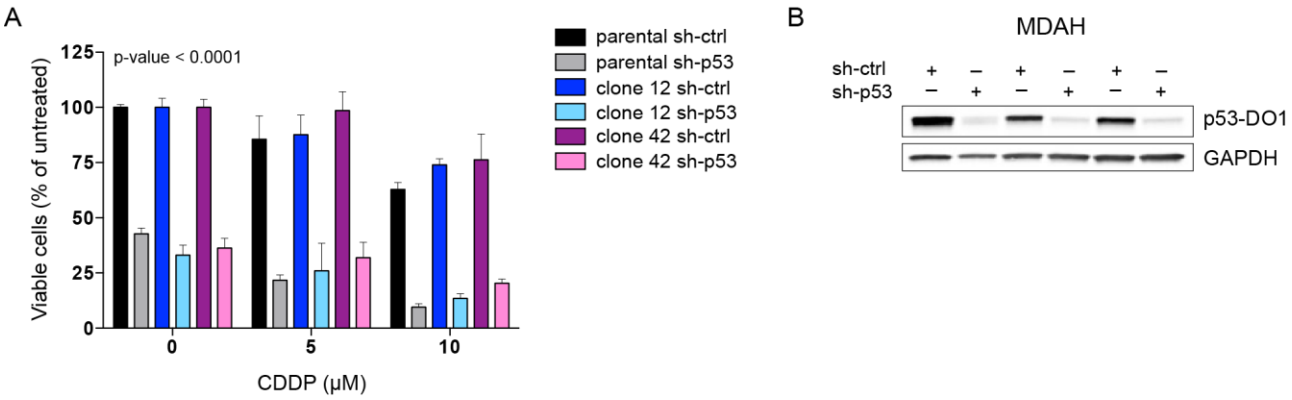

Figure 39. Down modulation of p53 expression induces cell death. (A) Dose-response curves of MDAH parental and PT-res single cell clones, transduced with sh-ctrl or sh-p53 and treated with increasing doses of cisplatin (CDDP) for 16 hours and released for 24 hours. Data are expressed as percentage of viable cells respect to the sh-ctrl untreated parental cells and represent the mean (±SD) of 3 biological replicates. Statistical significance was determined by two- way ANOVA test; a multiple comparison analysis was done to determine significant differences among groups. p-value is reported in the graph. B) Western Blot analysis evaluating p53 expression in parental and PT-res clones, transduced with sh- ctrl or sh-p53 used in (A). GAPDH was used as loading control. Adapted from Lorenzon et al., 2020.

Results showed that down modulation of p53 expression induced a marked cell death level per se, suggesting that MDAH cells are addicted to the expression of mutant TP53, rendering the evaluation of PT-sensitivity difficult to be evaluated in this experimental setting.

Based on these results, we used a different approach and evaluated if the double mutant p53$^{S185G/R273H}$ could play a role in some of the biological characteristics of the PT-res clones. We used the p53^{NULL} EOC cell line, SKOV-3, in which we overexpressed the p53^{R273H} or the p53$^{S185G/R273H}$ proteins, by transfecting them with pEGFP plasmids carrying the two different mutants. Although the transfecting efficacy ensures that the two proteins were equally expressed, the double mutant p53$^{S185G/R273H}$ had a higher phosphorylation of Ser 37 and, partially, of Ser 15 of p53, accompanied by a decreased expression of NCAPH (Figure 40A) mimicking what previously observed in PT-res clones (Figure 36B).

Using SKOV-3 over-expressing cells, we also examined whether the regulation of genes belonging to the p53^{MUT} signature (Girardini et al., 2011) was altered. Through qRT-PCR

analyses we evaluated the expression of the two genes differentially regulated in MDAH PT-res clones (Figure 40B). A slightly decreased mRNA expression of NCAPH and a consistent increased mRNA expression for DEPDC1 was observed in SKOV-3 double mutant $p53^{S185G/R273H}$ when compared to $p53^{R273H}$ over-expressing cells (Figure 40B). On the contrary, the expression of CCNE2 was not modified by $p53^{S185G/R273H}$ in this model (not shown), suggesting that context dependent regulation of gene expression exist.

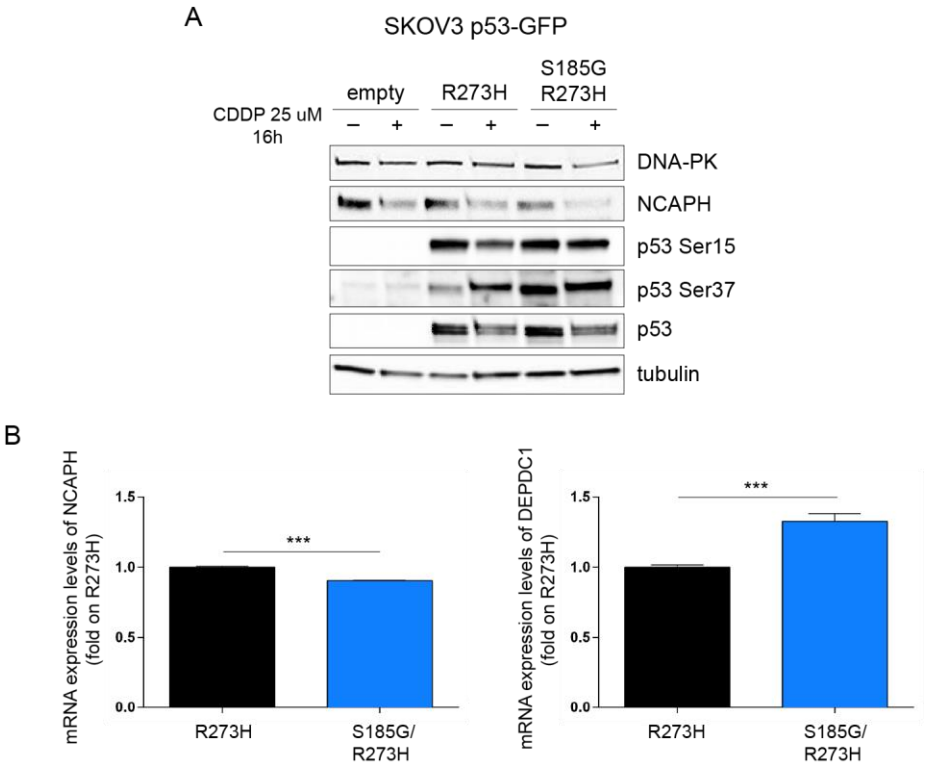

Figure 40. SKOV-3 $p53^{S185/R273H}$ over-expressing cells mimick MDAH PT-res clones gene regulation. (A) Western blot analyses evaluating the expression of DNA-PK, NCAPH, phosphorylated p53 (Ser 15 and Ser37) in SKOV-3 cells stably transfected with pEGFP-$p53^{R273H}$ or pEGFP-$p53^{R273H/S185G}$ double mutant. Cells were treated or not with CDDP for 16 hours. Tubulin was used as loading control. (B) qRT-PCR analyses of the indicated genes in SKOV-3 $p53^{R273H}$ or $p53^{S185G/R273H}$ over-expressing cells. mRNA levels were analyzed in triplicate and normalized using GAPDH housekeeping gene. Data are expressed as fold of mRNA expression in $p53^{R273H}$ or $p53^{S185G/R273H}$ over-expressing cells respect to empty condition and represent the mean (± SD) of at least of three independent experiments. Statistical significance was determined by a two-tailed unpaired Student's t-test (*$p < 0.05$ and **$p < 0.01$). Adapted from Lorenzon et al., 2020.

Importantly, the stable expression of $p53^{S185G/R273H}$ increased the resistance to platinum of SKOV-3 cells significantly better than the $p53^{R273H}$ single mutant (Figure 41), supporting a role of this double p53 mutant in the onset of platinum resistance of MDAH cells.

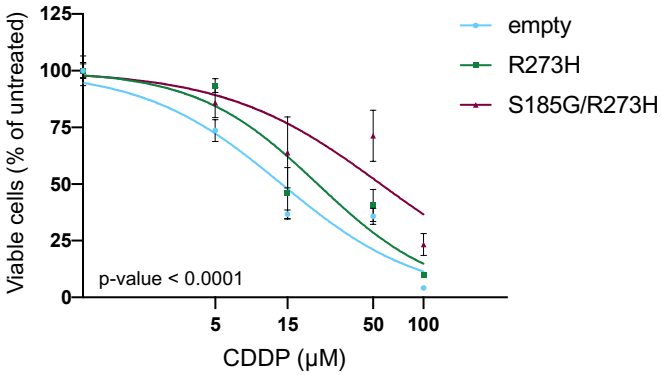

Figure 41. The expression of p53$^{S185G/R273H}$ induces an increase of SKOV-3 cells platinum resistance. Nonlinear regression analysis of cell viability assay of cells described above and treated with increasing doses of CDDP for 72 hours. Data are expressed as percentage of viable cells respect to the untreated cells and represent the mean (±SD) of 3 biological replicates. Fisher's exact test was used to calculate the global p-value reported in the graph. Adapted from Lorenzon et al., 2020.

To understand if the increased resistance to platinum of SKOV-3 p53$^{S185G/R273H}$ transfected cells was accompanied by an increased number of multinucleated cells, we evaluated the number of MNGCs in SKOV-3 cells transfected with p53^{R273H} or with p53$^{S185G/R273H}$ by immunofluorescence analyses, specifically looking at the number of multinucleated in cells expressing the p53 proteins.

Results showed that p53$^{S185G/R273H}$ markedly increased the number of multinucleated SKOV-3 cells (Figure 42A) respect to cells expressing p53^{R273H}. Nevertheless, p53$^{S185G/R273H}$ expression reduced SKOV-3 cell growth when compared to cells expressing p53^{R273H} single mutant (Figure 42B), overall, recapitulating most of the phenotype observed in PT-res cells.

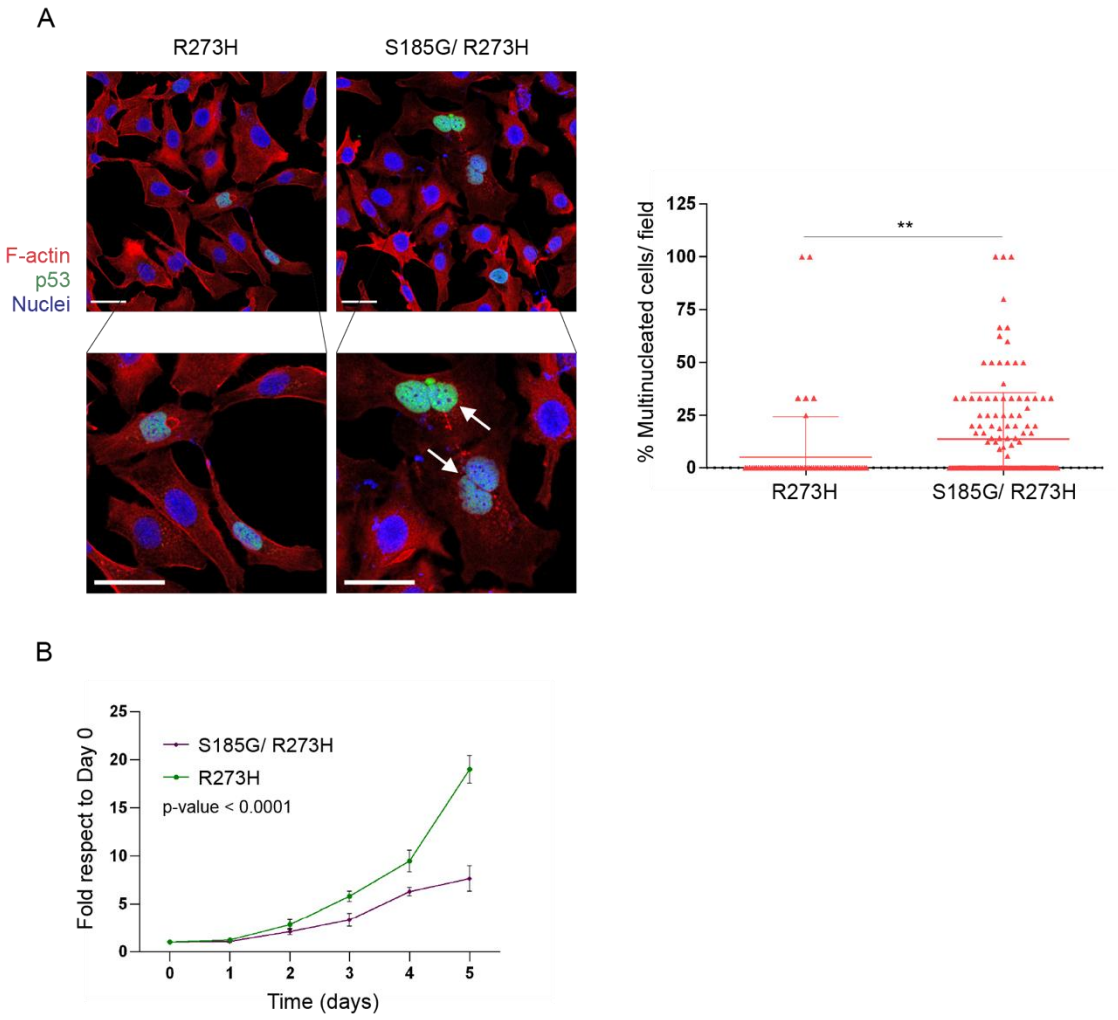

Figure 42. SKOV-3 p53$^{S185/R273H}$ over-expressing cells are characterized by an increased number of multinucleated cells with an impaired growth rate. (A) Representative images of SKOV-3 cells transfected with p53^{R273H} or p53$^{S185G/R273H}$ double mutant stained for F-actin (red) and p53 (green). Nuclei are pseudo colored in blue (TO-PRO-3). Bottom panels show the indicated zoomed area for each condition (2× zoom) in which white arrows indicate multinucleated cells. Scale bar = 44 μm. On the right, the number of multinucleated cells counted among p53 positive cells/field is reported (mean ± SD). The entire coverslips were counted. Statistical significance was determined by a two-tailed unpaired Student's t-test (*$p < 0.05$ and **$p < 0.01$). (B) Growth curves of SKOV-3 cells stably transfected with p53^{R273H} or p53$^{S185G/R273H}$ double mutant. Data are expressed as fold increase with respect to day 0. Global statistical significance was determined by two-way ANOVA test, global $p < 0.0001$. Adapted from Lorenzon et al., 2020.

Discussion

The development of platinum resistance seems a dynamic process. Patients who initially respond to platinum-based chemotherapy end up becoming resistant. This suggests that it is necessary to investigate the mechanisms at the base of resistance development (Tapia and Diaz-Padilla, 2013). In this PhD thesis, we reported the selection of seven isogenic cisplatin resistant cell lines derived from high grade EOC, and the molecular and biological characterization of three of them: MDAH-2774, TOV-112D and OVSAHO. To our knowledge this is the first report comparing three different EOC models of acquired resistance to cisplatin. Through this work strategy we were able to establish platinum resistance as a multifactorial and complex molecular process caused by different molecular alterations, although common phenotypic changes can be observed.

One important feature of the platinum resistant cells selected was the common ability to resolve platinum-induced DNA damage (Figure 20), strengthened by the concomitant altered expression of selected transporters of the drug (Figure 22). These two characteristics of PT-res cells then resulted in a decreased accumulation of DNA damages (i.e γH2AX expression). We observed that cross-resistance to other drugs often used in the therapy of platinum resistant ovarian cancer patients (like taxol and doxorubicin), was cell-type specific (Figure 13). Thus, identifying biomarkers of cross-resistance would end in significant clinical benefit for patients, avoiding ineffective treatments.

Interestingly, we have observed, at least *in vitro*, that the acquired resistant phenotype is maintained regardless the presence or absence of platinum in cell culture medium, suggesting that the clinical hypothesis postulating that it is worth to re-use platinum based therapies after a platinum-free interval, could be used as a therapeutic strategy only in platinum-sensitive ovarian cancer patients.

Another common alteration due to the acquisition of the resistant phenotype was an evident morphological change in PT-resistant cells respect to parental ones (Figure 15). This involved the reorganization of cytoskeleton (Figure 17), cell-cell junctions (Figure 18) and ability to adhere to mesothelium layer (Figure 19), suggesting that EMT and MET processes could have a role in a different response to platinum treatment (Figure 16). This result was also sustained by a different expression of SNAIL, TWIST-1 and ZEB1 in our PT-resistant cells (Figure 16), indicating that the resistant phenotype is accompanied by an induction of EMT-like process. All these findings encourage us to further investigate the

driven mechanisms of increased ability to disseminate in the peritoneal cavity and to adhere at distant sites as key properties of PT-resistant cells.

In the second part of this work we more deeply characterized several PT-resistant clones derived from single-cell cloning selection of MDAH-2774 PT-resistant pools. We reported that these cells showed an impaired growth rate respect to parental ones (Figure 26A), a deregulated cell division (Figure 28A and 31) with the appearance of a subpopulation of larger, multinucleated giant cells (MNGCs), not present in parental cells (Figure 26B and 30). It is described that the proportion of MNGCs increases markedly under stressful conditions. This increase can be provoked by replicative stress, hypoxia and after exposure to anticancer agents (as chemotherapy) (Parekh et al., 2018; Mirzayans et al., 2017; Mirzayans et al., 2018; Mittal et al., 2017). Although giant cells are often scored as "dead" because of their state of dormancy, they are associated with metastasis and resistance to chemotherapy, so targeting giant cells before they can promote tumor repopulation might be an effective anti-cancer strategy (Mirzayans et al., 2018). MNGCs secrete soluble signaling factors, including ROS, collectively known as SASP or senescence associated secretory phenotype in which TP53 plays crucial roles. In particular it has been proposed that SASP suppresses or promotes tumorigenesis depending on the TP53 status (Watanabe et al., 2017). This is coherent with the higher production of ROS levels we observed in MDAH PT-res cells (Figure 33). It is relevant to note that caspase 3 activation (Figure 32), in our model, could be also linked to an apoptosis-independent function, pro-survival, given than it has been already described as soluble factor characterizing the SASP phenotype of MNGCs (Mirzayans et al., 2017; Mirzayans et al., 2016; Liu et al., 2015). Which is the role of $TP53^{MUT}$ in the generation of MNGCs is still unclear but since it has been proposed that MNGCs could represent an adaptive response of apoptosis-reluctant cells, $TP53^{MUT}$ could play a pivotal role in allowing aberrant mitotic cells to complete the M phase and eventually survive as MNGCs. Here we report that MDAH PT-resistant cells acquired, under the pressure of platinum selection, a secondary mutation (the S185G missense substitution) in TP53, in addition to the already present R273H pathogenic missense substitution (Figure 38). This $p53^{S185G/R273H}$ double mutant was found in all tested clones and pools. Yet, while the R273H substitution is homozygous in MDAH cells the S185G seems to be heterozygous. $p53^{S185G}$ is still categorized as a mutation of unknown significance and it has been described in the Cosmic database only in one case of ovarian endometrioid carcinoma and one case of esophageal carcinoma. Surprisingly, in both cases $p53^{S185G}$ substitution

was found in tumors with known pathogenic TP53 mutations (Ralhan et al., 2000; Neungton et al., 2002). It is therefore possible that the S185G mutation confers a specific advantage only to a $p53^{MUT}$ protein.

To understand if $p53^{S185G}$ mutation appeared as the selection of an already existing missense mutation or as a platinum-induced mutation we deeply sequenced the parental cells (median coverage depth for TP53 was 5600X) in search of possible MDAH subclones carrying this substitution. We found that MDAH parental cells presented only the $p53^{R273H}$ mutation already described, suggesting that pressure of PT selection induced the appearance of this co-occurring mutation.

$p53^{S185G}$ appearance was linked to higher pS37 phosphorylation levels, not only in PT-res clones but also in transfected SKOV-3 ($p53^{NULL}$) cells, supposing its involvement in increased activity to an already mutated TP53 (Figure 36B and 39). How $p53^{S185G}$ affects pS37 is still unknown, although we could likely exclude that it could be due to an increased association between TP53 and DNA-PK_{CS} (Figure 37A). Interestingly, others and we demonstrated that $TP53^{MUT}$ specifically regulates the transcription of genes involved in the mitotic process (Girardini et al., 2011; Sonego et al., 2013), supporting the possibility that it confers additional surviving possibilities to cells with aberrant mitosis, otherwise committed to die for mitotic catastrophe. The deregulation of some of these genes (i.e. CCNE2, DEPDC1, NCAPH and C21orf45) observed in PT-res MDAH clones and partially in SKOV-3 cells is in line with this possibility (Figure 34 and 40). However, further studies are necessary to clarify the molecular mechanisms through which $TP53^{MUT}$ contributes to MNGCs formation. In addition, the ectopic expression of $p53^{S185G/R273H}$ had functional consequences since it significantly increased the resistance to PT in SKOV-3 cells and was associated with PT-resistance in MDAH cells (Figure 41). Based on the phenotypes observed in MDAH PT-res cells, we hypothesized that the more active $p53^{S185G/R273H}$ protein could be partially responsible for the bypass of the G2/M checkpoints normally activated upon DNA damage by regulating mitotic regulators. This altered regulation eventually resulted in a deregulated cell division with the appearance of large MNGCs. Although we partially proved this point using the SKOV-3 model, we cannot verify the effective contribution of TP53 mutation on the phenotypes observed in MDAH cells, since these cells seem to be addicted to mutant TP53 expression. Therefore, more experiments and more appropriate study models are needed to definitively prove this point.

However, TOV-112D and OVSAHO PT-resistant cell lines, that were generated with the same “pulse” method of MDAH cells (Figure 11), did not show defects in cell proliferation, caspase 3 activation and MNGCs formation. We sequenced TP53 in both OVSAHO and TOV112D cells and, while we confirmed the presence of the mutation reported in the literature (R342* and R175H, respectively), we did not observe in these cells the appearance of the additional $p53^{S185G}$, indirectly supporting its involvement in the typical phenotype of MDAH PT-res cells. The Gene Set Enrichment Analysis (GSEA) of MDAH, OVSAHO and TOV112D PT-res cells we recently performed, evidenced that only MDAH PT-res cells had alteration in pathways controlling cell cycle progression and cell division (Sonego et al., 2017).

Overall our data demonstrated that platinum chemotherapy could induce additional mutations in TP53 and that the expression of double mutant $p53^{R273H/S185G}$ could affect the generation of PT-resistance by regulating the progression trough mitosis. Future more detailed works will be necessary to specifically unveil the underlying molecular mechanisms.

Materials and Methods

5.1 Cell cultures

MDAH-2774 (CRL-10303), TOV-112D (CRL-11731), TOV-21G (CRL-11730), SKOV-3 (HTB-77), ES-2 (CRL-1978) cells were from ATCC; OVCAR-8 (60-0507712) cells were from The National Cancer Institute Developmental Therapeutics Program Tumor Repository; while OVSAHO (JCRB0098) cells were from JCRB Cell Bank. All cell lines were maintained in RPMI-1640 medium (Sigma-Aldrich Co.) containing 10% heat-inactivated FBS, 100 U/ml penicillin and streptomycin (complete medium) at 37°C in a 5% CO_2 atmosphere. Cisplatin-resistant (PT-res) isogenic cells were generated by treating EOC parental cells for growth for 2 hours with a cisplatin dose 10-fold higher than the calculated IC50 and then allowing to re-grow in drug-free complete medium (pulse treatment). The subsequent drug treatment was administrated when the cells reached again a 70-80% of confluence. In total PT-res cells received 20 pulse treatments. At the end of treatments, a single cell cloning was performed in order to evaluate the homogeneity of these PT-res cell populations. The cisplatin IC50 of clones was tested. All the experiments were performed with cells kept in cisplatin-free medium for $\geq$2 months unless otherwise stated. All cell lines were routinely authenticated in our lab using the Cell ID TM System (Promega) protocol and using Genemapper ID Ver 3.2.1 to identify DNA STR profiles.

5.2 Compounds and drugs treatment

Cisplatin was purchased from TEVA (Italia), Paclitaxel (TAXOL®) from ACTAVIS (Dublin, Ireland) and Doxorubicin from Ebewe (Italia). Cycloheximide (CHX) was purchased from Sigma. ROS analyses were done using 2',7'-dichlorodihydrofluorescein diacetate (H2-DCF-DA) (Sigma). 2′,7′-Dichlorofluorescin diacetate is a cell-permeable non-fluorescent probe. 2′,7′-Dichlorofluorescin diacetate is de-esterified intracellularly and turns to highly fluorescent 2′,7′-dichlorofluorescein upon oxidation. Double thymidine block was performed incubating cells with thymidine (2.5 mM), acquired from Sigma.

5.3 Cell viability assay

Dose-response curves were performed essentially as described previously (Dall'Acqua et al., 2017). EOC cells were seeded in 96-well culture plates and treated with increasing doses of cisplatin, Taxol or Doxorubicin for 72 hours. For dose-response curves of p53-

silenced MDAH, cells were seeded in 96-well culture plates and after 24 hours transduced with sh-ctrl or sh-p53 lentiviral particles (Mission Sigma TRCN0000003756). 48 hours after transduction cells were treated with increasing doses of CDDP for 16 hours and released with complete medium for 24 hours. Cell viability was determined using the CellTiter 96 Aqueous cell proliferation assay kit (Promega). Absorbance was detected at 492 nm using a microplate reader (Infinite® M1000 Pro, Tecan).

5.4 Vectors and transfections

The p53R273H mutant was subcloned in the pEGFP-C1 vector (Clontech) and in the pLPC vector (Provided by Dr R. Maestro) from the pCMV/Neo-p53R273H (Addgene#16439) into the BamHI restriction site. The pEGFP-p53 and pLPC-p53 double mutant were generated using a QuikChange Site-Directed Mutagenesis Kit (Agilent) using oligonucleotides carrying the indicated mutation. Plasmids were transfected in SKOV-3 cells using FuGENE HD Transfection Reagent (Promega) according to the manufacturer's indications. Stable expressing clones were selected by culturing cells with G418 (0.5 mg/ml) (pEGFP) or puromycin (1 ug/ml) (pLPC). For lentiviral production, 293FT cells (Invitrogen) were co-transfected, using a standard calcium phosphate precipitation, with the lentiviral based shRNA constructs (pLKO) and lentiviral vectors pGag-Pol (Sigma) and pVSV-G (Invitrogen). Seventy-two hours after transfection, medium containing viral particles was used to transduce EOC cell lines. pLKO vectors encoding for control and p53 (TRCN0000003756) shRNAs were purchased from Sigma.

5.5 Cell cycle analysis by flow cytometry

EOC cells (pools) were plated in 60-mm dishes (8×10^5 cells/dish) and after 24 hours treated with cisplatin. Cells were harvested at the indicated time points. EOC cells (MDAH clones) were plated in 60 mm dishes and collected after 48 hours for the exponentially growing condition analysis. For the synchronized cells condition was done a double thymidine block to arrest cells in G1/S phase. Cells were then released and collected at the indicated time points for the cell cycle analysis. Once harvested, cells were washed with 1x PBS, fixed in ice-cold 70% ethanol adding drop wise to the pellet while vortexing to minimize clumping and stored at -20 °C overnight. Fixed cells were then washed in 1x PBS and re-suspended in propidium iodide (PI) staining solution (50 μg/ml PI + 200 μg/ml RNaseA, in 1x PBS). Stained cells were subjected to flow cytometry analysis with a BD FACScan™ or a BD FACSCalibur™ flow cytometer. Distribution of cells in G1, S and G2/M

phases of the cell cycle was analyzed with the WinMDI2.9 software as described (Fabris et al., 2015) for EOC pools, with ModFit LT™ software for MDAH clones. Plots of MDAH clones were realized with FlowJo software.

5.6 Preparation of cell lysates, Immunoblotting, and Immunoprecipitation

Cell lysates were prepared using cold RIPA buffer [150 mM NaCl, 50 mM TRIS-HCl (pH 8), 0.1% SDS, 1% Igepal, and 0.5% NP-40] containing proteases inhibitor cocktail (Roche), phosphatase inhibitors (1 mM Na_3VO_4 and 10 mM NaF, Sigma-Aldrich) plus 1 mM DTT. Protein concentrations were determined using the Bio-Rad protein assay (Bio-Rad). For immunoblotting, equal concentrations of protein samples were separated by 4–20% SDS-polyacrylamide gel electrophoresis (SDS-PAGE) (Criterion precast gel, Bio-Rad) and blotted onto a nitrocellulose membrane (Amersham, GE Healthcare). Immunoprecipitations were performed using 600µg of cell lysate in HNTG buffer (20 mM HEPES, 150 mM NaCl, 10% glycerol, 0.1% Triton X-100) plus 1 µg of anti DNA-PKcs antibody (H-163 sc-9051, Santa Cruz Inc.) and incubating overnight at 4°C. The immunocomplexes were precipitated by adding protein A agarose-conjugated for additional 1 hours and 30 min at 4°C and finally separated on SDS-PAGE, for western blot analysis. Immunoblotting were performed using the following primary antibodies: DNA-PKcs (H-163 sc-9051, 1:1000), cyclin A (H-432 sc-751, 1:200), cyclin B1 (GNS1 sc-245, 1:200), phospho Rb (Ser780) (sc-12901, 1:500), stathmin (E-3 sc-55531, 1:1000), p53 (DO-1 sc-126, 1:1000) and vinculin (7F9 sc-73614, 1:1000), Twist-1 (Twist2C1a sc-81417, 1:200) were from Santa Cruz Inc.; phospho-p53 (Ser15) (#9284, 1:500), phospho-p53 (Ser37) (#9289, 1:500), phospho-H3 (Ser10) (D7N8E #53348, 1:500), Histone H3 (D1H2 #4499, 1:750), phospho-cdc2 (Tyr15) (10A11 #4539, 1:500), Zeb1 (D80D3 #3396, 1:500), Slug (C19G7 #9585, 1:500), Snail (C15D3 #3879, 1:1000) were from Cell Signaling Technology; cyclin E2 (EP454Y ab40890, 1:1000), NCAPH (ab154105, 1:300) were from Abcam; DEPDC1 (1:500) was a kind gift from Prof G. Del Sal (Trieste University); GAPDH (6C5 CB1001, 1:1000), phospho-histone H2AX (Ser139) (γH2AX) (JBW301 #05-636, 1:500), were from EMD Millipore; CDK1 (C12720, 1:500) was from BD Transduction Laboratories; α-tubulin (DM1A T9026, 1:5000) was from Sigma-Aldrich.

5.7 Protein stability

p53 protein stability was evaluated in MDAH-2774 parental and PT-res clones treated with CHX (10 mg/ml) for the indicated time points. The p53 expression was calculated as

remaining fraction respect to T0 (mean ± SD of 3 different experiments), normalized respect to GAPDH expression.

5.8 RNA isolation and Real-time polymerase chain reaction

Total RNA was isolated using TriZol reagent (Life Technologies) following the manufacturer's instructions. 2 μg of total RNA was retro-transcribed using random hexamers and the AMV Reverse Transcriptase (Promega). 1/20 of the obtained cDNAs were then amplified using primers for the human FAM64A, CENPA, BUB1, NCAPH, C21orf45, DEPDC1, CCNE2, WDR67, CPSF6, EPB41L (Girardini et al., 2011; Sonego et al., 2013). Standard curves (10-fold dilution from 10^{-1} to 10^{-4} attomoles) were prepared and analyzed by quantitative reverse transcription polymerase chain reaction (qRT-PCR) using the CFX96™ Real-time PCR Detection System (Bio-Rad).

5.9 *In vitro* cell proliferation

For growth curve analyses, MDAH-2774 parental and PT-res pools (pool#1 and pool#2) and SKOV-3 cells stably transfected with pLPC- $p53^{R273H}$ or pEGFP-$p53^{R273H/S185G}$ double mutant were cultured in 6-well plates. Viable cells were counted daily in triplicate for 5 days, by trypan-blue dye exclusion method. For cell proliferation, PT-res clones (#12, #19, #42 and #51) were seeded in sextuplicate in 96-well plates and cell proliferation was determined daily (for 5 days) by MTS assay using the CellTiter 96 AQueous cell proliferation assay kit (Promega). All experiments were repeated at least three times.

5. 10 EOC adhesion on mesothelial cells and Immunofluorescence analyses

Mesothelial cells (derived from pleural lavage) were seeded on glass coverslips and allowed to grow until they reached complete confluence. 1.5×10^5 EOC cells detached with 5 mM EDTA, labeled with vital green fluorescent lipophilic tracer DiO (Invitrogen) and washed with PBS were then plated on mesothelial layer in serum free medium for 24 hours.

For immunofluorescence analyses cells plated on coverslips were fixed in PBS-4% paraformaldehyde (PFA) at room temperature (RT), blocked in PBS-1% bovine serum albumin (BSA), permeabilized in PBS 0.2% Triton X-100. Stains were performed with primary antibodies: anti-α-tubulin-fluorescein isothiocyanate (FITC) (clone DH1A, F2168, 1:150), γ-tubulin (clone GTU-88, T6557, 1:1000) (Sigma Aldrich); ZO-1 (D7D12 #8193, 1:50), cleaved caspase 3 (Asp175) (#9661, 1:300), phospho- histone H3 (Ser10) (D7N8E

#53348, 1:300) (Cell Signaling), p53 (DO-1 sc-126, 1:200) from Santa Cruz Inc.; and γ-catenin (610253, 1:50) (BD Biosciences). Then samples were washed in PBS and incubated with secondary antibodies (Alexa-Fluor 488-, 568- or 633- conjugated anti-mouse or anti-rabbit antibodies; Invitrogen) for 1 hour at RT. PI (5 µg/ml + RNaseA) or TO-PRO-3 iodide (Invitrogen) were used to visualize nuclei and Alexa-Fluor 647- or 546-Phalloidin (Invitrogen) for F-actin staining. Coverslips were mounted with glycerol/0.25% DABCO and analyzed using the Leica Time Lapse AF6000LX workstation, the TCS-SP2 or the TCS-SP8 Confocal Systems (Leica Microsystems Heidelberg GmbH) interfaced with the Leica Confocal Software (LCS) or the Leica Application Suite (LAS) software.

5.11 Next Generation Sequencing (NGS)

For TP53 sequencing of PT-res pool cells, genomic DNA was extracted from cultured cells using Maxwell 16 DNA purification kit (Promega). 50 ng of genomic DNA was amplified with TruSeq Custom Amplicon kit (TSCA, Illumina) specially designed for the targeted sequencing of TP53 (13 amplicons) among others. Libraries were run in an Illumina MiSeq instrument achieving a median coverage >1000 reads. Data were aligned to human reference genome hg18 and analyzed, after quality control, using Variant Studio and IGV program, reporting only variants with a mutant allelic frequency (MAF) greater than 5%. We considered not only variants inside the coding sequence, but also the ones inside the 5'-, 3'-untranslated regions (UTRs) and inside splicing regulatory elements (Diederichs S et al 2016, http://p53.iarc.fr/TP53GeneVariations.aspx). Validation of NGS data was performed on PT-res clones by Sanger method.

5.12 Cisplatin-DNA (Pt-DNA) adduct detection by Dot-blot

To detect cisplatin-DNA adducts, genomic DNA was isolated using the Maxwell® DNA-purification kit (Promega) from cells treated as indicated. DNA (500 ng) was denatured at 100 °C for 10 min and spotted onto nitrocellulose membranes (Hybond C; Amersham) using a dot-blot apparatus (Easy-Titer® ELIFA, Pierce). The membranes were then baked for 2 hours at 80 °C and subjected to standard Immunoblot assay using an anti-cisplatin-DNA Adducts (1:500) antibody (EMD Millipore, clone ICR4).

5.13 Reactive Oxygen Species (ROS) analyses

To determine the quantification of intracellular ROS, cells were plated in 60 mm dishes and treated or not with CDDP for 24 hours. After treatment, cells were incubated with 2',7'-

dichlorodihydrofluorescein diacetate (H2-DCF-DA) (Sigma) 2,5 μM in RPMI without phenol red for 30 minutes at 37°C and 5% CO2. Cells were washed in PBS 1X and collected by trypsinization in 1 ml of PBS 1X and analyzed using the BD FACSCanto™ II flow cytometer. The H2-DCF-DA molecule was excited with an excitation wavelength of 504 nm and the emission wavelength of 529 nm was detected and recorded by the instrument. For each sample were analyzed 20000 events, applying a gating strategy to exclude the debris. All the data were analyzed using the BD FACSDiva™ Software.

5.14 Double thymidine block

To synchronize cells a double thymidine block was performed. Cells were plated in 60 mm dishes and after 24 hours incubated with thymidine (2.5 mM) for 16 hours. Cells were then washed with 1x PBS and incubated with fresh complete medium for 9 hours before the second round of thymidine (2.5 mM) for 16 hours. Synchronized cells were then washed with 1x phosphate-buffered saline (PBS), released with complete medium and collected at the indicated time points for analysis of cell cycle by propidium iodide (PI)-DNA staining, or analysis of protein by Western blot.

5.15 Statistical analyses

All statistical analysis was done using Graphpad Prism 8 software and appropriate methods were employed. Standard deviations were used for designating error bars. Comparisons of two different groups were done with the help of Student's t-test and multiple groups were compared using ANOVA test. p-value ≤ 0.05 was considered significant (*$p \leq 0.05$, **$p \leq 0.01$, ***$p \leq 0.001$, ****$p \leq 0.0001$).

Table 1

Real-time PCR primers

Name	Sequence (5'-3')
BUB1 f	ATTCAAGCCACAGAGTGGAGCAG
BUB1 r	AGAACTTGTGTTGGCAACCTTATGTG
C21ORF45 f	GCGACTCGCTGAGCTGGGTG
C21ORF45 r	CCCCGCGCAGCACAAAGTCT
CCNE2 f	TGAGCCGAGCGGTAGCTGGT
CCNE2 r	GGGCTGGGGCTGCTGCTTAG
CENPA f	CTTCCTCCCATCAACACAGTCG
CENPA r	TGCTTCTGCTGCCTCTTGTAGG
CPSF6 f	AGGGGCTGTTCCTGGTGGGG
CPSF6 r	GGCCCAGCTAGAGGAGGAGGC
DEPDC1 f	TGGGTATTATCTGCCATGAAGTGCCT
DEPDC1 r	AGGTTGCAGCAAGCCCAAAATGT
EPB41L4B f	CGACGGGACCGAAGTGAGCG
EPB41L4B r	CAGTGCGCAACCTGGGCAGA
FAM64A f	CTCCAGGCTGCAGCTCGCTC
FAM64A r	CAGCCGGGTGCTCTTCTGGC
NCAPH f	GAGGAGCCTGCCCCCTGTCA
NCAPH r	TGGGCCTCCTGCTGCTGACT
WDR67 f	AGGCAACAAGGAGAGCGGCA
WDR67 r	AGCAGTCGCCTGTGCCATCA

PCR and sequencing primers

Name	Sequence (5'-3')
p53 exon5 f	GCCGTCTTCCAGTTGCTTTA
p53 exon5 r	ACACGCAAATTTCCTTCCAC
p53 exon8 f	GGGAGTAGATGGAGCCTGGT
p53 exon8 r	GTTGGGCAGTGCTAGGAAAG

Table 1. List of primers used for Real-time PCR, PCR and sequencing.

References

Agarwal, R., and Kaye, S.B. (2003). **Ovarian cancer: strategies for overcoming resistance to chemotherapy.** Nat. Rev. Cancer *3*, 502–516.

Ahmed, N., Abubaker, K., Findlay, J., and Quinn, M. (2010). **Epithelial mesenchymal transition and cancer stem cell-like phenotypes facilitate chemoresistance in recurrent ovarian cancer.** Curr Cancer Drug Targets *10*, 268–278.

Badciong, J.C., and Haas, A.L. (2002). **MdmX is a RING finger ubiquitin ligase capable of synergistically enhancing Mdm2 ubiquitination.** J. Biol. Chem. *277*, 49668–49675.

Basourakos, S.P., Li, L., Aparicio, A.M., Corn, P.G., Kim, J., and Thompson, T.C. (2017). **Combination Platinum-based and DNA Damage Response-targeting Cancer Therapy: Evolution and Future Directions.** Curr. Med. Chem. *24*, 1586–1606.

Bastiat, G., Pritz, C.O., Roider, C., Fouchet, F., Lignières, E., Jesacher, A., Glueckert, R., Ritsch-Marte, M., Schrott-Fischer, A., Saulnier, P., et al. (2013). **A new tool to ensure the fluorescent dye labeling stability of nanocarriers: a real challenge for fluorescence imaging.** J Control Release *170*, 334–342.

Batty, P., and Gerlich, D.W. (2019). **Mitotic Chromosome Mechanics: How Cells Segregate Their Genome.** Trends Cell Biol. *29*, 717–726.

Beaufort, C.M., Helmijr, J.C.A., Piskorz, A.M., Hoogstraat, M., Ruigrok-Ritstier, K., Besselink, N., Murtaza, M., van IJcken, W.F.J., Heine, A.A.J., Smid, M., et al. (2014). **Ovarian cancer cell line panel (OCCP): clinical importance of in vitro morphological subtypes.** PLoS ONE *9*, e103988.

van den Berghe, P.V.E., Folmer, D.E., Malingré, H.E.M., van Beurden, E., Klomp, A.E.M., van de Sluis, B., Merkx, M., Berger, R., and Klomp, L.W.J. (2007). **Human copper transporter 2 is localized in late endosomes and lysosomes and facilitates cellular copper uptake.** Biochem. J. *407*, 49–59.

Bieging, K.T., and Attardi, L.D. (2012). **Deconstructing p53 transcriptional networks in tumor suppression.** Trends Cell Biol. *22*, 97–106.

Blair, B.G., Larson, C.A., Safaei, R., and Howell, S.B. (2009). **Copper transporter 2 regulates the cellular accumulation and cytotoxicity of Cisplatin and Carboplatin.** Clin. Cancer Res. *15*, 4312–4321.

Blair, B.G., Larson, C.A., Adams, P.L., Abada, P.B., Safaei, R., and Howell, S.B. (2010). **Regulation of copper transporter 2 expression by copper and cisplatin in human ovarian carcinoma cells.** Mol. Pharmacol. *77*, 912–921.

Borst, P., and Elferink, R.O. (2002). **Mammalian ABC transporters in health and disease.** Annu. Rev. Biochem. *71*, 537–592.

Brachova, P., Thiel, K.W., and Leslie, K.K. (2013). **The consequence of oncomorphic TP53 mutations in ovarian cancer.** Int J Mol Sci *14*, 19257–19275.

Brady, C.A., Jiang, D., Mello, S.S., Johnson, T.M., Jarvis, L.A., Kozak, M.M., Kenzelmann Broz, D., Basak, S., Park, E.J., McLaughlin, M.E., et al. (2011). **Distinct p53 transcriptional programs dictate acute DNA-damage responses and tumor suppression.** Cell *145*, 571–583.

Brosh, R., and Rotter, V. (2009). **When mutants gain new powers: news from the mutant p53 field.** Nat. Rev. Cancer *9*, 701–713.

Caldon, C.E., Sergio, C.M., Burgess, A., Deans, A.J., Sutherland, R.L., and Musgrove, E.A. (2013). **Cyclin E2 induces genomic instability by mechanisms distinct from cyclin E1.** Cell Cycle *12*, 606–617.

Cancer Genome Atlas Research Network (2011). **Integrated genomic analyses of ovarian carcinoma.** Nature *474*, 609–615.

Cass, I., Baldwin, R.L., Varkey, T., Moslehi, R., Narod, S.A., and Karlan, B.Y. (2003). **Improved survival in women with BRCA-associated ovarian carcinoma.** Cancer *97*, 2187–2195.

Castellarin, M., Milne, K., Zeng, T., Tse, K., Mayo, M., Zhao, Y., Webb, J.R., Watson, P.H., Nelson, B.H., and Holt, R.A. (2013). **Clonal evolution of high-grade serous ovarian carcinoma from primary to recurrent disease.** J. Pathol. *229*, 515–524.

Chang, G. (2003). **Multidrug resistance ABC transporters.** FEBS Lett. *555*, 102–105.

Chen, D., Ito, S., Hyodo, T., Asano-Inami, E., Yuan, H., and Senga, T. (2017). **Phosphorylation of DEPDC1 at Ser110 is required to maintain centrosome organization during mitosis.** Exp. Cell Res. *358*, 101–110.

Choi, C.-H. (2005). **ABC transporters as multidrug resistance mechanisms and the development of chemosensitizers for their reversal.** Cancer Cell Int. *5*, 30.

Choi, Y.H., and Yu, A.-M. (2014). **ABC Transporters in Multidrug Resistance and Pharmacokinetics, and Strategies for Drug Development.** Curr Pharm Des *20*, 793–807.

Ciarimboli, G. (2014). **Membrane transporters as mediators of cisplatin side-effects.** Anticancer Res. *34*, 547–550.

Cooke, S.L., and Brenton, J.D. (2011). **Evolution of platinum resistance in high-grade serous ovarian cancer.** Lancet Oncol. *12*, 1169–1174.

Couch, F.J., Nathanson, K.L., and Offit, K. (2014). **Two decades after BRCA: setting paradigms in personalized cancer care and prevention.** Science *343*, 1466–1470.

Dai, L., Li, C., Shedden, K.A., Misek, D.E., and Lubman, D.M. (2009). **Comparative proteomic study of two closely related ovarian endometrioid adenocarcinoma cell lines using clEF fractionation and pathway analysis.** Electrophoresis *30*, 1119–1131.

Dall'Acqua, A., Sonego, M., Pellizzari, I., Pellarin, I., Canzonieri, V., D'Andrea, S., Benevol, S., Sorio, R., Giorda, G., Califano, D., et al. (2017). **CDK6 protects epithelial**

ovarian cancer from platinum-induced death via FOXO3 regulation. EMBO Mol Med *9*, 1415–1433.

Deans, A.J., and West, S.C. (2011). **DNA interstrand crosslink repair and cancer.** Nat. Rev. Cancer *11*, 467–480.

Domcke, S., Sinha, R., Levine, D.A., Sander, C., and Schultz, N. (2013). **Evaluating cell lines as tumour models by comparison of genomic profiles.** Nat Commun *4*, 2126.

Eischen, C.M. (2017). **Role of Mdm2 and Mdmx in DNA repair.** J Mol Cell Biol *9*, 69–73.

Farmer, H., McCabe, N., Lord, C.J., Tutt, A.N.J., Johnson, D.A., Richardson, T.B., Santarosa, M., Dillon, K.J., Hickson, I., Knights, C., et al. (2005). **Targeting the DNA repair defect in BRCA mutant cells as a therapeutic strategy.** Nature *434*, 917–921.

Fink, D., Nebel, S., Aebi, S., Zheng, H., Cenni, B., Nehmé, A., Christen, R.D., and Howell, S.B. (1996). **The role of DNA mismatch repair in platinum drug resistance.** Cancer Res. *56*, 4881–4886.

Freimund, A.E., Beach, J.A., Christie, E.L., and Bowtell, D.D.L. (2018). **Mechanisms of Drug Resistance in High-Grade Serous Ovarian Cancer.** Hematol. Oncol. Clin. North Am. *32*, 983–996.

Galluzzi, L., Vitale, I., Michels, J., Brenner, C., Szabadkai, G., Harel-Bellan, A., Castedo, M., and Kroemer, G. (2014). **Systems biology of cisplatin resistance: past, present and future.** Cell Death Dis *5*, e1257.

Gifford, G., Paul, J., Vasey, P.A., Kaye, S.B., and Brown, R. (2004). **The acquisition of hMLH1 methylation in plasma DNA after chemotherapy predicts poor survival for ovarian cancer patients.** Clin. Cancer Res. *10*, 4420–4426.

Girardini, J.E., Napoli, M., Piazza, S., Rustighi, A., Marotta, C., Radaelli, E., Capaci, V., Jordan, L., Quinlan, P., Thompson, A., et al. (2011). **A Pin1/mutant p53 axis promotes aggressiveness in breast cancer.** Cancer Cell *20*, 79–91.

Glavinas, H., Krajcsi, P., Cserepes, J., and Sarkadi, B. (2004). **The role of ABC transporters in drug resistance, metabolism and toxicity.** Curr Drug Deliv *1*, 27–42.

Holmes, D. (2015). **The problem with platinum.** Nature *527*, S218-219.

Horwitz, S.B. (1994). **Taxol (paclitaxel): mechanisms of action.** Ann. Oncol. *5 Suppl 6*, S3-6.

Huang, C.P., Fofana, M., Chan, J., Chang, C.J., and Howell, S.B. (2014). **Copper transporter 2 regulates intracellular copper and sensitivity to cisplatin.** Metallomics *6*, 654–661.

Huerta, L., López-Balderas, N., Larralde, C., and Lamoyi, E. (2006). **Discriminating in vitro cell fusion from cell aggregation by flow cytometry combined with fluorescence resonance energy transfer.** J. Virol. Methods *138*, 17–23.

Jackson, J.G., Pant, V., Li, Q., Chang, L.L., Quintás-Cardama, A., Garza, D., Tavana, O., Yang, P., Manshouri, T., Li, Y., et al. (2012). **p53-mediated senescence impairs the apoptotic response to chemotherapy and clinical outcome in breast cancer.** Cancer Cell *21*, 793–806.

Jayson, G.C., Kohn, E.C., Kitchener, H.C., and Ledermann, J.A. (2014). **Ovarian cancer.** Lancet *384*, 1376–1388.

Joerger, A.C., and Fersht, A.R. (2007). **Structure-function-rescue: the diverse nature of common p53 cancer mutants.** Oncogene *26*, 2226–2242.

Johnson, R.D., and Jasin, M. (2001). **Double-strand-break-induced homologous recombination in mammalian cells.** Biochem. Soc. Trans. *29*, 196–201.

Johnson, T.M., Hammond, E.M., Giaccia, A., and Attardi, L.D. (2005). **The p53QS transactivation-deficient mutant shows stress-specific apoptotic activity and induces embryonic lethality.** Nat. Genet. *37*, 145–152.

Kanska, J., Zakhour, M., Taylor-Harding, B., Karlan, B.Y., and Wiedemeyer, W.R. (2016). **Cyclin E as a potential therapeutic target in high grade serous ovarian cancer.** Gynecol. Oncol. *143*, 152–158.

Katano, K., Safaei, R., Samimi, G., Holzer, A., Rochdi, M., and Howell, S.B. (2003). **The copper export pump ATP7B modulates the cellular pharmacology of carboplatin in ovarian carcinoma cells.** Mol. Pharmacol. *64*, 466–473.

Katano, K., Safaei, R., Samimi, G., Holzer, A., Tomioka, M., Goodman, M., and Howell, S.B. (2004). **Confocal microscopic analysis of the interaction between cisplatin and the copper transporter ATP7B in human ovarian carcinoma cells.** Clin. Cancer Res. *10*, 4578–4588.

Kato, S., Han, S.-Y., Liu, W., Otsuka, K., Shibata, H., Kanamaru, R., and Ishioka, C. (2003). **Understanding the function-structure and function-mutation relationships of p53 tumor suppressor protein by high-resolution missense mutation analysis.** Proc. Natl. Acad. Sci. U.S.A. *100*, 8424–8429.

Kawamura, K., Izumi, H., Ma, Z., Ikeda, R., Moriyama, M., Tanaka, T., Nojima, T., Levin, L.S., Fujikawa-Yamamoto, K., Suzuki, K., et al. (2004). **Induction of centrosome amplification and chromosome instability in human bladder cancer cells by p53 mutation and cyclin E overexpression.** Cancer Res. *64*, 4800–4809.

Kelland, L. (2007). **The resurgence of platinum-based cancer chemotherapy.** Nat. Rev. Cancer *7*, 573–584.

Khoo, K.H., Hoe, K.K., Verma, C.S., and Lane, D.P. (2014). **Drugging the p53 pathway: understanding the route to clinical efficacy.** Nat Rev Drug Discov *13*, 217–236.

Krishnakumar, R., and Kraus, W.L. (2010). **The PARP side of the nucleus: molecular actions, physiological outcomes, and clinical targets.** Mol. Cell *39*, 8–24.

Kruiswijk, F., Labuschagne, C.F., and Vousden, K.H. (2015). **p53 in survival, death and metabolic health: a lifeguard with a licence to kill.** Nat. Rev. Mol. Cell Biol. *16*, 393–405.

Kuhn, E., Wang, T.-L., Doberstein, K., Bahadirli-Talbott, A., Ayhan, A., Sehdev, A.S., Drapkin, R., Kurman, R.J., and Shih, I.-M. (2016). **CCNE1 amplification and centrosome number abnormality in serous tubal intraepithelial carcinoma: further evidence supporting its role as a precursor of ovarian high-grade serous carcinoma.** Mod. Pathol. *29*, 1254–1261.

Kurman, R.J., and Shih, I.-M. (2010). **The origin and pathogenesis of epithelial ovarian cancer: a proposed unifying theory.** Am. J. Surg. Pathol. *34*, 433–443.

Lee, Y.-Y., Choi, C.H., Do, I.-G., Song, S.Y., Lee, W., Park, H.S., Song, T.J., Kim, M.K., Kim, T.-J., Lee, J.-W., et al. (2011). **Prognostic value of the copper transporters, CTR1 and CTR2, in patients with ovarian carcinoma receiving platinum-based chemotherapy.** Gynecol. Oncol. *122*, 361–365.

Li, M., Brooks, C.L., Wu-Baer, F., Chen, D., Baer, R., and Gu, W. (2003). **Mono- versus polyubiquitination: differential control of p53 fate by Mdm2.** Science *302*, 1972–1975.

Liang, Z.D., Long, Y., Tsai, W.-B., Fu, S., Kurzrock, R., Gagea-Iurascu, M., Zhang, F., Chen, H.H.W., Hennessy, B.T., Mills, G.B., et al. (2012). **Mechanistic basis for overcoming platinum resistance using copper chelating agents.** Mol. Cancer Ther. *11*, 2483–2494.

Liu, X., He, Y., Li, F., Huang, Q., Kato, T.A., Hall, R.P., and Li, C.-Y. (2015). **Caspase-3 promotes genetic instability and carcinogenesis.** Mol. Cell *58*, 284–296.

Lu, H. (2017). **p53 and MDM2: their Yin-Yang intimacy.** J Mol Cell Biol *9*, 1–2.

Lukin, D.J., Carvajal, L.A., Liu, W., Resnick-Silverman, L., and Manfredi, J.J. (2015). **p53 Promotes cell survival due to the reversibility of its cell-cycle checkpoints.** Mol. Cancer Res. *13*, 16–28.

Madariaga, A., Lheureux, S., and Oza, A.M. (2019). **Tailoring Ovarian Cancer Treatment: Implications of BRCA1/2 Mutations.** Cancers (Basel) *11*.

Mangala, L.S., Zuzel, V., Schmandt, R., Leshane, E.S., Halder, J.B., Armaiz-Pena, G.N., Spannuth, W.A., Tanaka, T., Shahzad, M.M.K., Lin, Y.G., et al. (2009). **Therapeutic Targeting of ATP7B in Ovarian Carcinoma.** Clin Cancer Res *15*, 3770–3780.

Mantovani, F., Collavin, L., and Del Sal, G. (2019). **Mutant p53 as a guardian of the cancer cell.** Cell Death Differ. *26*, 199–212.

Mirzayans, R., Andrais, B., Kumar, P., and Murray, D. (2016). **The Growing Complexity of Cancer Cell Response to DNA-Damaging Agents: Caspase 3 Mediates Cell Death or Survival?** Int J Mol Sci *17*.

Mirzayans, R., Andrais, B., Kumar, P., and Murray, D. (2017a). **Significance of Wild-Type p53 Signaling in Suppressing Apoptosis in Response to Chemical Genotoxic Agents: Impact on Chemotherapy Outcome.** Int J Mol Sci *18*.

Mirzayans, R., Andrais, B., Scott, A., Wang, Y.W., Kumar, P., and Murray, D. (2017b). **Multinucleated Giant Cancer Cells Produced in Response to Ionizing Radiation Retain Viability and Replicate Their Genome.** Int J Mol Sci *18*.

Mirzayans, R., Andrais, B., and Murray, D. (2018). **Roles of Polyploid/Multinucleated Giant Cancer Cells in Metastasis and Disease Relapse Following Anticancer Treatment.** Cancers (Basel) *10*.

Mittal, K., Donthamsetty, S., Kaur, R., Yang, C., Gupta, M.V., Reid, M.D., Choi, D.H., Rida, P.C.G., and Aneja, R. (2017). **Multinucleated polyploidy drives resistance to Docetaxel chemotherapy in prostate cancer.** Br. J. Cancer *116*, 1186–1194.

Motwani, M., Li, X., and Schwartz, G.K. (2000). **Flavopiridol, a cyclin-dependent kinase inhibitor, prevents spindle inhibitor-induced endoreduplication in human cancer cells.** Clin. Cancer Res. *6*, 924–932.

Muller, P.A.J., and Vousden, K.H. (2014). **Mutant p53 in cancer: new functions and therapeutic opportunities.** Cancer Cell *25*, 304–317.

Muller, P.A.J., Vousden, K.H., and Norman, J.C. (2011). **p53 and its mutants in tumor cell migration and invasion.** J. Cell Biol. *192*, 209–218.

Neungton, N., Neungton, S., Leelaphatanadit, C., Dangrat, C., and Soiampornkul, R. (2002). **p53 tumor suppressor gene mutation in ovarian cancer in Thai patients.** J Med Assoc Thai *85*, 658–667.

Ofir-Rosenfeld, Y., Boggs, K., Michael, D., Kastan, M.B., and Oren, M. (2008). **Mdm2 regulates p53 mRNA translation through inhibitory interactions with ribosomal protein L26.** Mol. Cell *32*, 180–189.

Oliner, J.D., Pietenpol, J.A., Thiagalingam, S., Gyuris, J., Kinzler, K.W., and Vogelstein, B. (1993). **Oncoprotein MDM2 conceals the activation domain of tumour suppressor p53.** Nature *362*, 857–860.

Olotu, F.A., and Soliman, M.E.S. (2018). **From mutational inactivation to aberrant gain-of-function: Unraveling the structural basis of mutant p53 oncogenic transition.** J. Cell. Biochem. *119*, 2646–2652.

Oren, M., and Kotler, E. (2016). **p53 mutations promote proteasomal activity.** Nat. Cell Biol. *18*, 833–835.

Oren, M., and Rotter, V. (2010). **Mutant p53 Gain-of-Function in Cancer.** Cold Spring Harb Perspect Biol *2*.

Pan, D., Klare, K., Petrovic, A., Take, A., Walstein, K., Singh, P., Rondelet, A., Bird, A.W., and Musacchio, A. (2017). **CDK-regulated dimerization of M18BP1 on a Mis18 hexamer is necessary for CENP-A loading.** Elife *6*.

Parekh, A., Das, S., Parida, S., Das, C.K., Dutta, D., Mallick, S.K., Wu, P.-H., Kumar, B.N.P., Bharti, R., Dey, G., et al. (2018). **Multi-nucleated cells use ROS to induce breast cancer chemo-resistance in vitro and in vivo.** Oncogene *37*, 4546–4561.

Patch, A.-M., Christie, E.L., Etemadmoghadam, D., Garsed, D.W., George, J., Fereday, S., Nones, K., Cowin, P., Alsop, K., Bailey, P.J., et al. (2015). **Whole-genome characterization of chemoresistant ovarian cancer.** Nature *521*, 489–494.

Peng, G., and Lin, S.-Y. (2011). **Exploiting the homologous recombination DNA repair network for targeted cancer therapy.** World J Clin Oncol *2*, 73–79.

Prat, J. (2015). **FIGO's staging classification for cancer of the ovary, fallopian tube, and peritoneum: abridged republication.** J Gynecol Oncol *26*, 87–89.

Ralhan, R., Arora, S., Chattopadhyay, T.K., Shukla, N.K., and Mathur, M. (2000). **Circulating p53 antibodies, p53 gene mutational profile and product accumulation in esophageal squamous-cell carcinoma in India.** Int. J. Cancer *85*, 791–795.

Rouleau, M., Patel, A., Hendzel, M.J., Kaufmann, S.H., and Poirier, G.G. (2010). **PARP inhibition: PARP1 and beyond.** Nat. Rev. Cancer *10*, 293–301.

Samimi, G., Safaei, R., Katano, K., Holzer, A.K., Rochdi, M., Tomioka, M., Goodman, M., and Howell, S.B. (2004). **Increased expression of the copper efflux transporter ATP7A mediates resistance to cisplatin, carboplatin, and oxaliplatin in ovarian cancer cells.** Clin. Cancer Res. *10*, 4661–4669.

Sonego, M., Schiappacassi, M., Lovisa, S., Dall'Acqua, A., Bagnoli, M., Lovat, F., Libra, M., D'Andrea, S., Canzonieri, V., Militello, L., et al. (2013). **Stathmin regulates mutant p53 stability and transcriptional activity in ovarian cancer.** EMBO Mol Med *5*, 707–722.

Sonego, M., Pellizzari, I., Dall'Acqua, A., Pivetta, E., Lorenzon, I., Benevol, S., Bomben, R., Spessotto, P., Sorio, R., Gattei, V., et al. (2017). **Common biological phenotypes characterize the acquisition of platinum-resistance in epithelial ovarian cancer cells.** Sci Rep *7*, 7104.

Sonnenblick, A., de Azambuja, E., Azim, H.A., and Piccart, M. (2015). **An update on PARP inhibitors--moving to the adjuvant setting.** Nat Rev Clin Oncol *12*, 27–41.

Spiller, F., Medina-Pritchard, B., Abad, M.A., Wear, M.A., Molina, O., Earnshaw, W.C., and Jeyaprakash, A.A. (2017). **Molecular basis for Cdk1-regulated timing of Mis18 complex assembly and CENP-A deposition.** EMBO Rep. *18*, 894–905.

Spötl, L., Sarti, A., Dierich, M.P., and Möst, J. (1995). **Cell membrane labeling with fluorescent dyes for the demonstration of cytokine-induced fusion between monocytes and tumor cells.** Cytometry *21*, 160–169.

Sung, P., and Klein, H. (2006). **Mechanism of homologous recombination: mediators and helicases take on regulatory functions.** Nat. Rev. Mol. Cell Biol. *7*, 739–750.

Tapia, G., and Diaz-Padilla, I. (2013). **Molecular Mechanisms of Platinum Resistance in Ovarian Cancer. Ovarian Cancer - A Clinical and Translational Update.**

The Cancer Genome Atlas. (2011). **Integrated Genomic Analyses of Ovarian Carcinoma.** Nature *474*, 609–615.

van Veen, H.W., and Konings, W.N. (1998). **The ABC family of multidrug transporters in microorganisms.** Biochim. Biophys. Acta *1365*, 31–36.

Venot, C., Maratrat, M., Sierra, V., Conseiller, E., and Debussche, L. (1999). **Definition of a p53 transactivation function-deficient mutant and characterization of two independent p53 transactivation subdomains.** Oncogene *18*, 2405–2410.

Vogelstein, B., Lane, D., and Levine, A.J. (2000). **Surfing the p53 network.** Nature *408*, 307–310.

Vousden, K.H., and Prives, C. (2009). **Blinded by the Light: The Growing Complexity of p53.** Cell *137*, 413–431.

Wade, M., Li, Y.-C., and Wahl, G.M. (2013). **MDM2, MDMX and p53 in oncogenesis and cancer therapy.** Nat. Rev. Cancer *13*, 83–96.

Watanabe, S., Kawamoto, S., Ohtani, N., and Hara, E. (2017). **Impact of senescence-associated secretory phenotype and its potential as a therapeutic target for senescence-associated diseases.** Cancer Sci. *108*, 563–569.

Wiman, K.G. (2010). **Pharmacological reactivation of mutant p53: from protein structure to the cancer patient.** Oncogene *29*, 4245–4252.

Yamamoto, S., and Iwakuma, T. (2018). **Regulators of Oncogenic Mutant TP53 Gain of Function.** Cancers (Basel) *11*.

Yan, X.-D., Li, M., Yuan, Y., Mao, N., and Pan, L.-Y. (2007). **Biological comparison of ovarian cancer resistant cell lines to cisplatin and Taxol by two different administrations.** Oncol. Rep. *17*, 1163–1169.

Yin, L., Jiang, L.-P., Shen, Q.-S., Xiong, Q.-X., Zhuo, X., Zhang, L.-L., Yu, H.-J., Guo, X., Luo, Y., Dong, J., et al. (2017). **NCAPH plays important roles in human colon cancer.** Cell Death Dis *8*, e2680.

Yoshida, K., and Miki, Y. (2004). **Role of BRCA1 and BRCA2 as regulators of DNA repair, transcription, and cell cycle in response to DNA damage.** Cancer Sci. *95*, 866–871.

Zhitomirsky, B., and Assaraf, Y.G. (2016). **Lysosomes as mediators of drug resistance in cancer.** Drug Resist. Updat. *24*, 23–33.

Zhou, C., Wang, P., Tu, M., Huang, Y., Xiong, F., and Wu, Y. (2019). **DEPDC1 promotes cell proliferation and suppresses sensitivity to chemotherapy in human hepatocellular carcinoma.** Biosci. Rep. *39*.

Zhou, X., Cao, B., and Lu, H. (2017). **Negative auto-regulators trap p53 in their web.** J Mol Cell Biol *9*, 62–68.

Publications

Sonego M., Pellizzari I., Dall'Acqua A., Pivetta E., Lorenzon I., Benevol S., Bomben R., Spessotto P., Sorio R., Gattei V., et al. (2017). **Common biological phenotypes characterize the acquisition of platinum-resistance in epithelial ovarian cancer cells.** Sci Rep 7(1):7104, https://www.nature.com/articles/s41598-017-07005-1

Lorenzon I., Sonego M., Pellarin I., Pellizzari I., D'Andrea S., Belletti B., Baldassarre G. and Schiappacassi M. (2020). **Identification and characterization of a new platinum-induced TP53 mutation in MDAH ovarian cancer cells.** Cells 9(1)36, https://doi.org/10.3390/cells9010036

Ranzuglia V., Lorenzon I., Pellarin I., Sonego M., Dall'Acqua A., D'Andrea S., Lovisa S., Segatto I., Coan M., Polesel J., Serraino D., Sabatelli P., Spessotto P., Belletti B., Baldassarre G. and Schiappacassi M. **Serum- and Glucocorticoid- inducible Kinase 2, SGK2, is a novel autophagy regulator that modulates platinum drugs response in cancer cells.** *(submitted)*

Scientific meetings

Lorenzon I., Pellarin I., Ranzuglia V., Sonego M., Dall'Acqua A., Belletti B., Baldassarre G. and Schiappacassi M. **Inhibition of SGK2, a novel autophagy modulator, sensitizes cancer cells to platinum drugs.** ABCD (Associazione di Biologia Cellulare e del Differenziamento) Congress Bologna 2019

Acknowledgments

I am grateful to all my group members (SCICC lab), in particular I thank Dr.ssa Monica Schiappacassi, Dr.ssa Maura Sonego and Dr. Gustavo Baldassarre for accepted me in the lab and for giving me the opportunity to carry out my PhD project, helping and supporting me.